CHALMERS
UNIVERSITY OF TECHNOLOGY

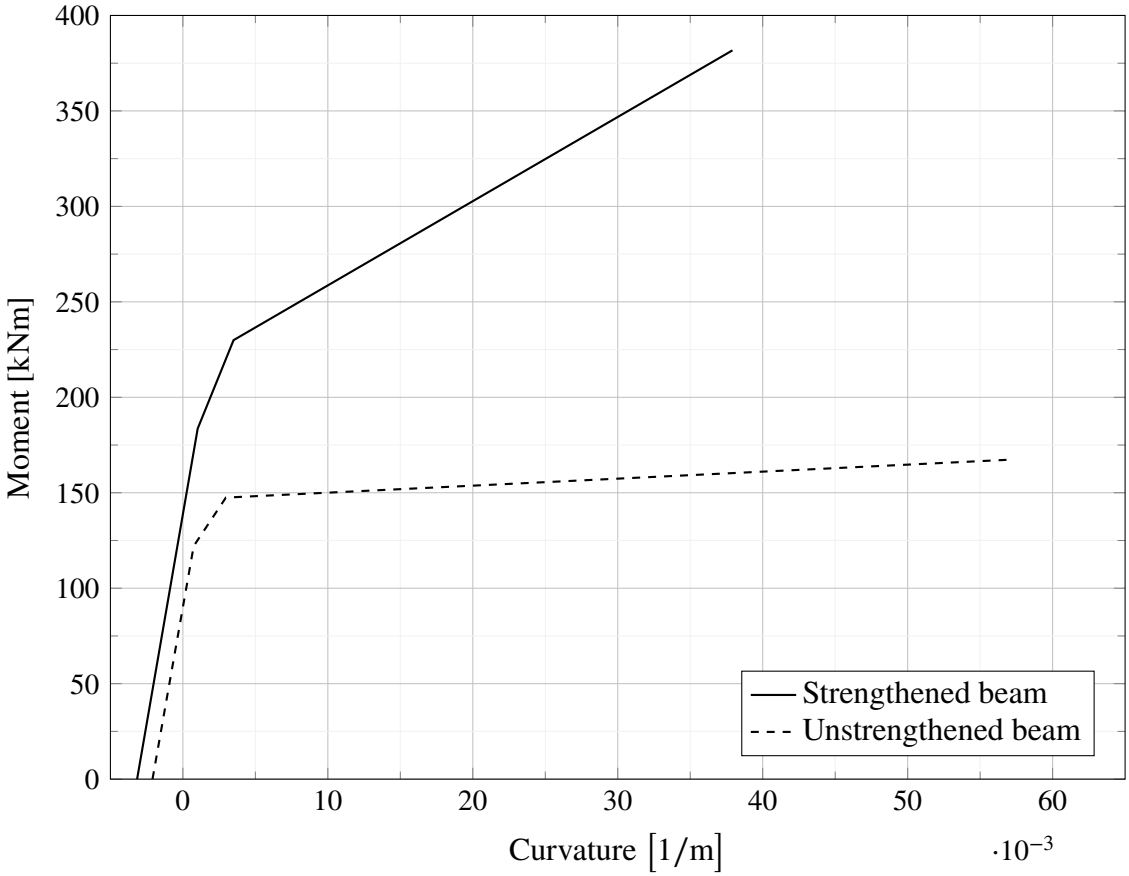

An analytical approach for flexural strengthening of double-T slabs with prestressed CFRP laminates

Master's Thesis in the Master's Programme Structural Engineering and Building Technology

PATRIK DYRESJÖ
MATTIAS ESKILSSON

Department of Civil and Environmental Engineering
Division of Structural Engineering
Steel and Timber Structures
CHALMERS UNIVERSITY OF TECHNOLOGY
Gothenburg, Sweden 2016
Master's Thesis BOMX02-16-72

MASTER'S THESIS BOMX02-16-72

An analytical approach for flexural strengthening of double-T slabs with prestressed CFRP laminates

Master's Thesis in the Master's Programme Structural Engineering and Building Technology

PATRIK DYRESJÖ

MATTIAS ESKILSSON

Department of Civil and Environmental Engineering
Division of Structural Engineering
Steel and Timber Structures
CHALMERS UNIVERSITY OF TECHNOLOGY

Gothenburg, Sweden 2016

An analytical approach for flexural strengthening of double-T slabs with prestressed CFRP laminates

Master's Thesis in the Master's Programme Structural Engineering and Building Technology

PATRIK DYRESJÖ

MATTIAS ESKILSSON

Examensarbete BOMX02-16-72/Institutionen för bygg- och miljöteknik,
Chalmers tekniska högskola 2016

Department of Civil and Environmental Engineering
Division of Structural Engineering
Steel and Timber Structures
Chalmers University of Technology
SE-412 96 Gothenburg
Sweden
Telephone: +46 (0)31-772 1000

Cover:
Comparison of moment-curvature relationship between a unstrengthened and strengthened double-T slab.
Chalmers Reproservice
Gothenburg, Sweden 2016

An analytical approach for flexural strengthening of double-T slabs with prestressed CFRP laminates

Master's Thesis in the Master's Programme Structural Engineering and Building Technology

PATRIK DYRESJÖ
MATTIAS ESKILSSON
Department of Civil and Environmental Engineering
Division of Structural Engineering
Steel and Timber Structures
Chalmers University of Technology

ABSTRACT

The usage of a building sometimes changes during its lifespan, which may result in a need for strengthening the structural system due to additional loads. A feasibility study on developing the roof of an old cultural building located in Gothenburg, Sweden into a public and urban space was conducted by COWI AB during the summer of 2015. It was concluded that the roof structure consisting of double-T slabs were in need of strengthening in order to withstand the higher loads and suggested applying prestressed carbon fibre reinforced polymers, CFRP.

The research on strengthening reinforced concrete members with prestressed CFRP is well established, yet strengthening of prestressed concrete and how to analytically assess the enhanced member is less explored.

The aim of this master's thesis is to develop an analytical approach which describes the flexural behaviour of a prestressed concrete beam strengthened with prestressed CFRP laminates. Furthermore, the approach is used to determine the theoretical increase in load-bearing capacity for a double-T slab connected to the cultural building in Gothenburg.

An analytical approach which describes the moment-curvature relationship consisting of linear branches between the states prior to strengthening, after strengthening, concrete cracking, yielding of the prestressing steel and failure is presented. The evaluated results obtained from analysing the double-T slab partially verifies the validity of the analytical approach. Furthermore, the results shows that in order to sufficiently increase the cracking load the required prestressing force leads to high interfacial shear stresses which will be difficult for the concrete to handle without proper anchorage. To limit the stresses developed in the CFRP-concrete interface and for the anchorage to not interfere with the prestressing wires, it is recommended to use a non-mechanical anchorage system which gradually increases the prestressing force in the laminate. These systems have in previous research shown to anchor a prestressing force up to 120 kN per laminate.

The flexural cracking and failure capacities of the studied double-T slab may be increased by 50% and 130%, respectively, which is considered sufficient when related to the predicted loads associated with the suggested development of the roof. It is concluded that applying prestressed CFRP laminates to the double-T slabs of the cultural building may enable the roof to be developed into a public and urban space, yet further research is required to validate the analytical approach.

Keywords: Prestressed CFRP, prestressed concrete strengthening, double-T slabs, non-mechanical anchorage

En analytisk modell för böjförstärkning av TT-element förspända med CFRP-laminat

Examensarbete inom masterprogrammet Structural Engineering and Building Technology

PATRIK DYRESJÖ
MATTIAS ESKILSSON
Institutionen för bygg- och miljöteknik
Avdelningen för Konstruktionsteknik
Stål- och träbyggnad
Chalmers tekniska högskola

SAMMANFATTNING

Användandet av en byggnad ändras ibland under dess livslängd, vilket kan resultera i ett behov av att förstärkning det bärande systemet på grund av ökade yttre laster. Under sommaren 2015 utförde COWI AB en förstudie om att omvandla taket på en gammal kulturbyggnad i Göteborg till en offentlig plats. Det kunde då fastställas att takkonstruktionen, bestående av TT-element, var i behov av förstärkning för att klara den högre belastningen. Den förstärkningsmetod som föreslogs var applicering av förspända kolfiberarmerade polymerer, CFRP.

Forskningen på förstärkning av armerade betongelement med hjälp av förspänd CFRP är väletablerad, däremot är förstärkning av förspända betongelement och hur det förstärkta elementen ska analyseras mindre utforskat.

Syftet med detta examensarbete är att utveckla en analytisk metod som beskriver beteendet av en förspänd betongbalk utsatt för böjning när den förstärkts med förspända CFRP-laminat. Metoden används sedan för att bestämma den teoretiskt möjliga ökningen i bärförmåga för ett TT-element kopplat till kulturbyggnaden i Göteborg.

En analytisk modell som beskriver moment-krökningsförhållandet som raka linjer mellan stadierna före förstärkning, efter förstärkning, sprickbildning, flytning av förspänningsstålet och brott är framtagen. De utvärderade resultaten från analyseringen av TT-elementet verifierar delvis validiteten av den analytiska modellen. Resultaten visar också på att om en tillräcklig ökning av spricklasten ska åstadkommas kommer den nödvändiga förspänningskraften leda till höga skjuvspänningar i kontaktytan mellan betongen och CFRP-laminatet. Utan ordentlig förankring kommer dessa spänningar vara svåra för betongen att hantera. För att begränsa spänningarna som uppstår i kontaktytan samt för att förankringen inte ska påverka förspänningstrådarna, rekommenderas användning av ett icke-mekaniska förankringssystem som gradvis ökar förspänningskraften i laminatet. Dessa system har i tidigare forskning visat att en förspänningskraft upp till 120 kN per laminat kan förankras.

Böjkapaciteten vid sprickbildning och brott för det studerade TT-elementet kan ökas med respektive 50 % och 130 %, vilket anses vara tillräckligt i jämförelse med de antagna lastförutsättningarna från den föreslagna omvandlingen av taket. Det fastställs att applicering av förspända CFRP-laminat på TT-elementen i kulturbyggnaden troligen gör det möjligt att omvandla taket till en offentlig plats, men att ytterligare forskning krävs för att validera den analytiska modellen.

Nyckelord: Förspänd CFRP, förstärkning av förspänd betong, TT-element, icke-mekanisk förankring

Contents

Preface

In this master's thesis an analytical approach for strengthening of double-T slabs with prestressed CFRP laminates were developed and used to study the possibility to strengthen the roof of Frölunda kulturhus in Gothenburg, Sweden. The project was carried out between the months of February and June 2016 at COWI AB, Gothenburg.

We would like to thank Johan Ström at COWI for initiating the thesis project and for the continuous support throughout the work. We would also like to thank our supervisor Pontus Nilsson at COWI who has contributed with his valuable experience and always were available for discussions. Furthermore, we would like to thank our examiner and supervisor Associate Professor Reza Haghani from the Division of Structural Engineering for supporting the thesis and helping us with guidance when we had more questions than answers.

Patrik would like to thank his wife Madeleine for all love and support during his long journey to becoming a structural engineer.

Finally, a special thanks to Oscar Pagrotsky and all other co-workers at COWI for their shown interest and will to discuss any question we threw their way.

Gothenburg, June 2016

Patrik Dyresjö & Mattias Eskilsson

Notations

Abbrevations

AFRP	Aramid fibre reinforced polymer
CDC	Critical diagonal crack
CFRP	Carbon fibre reinforced polymer
CGI	Corrugated galvanised iron
CTE	Coefficient of thermal expansion
EB	Externally bonded
FIC	Flexural intermediate crack
FRP	Fibre reinforced polymer
GFRP	Glass fibre reinforced polymer
HM	High modulus
HS	High strength
NSM	Near surface mounted
PAN	Polyacrylonitrile
PBO	Poly phenylene benzobisoxazole
PC	Prestressed concrete
PE	Plate end
RC	Reinforced concrete
SBN 75	Svensk Bygg Norm 1975
SPC	Prestressed concrete strengthened with prestressed CFRP

Roman upper case letters

A_{f}	Cross-sectional area of the CFRP laminate
A_{p}	Prestressing steel area
E	Modulus of elasticity
$E_{\mathrm{c,ef}}$	Effective modulus of elasticity for concrete
E_{c}	Modulus of elasticity of strengthened member
E_{cm}	Mean modulus of elasticity of concrete
E_{f}	Modulus of elasticity of CFRP laminate
E_{fd}	Design modulus of elasticity of CFRP laminate
E_{p}	Modulus of elasticity of prestressing steel
E_{s}	Modulus of elasticity of steel reinforcement
$E_{\mathrm{c},\varphi}$	Creep modulus of elasticity
EI	Flexural rigidity
F	Force
F_{c}	Resultant force in concrete
$F_{\mathrm{cs,p}}$	Shrinkage force acting on the prestressing steel
$F_{\mathrm{cs,s}}$	Shrinkage force acting on the steel reinforcement
F_{P}	Prestressing force in CFRP laminate
F_{p1}	Prestressing force in CFRP laminate
F_{p2}	Prestressing force in CFRP laminate
G_{a}	Shear modulus of the adhesive
I	Moment of inertia

$I_{I,ef}$ Effective modulus of elasticity in state I
K_n Spring stiffness for spring in step n
L_f Length of CFRP laminate
M External moment
$M(x)$ Moment distribution
M_c Moment caused by resultant force in concrete
M_P Moment distribution for an axial force
M_{plate} Moment in CFRP plate
M_q Moment distribution for a uniformly distributed load
N_{plate} Normal force between CFRP plate and concrete
P Axial force
P_{0i} Initial prestressing force in the steel
P_f Axial force in the CFRP laminate
P_{f0} Initial prestressing force in the CFRP laminate
P_{max} Maximum axial force in CFRP laminate
P_{plate} Axial force in CFRP plate
$P_{0\infty}$ Final steel prestressing force after long time
T_g Glass transition temperature
W_c Section modulus of strengthened member

Roman lower case letters

a Distance between the support and the laminate end
$b(z)$ Width of cross-section in section z
b_f Width of double-T slab flange
b_{frp} Width of CFRP laminate
b_p Distance between point load and the support
$b_{w,b}$ Width in the bottom of the double-T slab web
$b_{w,t}$ Width in top of the double-T slab web
$d\theta_i$ Change in slope
d_f Distance from the top concrete fibre to the CFRP laminate
d_p Distance from the top concrete fibre to the prestressing steel
d_s Distance from the top concrete fibre to the steel reinforcement
d_z Distance from the top concrete fibre to level z
dx Infinitesimal length
e Eccentricity
e_f Eccentricity of CFRP laminate
e_p Eccentricity of prestressing steel
e_s Eccentricity of steel reinforcement
f_{cd} Design compressive concrete strength
f_{ck} Characteristic compressive concrete strength
$f_{ctk0,05}$ Low characteristic tensile concrete strength
f_{ctm} Mean tensile concrete strength
f_{fu} Ultimate strength of FRP
f_{fuk} Ultimate strength of CFRP

f_{fyd} Design yield stength of the steel reinforcement
$f_{p0,1k}$ Characteristic 0.1%-proof stress of prestressing steel
$f_{p0,2k}$ Characteristic 0.2%-proof stress of prestressing steel
f_{pd} Design yield stength of the prestressing steel
f_{puk} Characteristic ultimate stength of the prestressing steel
h Total height of member
h_w Height of double-T web
l_0 Length of span
n Coefficient for concrete stress-strain relationship
n_f Number of CFRP laminates
q Uniformly distributed load
q_l Long term uniformly distributed load
t Time
t_a Thickness of adhesive layer
t_f Thickness of double-T slab flange
t_{frp} Thickness of CFRP laminate
x^i Location of the neutral axis in state i
x_i Distance from studied section to infinitesimal area

Greek upper case letters

ΔF_i Force release in CFRP, where i is the release step
ΔF_p Increase in prestressing force in CFRP laminate per step
ΔP Prestressing force transfered to the concrete at each spring
Δf Change in deflection
$\Delta\epsilon$ Change in strain difference between concrete and CFRP
$\Delta\epsilon_c$ Change in concrete strain
$\Delta\epsilon_p$ Change in prestressing steel strain

Greek lower case letters

α_1, α_2 Angle
β A function of material and geometrical properties
γ_c Partial factor for concrete
γ_f Partial factor for CFRP
γ_{fE} Partial factor for CFRP modulus of elasticity
γ_p Partial factor for prestressing steel
γ_s Partial factor for steel reinforcement
$\delta(x_1)$ Deflection in section x_1
δ_P Deflection due to an axial force
δ_q Deflection due to a uniformly distributed load
δ_κ Ductility index
ε Strain
ε_c Concrete strain distribution
ε_{c2} Strain when maximum concrete strength is reached
ε_{cc} Strain the top concrete fibre

ε_{cf}	Concrete strain on the level of the CFRP laminate
ε_{cp}	Concrete strain on the level of the prestressing steel
ε_{cs}	Shrinkage strain after fully developed long term effects
ε_{ct}	Strain in the bottom concrete fibre
ε_{cu}, ε_{cu2}	Ultimate compressive strain of concrete
ε_{cz}	Concrete strain at level z
ε_{f}	Strain in the CFRP
ε_{f0}	Initial prestrain of the CFRP laminate
ε_{fu}	Ultimate strain of the FRP
ε_{fud}	Design ultimate strain of the CFRP laminate
ε_{p}	Strain in the prestressing steel
ε_{p0i}	Initial prestrain in the prestressing steel
ε_{pud}	Design ultimate strain of prestressing steel
ε_{puk}	Characteristic ultimate strain of prestressing steel
ε_{py}	Yield strain of prestressing steel
ε_{s}	Strain in the steel reinforcement
ε_{sy}	Yield strain of steel reinforcement
$\varepsilon_{p0\infty}$	Prestrain in the prestressing steel after long time
η	FRP stress limitation coefficient
θ_{A}	Support rotation at support A
κ	Curvature
$\kappa(x)$	Curvature distribution
λ	Constant
μ	Snow load shape coefficient
ν_{i}	Volume fraction of FRP constituent
ρ_{f}	Density of FRP element
ρ_{i}	Density of FRP constituent
σ	Stress
σ_{c}	Stress in the concrete
σ_{cc}	Stress in top concrete fibre
σ_{f}	Stress in the CFRP laminate
σ_{p}	Stress in the prestressing steel
$\sigma_{p}(t)$	Stress in the prestressing steel at time t
σ_{p0i}	Initial prestressing in prestressing steel
σ_{pi}	Stress in the prestressing steel after detensioning
σ_{s}	Stress in the steel reinforcement
$\tau(x)$	Shear stress in section x
τ_{max}	Maximum shear stress
φ	Creep coefficient of concrete
χ	Relaxation factor
ψ_{0}	Factor for combination value of a variable load
ω	Constant

Indices

aca	State after CFRP application
cr	Cracking state
crit	Critical state
i	Arbitrary studied state
pc	Prestressed concrete beam
pca	State prior to CFRP application
spc	Prestressed concrete beam strengthened with prestressed CFRP laminates
y	Yielding state
u	Failure state

1 Introduction

The life span of buildings typically exceed 50 years, during which the purpose of a structure may change several times. These changes can lead to additional loading, which the original building was not designed for. Strengthening is in these situations a cost-efficient and environmental friendly alternative to replacing parts of the structure.

In the early summer of 2015, the City Premises Administration in corporation with White AB contacted COWI AB regarding an assessment of the existing roof structure of Frölunda kulturhus – a cultural building located in the west part of Gothenburg. The vision put forward by White AB was to make parts of the roof accessible for the public and turn it into an urban space with plantings, benches and smaller buildings.

The cultural building was completed in 1980 and later expanded during 2001-2003. The structural system in the original part consist of prefabricated concrete columns, beams and double T-slabs, while the expansion is a steel column-beam system with CGI sheet roofing.

Double-T slabs are normally highly utilised members and optimised for their original purpose and may therefore be more problematic to strengthen than rectangular concrete beams, which is the most studied member in strengthening literature. The slabs are commonly supported beneath the web, allowing the member to have a constant cross-section along its length, see Figure 1.1a). However, to limit the construction height and shorten the construction time the slab can be designed to be supported beneath the deck, see Figure 1.1b). The cross-section will in that case not be constant in all sections, since the web is reduced towards the support. The double-T slabs used in Frölunda kulturhus is designed with the latter support type.

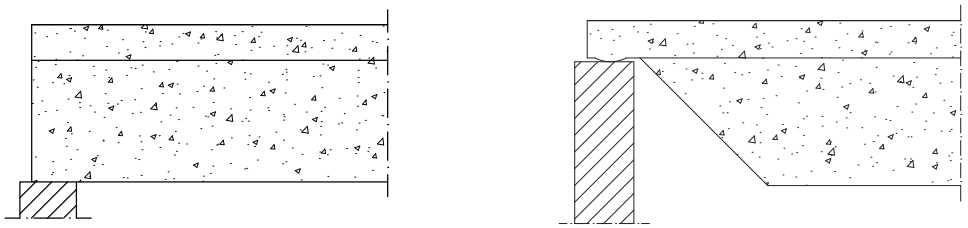

a) Web support. *b) Deck support.*

Figure 1.1 Support types of double-T slabs.

A feasibility study focusing on the concrete roofing of Frölunda kulturhus was carried out during the summer of 2015 and concluded that for the vision to be feasible, strengthening measures is needed in a number of locations. The client's requirement to not intrude on the existing ceiling height led to a suggestion of strengthening using prestressed carbon fibre reinforced polymers, CFRP, to increase the capacity of the existing double-T slabs. Prestressed CFRP, one of many different strengthening methods available, have in recent years been more frequently used while the price of carbon fibre has steadily dropped.

Prestressed concrete members can be analysed with a number of commercially available software. However, non of these supports analysis of strengthened members.

The conducted feasibility study identified a number of issues with the existing double-T slabs:

- Reduced shear resistance near support due to the reduced web height

- Insufficient load-bearing capacity in serviceability and ultimate limit state
- The thin web width may lead to problems of anchoring the CFRP to the web
- Reduced stiffness if the thin deck cracks during strengthening

1.1 Aim

In this master's thesis the aim is to develop an analytical approach which describes the flexural behaviour of a prestressed concrete beam strengthened with prestressed CFRP laminates. Furthermore, the approach is used in a case study which aims to determine the theoretical increase in load-bearing capacity for one of the double-T slabs in Frölunda kulturhus.

1.2 Limitations

The analytical approach will only consider the short term effects of the strengthening and assumes that the long term effects of the double-T slab is fully developed when the strengthening is performed. Since only the flexural behaviour is studied, the cross-section is assumed to be constant along the entire length of the member as the effects of the deck support is considered to mostly have influence on the shear capacity. The analysis is only considering the mid-section of the beam. Furthermore, only the flexural capacity in longitudinal direction is studied.

1.3 Methodology

First a literature study is conducted, where general knowledge about FRP materials, design procedures, prestressing techniques and their applications are presented, as well as how to design and produce double-T slabs. Following the literature study an analytical approach for a prestressed concrete beam strengthened with prestressed CFRP laminates is developed and adopted in Mathcad.

Secondly a case study is carried out in order to ensure the plausibility of the approach and to determine the theoretical increase in load-bearing capacity for a common double-T slab in Frölunda kulturhus.

1.4 Outline

Chapter 2 briefly introduces the concept of prestressing and describes prestressed concrete in general, which should be well known to the reader.

Chapter 3 describes the most common fibre reinforced polymers as well as their behaviour and properties under short and long term loading.

Chapter 4 describes frequently used techniques for strengthening concrete structures with non-prestressed and prestressed CFRP and the common failure modes of externally bonded CFRP.

Chapter 5 presents the behaviour of prestressed concrete strengthened with prestressed CFRP.

Chapter 6 presents the theory and verification of the analytical approach.

Chapter 7 defines the case study and the evaluation criteria. Furthermore, the results from adopting the analytical approach on the studied double-T slab in Frölunda kulturhus is presented.

Chapter 8 discusses and evaluates the results.

Chapter 9 lists the drawn conclusions.

2 Prestressed concrete

In modern structures, especially those produced with a high degree of prefabrication, it is not uncommon to find prestressed members. For a given length, these members have an improved load-carrying capacity in serviceability limit state and an equal or reducing thickness compared to its non-prestressed counterpart. For prestressed concrete members, this most importantly translates to delayed or prevented cracking and therefore reduced crack widths and deflection.

The concept of prestressing is based on that an eccentric compressive force applied within the tensile zone of a beam introduces a negative moment, which will act to bend the beam upwards, see Figure 2.1. This results in a reduction of the span moment as well as an increased shear capacity, mainly due to delayed shear cracks, and thus allows the member to carry additional load. For a sufficiently large prestressing force the entire cross-section will remain compressed for service loads and therefore prevent cracking (Engström, 2011).

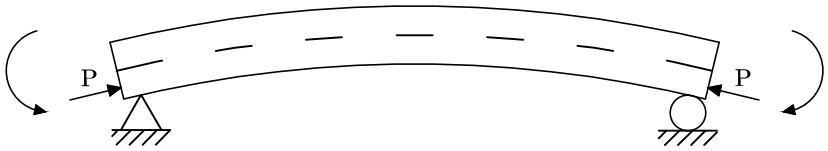

Figure 2.1 Beam subjected to a prestressing force which result in a upward camber.

Although prestressed concrete provides a number of advantages over reinforced concrete, there are additional effects which need to be considered in design. For prefabricated pretensioned members, these are mainly crushing of concrete and risk of cracking at detensioning, loss of prestressing force due to relaxation and shrinkage as well as loss of stiffness due to creep (Engström, 2011).

Detensioning refers to the step during production when the prestressing force is released and begins to act on the cross-section. At this state the only load counteracting the effects of the prestressing force is the self-weight of the member. To maintain its integrity it is essential that the stress at the compressed edge does not exceed the compressive strength of the concrete and that the stress at the tensile edge is limited so that cracking is prevented (Engström, 2011).

Relaxation is a long term effect which describes how a material subjected to constant strain displays a decrease in stress over time. As prestressing results in a certain amount of applied constant strain, the prestressing force will decrease with time when a material that exhibits this behaviour, such as steel, is used, see Figure 2.2 (Engström, 2011).

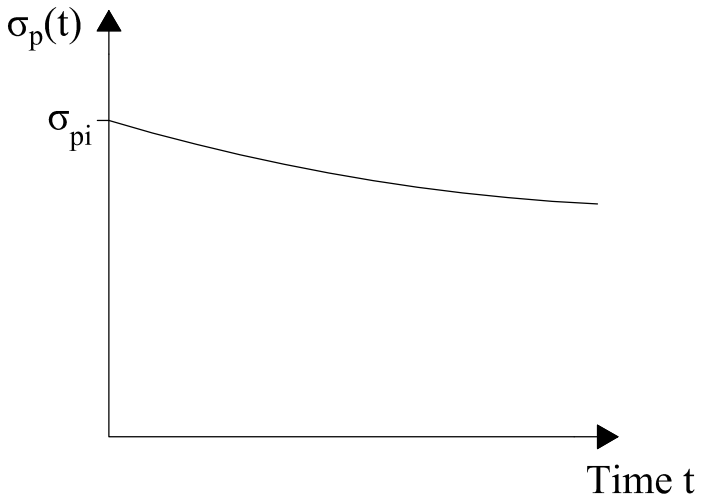

Figure 2.2 Loss in prestressing force due to steel relaxation as a function of time.

In addition to relaxation, the creep and shrinkage behaviour that concrete display when it is subjected to long term loading also result in a reduction of the prestressing force (Engström, 2011).

2.1 Manufacturing process

Prefabricated prestressed concrete members, such as double-T slabs, are manufactured in pretension beds, which consist of a mould with external supports. The prestressing steel run through the mould and is tensioned against the supports using a hydraulic jack before the concrete is cast. When the concrete has cured sufficiently, the prestressing steel is detensioned and the steel will try to shorten to its original length. This introduce a compressive force at the level of the steel, which will result in an upward bend of the member. The prestressed member is then removed from the mould for further curing. The principal steps are illustrated in Figure 2.3 (Engström, 2011).

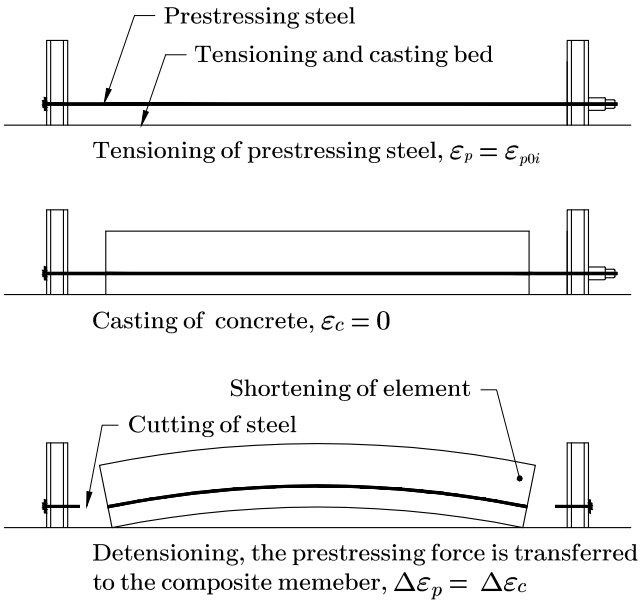

Figure 2.3 Principal steps during manufacturing of prestressed members in pretension beds.

2.2 Moment-curvature relationship

There are benefits with prestressing a concrete member, as has been described previously in this chapter. Even though delayed cracking is the main reason to prestress concrete members, the prestressing can be performed in different ways with different acceptance in the service state. The beam can either be fully prestressed or partially prestressed (Engström, 2011).

Fully prestressed members have a prestressing level which is large enough to prevent cracking in the service state. The prestressing can either be complete or incomplete, where complete prestressing only allows the concrete to be subjected to compressive stresses. If tensile stresses below the tensile strength of concrete is allowed, the prestressing is considered to be incomplete. Limited cracking may be accepted during manufacturing if the cracks closes when the beam is subjected to service load (Engström, 2011).

In *partially prestressed* members, controlled and limited cracking is accepted in the service state and the level of prestressing is adapted for certain demands to be fulfilled - such as crack widths or deflection. Many of the cracks which appear when the beam is subjected to high load will close when the load decreases, compared to a reinforced concrete beam where they remain (Engström, 2011).

As the load increases, the beam reaches different states before collapse. These states can be shown in a diagram as a moment-curvature relationship, see Figure 2.4. The change in behaviour and some of the benefits with prestressed concrete compared to reinforced concrete can also be seen, as the cracking and yielding moment is increased (Engström, 2011).

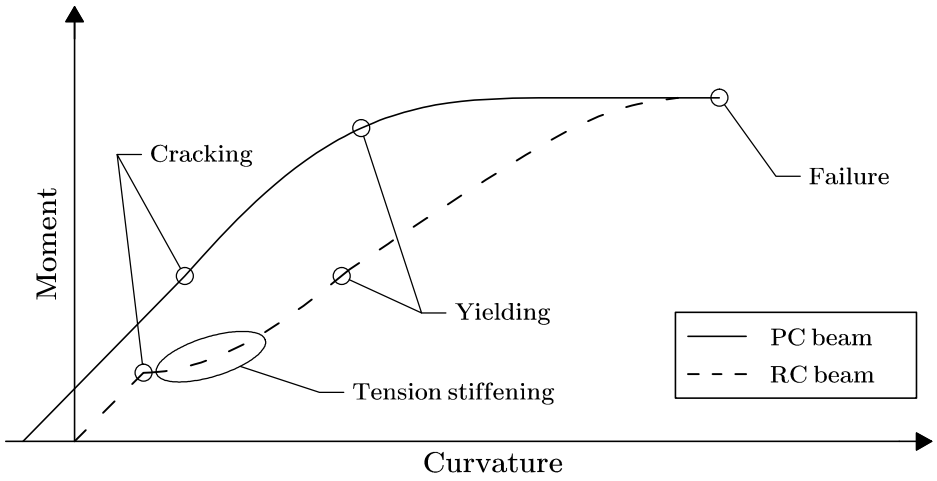

Figure 2.4 Principal moment-curvature diagram for a beam with and without prestressed steel.

Both the reinforced and the prestressed concrete member have linear behaviour up to cracking, with the difference that the prestressed member cracks at a higher moment due to the initial camber. As the member cracks, the cross-section enters state II, where the relationship still is linear but with a lesser slope due to the loss of stiffness in the concrete at the tensile zone of the cross-section. When the concrete cracks in the tensile zone, a new equilibrium system takes place, where the reinforcing steel becomes an essential part. Normally this leads to large steel stresses and strains, which also result in large structural deformations. Due to this fact, high strength steel cannot be utilised in practise since a

higher stress level results in higher steel strain, which would result in even larger structural deformations. A reinforced beam is normally in state II in the serviceability limit state. For the prestressed beam, the imposed compressive stress from the prestressing force is compensating for the limited tensile strength in the concrete. Cracks can, in case of fully prestressed, be totally prevented or in case of partially prestressed, be delayed by choosing the right prestressing force. It is possible to work with high steel stresses without large structural deformations, since the steel is prestressed (Engström, 2011).

For a simply supported reinforced concrete beam, the first crack appear in the the mid-span while more cracks can develop closer to the supports as the load continue to increase. In the beginning of the cracking phase, the uncracked sections with tensile concrete between the cracks will contribute to the overall stiffnesss. This phenomenon is called the tension stiffening effect and is observed in Figure 2.4 as a gradually transition towards a less stiff behaviour. The effect decreases as the moment increases and more sections become cracked and the beam is approaching a fully cracked state. Due to the prestressing the PC beam will have a varying rigidity in state II as the service load varies. The relationship will therefore be curved despite the fact that the concrete and the steel have linear elastic response (Engström, 2011).

If the load is increased further the steel in both RC and PC beams will reach its yield strength after which the deflection increases considerably. At failure, the flexural resistance of RC and PC beams with the same amount of steel is the same (Engström, 2011).

3 Fibre reinforced polymers

Reinforced plastics are an essential part of the modern society and are found in a vast variety of products, ranging from bathtubs and fishing rods to complex scientific products such as fibre reinforced polymers, FRP. FRP is the generic term for all reinforced plastics which use fibre as reinforcement, irrespective of what manufacturing process or fibre is used. Generally, a polymer containing additives, fillers and/or reinforcement is called a plastic (Rosato and Rosato, 2005); however in literature on FRP strengthening the term polymer is more frequently used.

FRP is a composite material consisting of two main constituents, the fibre and the matrix, which have significantly different properties. The resulting material exhibit characteristics that is a combination of the individual components and the amount, orientation and length of the fibres (Rosato and Rosato, 2005).

3.1 Matrices

The most important functions of a matrix is to bind the individual fibres together, allow for loads to be transferred between the fibres and supply the fibres with a protective layer against external mechanical and environmental damage. In order to guarantee protection during loading it is essential that the elongation at break of the matrix is considerably larger than that of the fibre, so that the fibre is not exposed before it fails (Zoghi, 2014).

The matrix is highly viscoelastic and the continuous medium which allow FRP to take most shapes. It consists of a polymer binder, fillers and additives, where the most commonly used binders for FRP strengthening are unsaturated polyester, vinyl ester and epoxy. These are all so called thermosetting resins which after curing solidifies and thereafter do not melt when exposed to high temperatures (Zoghi, 2014). The choice of matrix highly effects the transverse modulus of elasticity in one-directional FRP composites, as well as the buckling and shear resistance. In Table 3.1 some material properties of the resins are shown (Täljsten, Blanksvärd and Sas, 2016).

Table 3.1 Material properties of common matrices (Täljsten, Blanksvärd and Sas, 2016).

Matrix type	Density [kg/m^3]	Tensile strength [MPa]	Modulus of elasticity [GPa]	Ultimate strain [%]
Unsaturated polyester	1200-1400	34.5-104	2.1-3.45	1.0-6.5
Vinyl ester	1150-1350	73-81	3.0-3.5	4.0-5.0
Epoxy	2270	55-130	2.75-4.10	1.5-9.0

Unsaturated polyester can be tailored to fit the needs of many applications. However, improved stiffness and thermal stability come on the expense of lowered ductility. The resin display adequate chemical resistance, good processability and is dimensionally stable, but exhibit high shrinkage during curing which may introduce residual stresses in the material (Zoghi, 2014).

Vinyl ester, like unsaturated polyester, have low viscosity, short curing time and displays

high curing shrinkage. While the chemical and temperature properties are improved and the resin exhibit greater fracture toughness and good adhesion to glass fibres, the resin also has a higher price than polyester (Zoghi, 2014).

Epoxy is the most expensive resin of the commonly used FRP binders, but its mechanical and physical characteristics can be customised in order to comply with most requirements and is therefore widely used. It displays good resistance to creep, chemicals and solvents as well as have superior strength, low curing shrinkage and excellent adhesion properties. However, the curing time is longer than for polyester and vinyl ester (Zoghi, 2014).

3.2 Fibres

There is a large variety of fibre types available which can be used for a wide range of applications (Rosato and Rosato, 2005). In civil engineering applications the most commonly used fibre types today are glass, aramid and carbon (Täljsten, Blanksvärd and Sas, 2016); but there are studies on the use of other fibres, such as poly phenylene benzobisoxazole, PBO (Wu et al., 2003). Figure 3.1 show the stress-strain relation for these fibres together with steel reinforcement and prestressing steel.

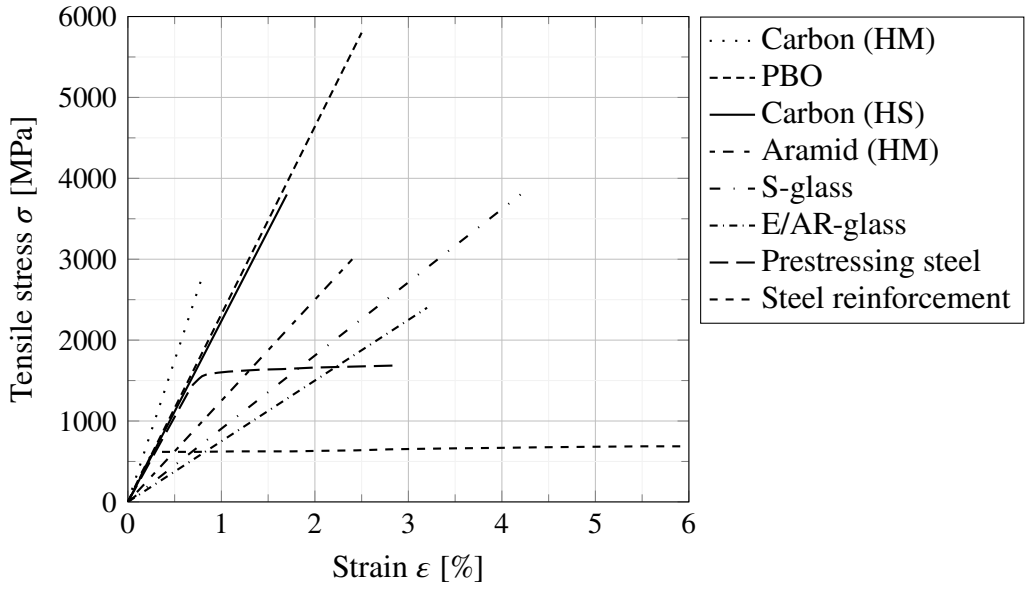

Figure 3.1 Stress-strain behaviour of various fibres compared to mild and prestressing steel (Zoghi, 2014; Toyobo Co. Ltd, 2005).

As seen in Figure 3.1, all fibres have a linear elastic behaviour up to its breaking point and is lacking a yield plateau as well as the strain hardening property which steel display. Thus, the fibres are much more brittle than steel. However, the fibres outperforms steel with low density, high strength and stiffness and consequently high strength-to-weight ratio. Table 3.2 show a comparison of material properties between the common fibres and steel.

Table 3.2 Material properties of common fibre types compared with steel reinforcement and prestressing steel (Zoghi, 2014; Täljsten, Blanksvärd and Sas, 2016; Toyobo Co. Ltd, 2005).

Material	Density [kg/m^3]	Tensile strength [MPa]	Modulus of elasticity [GPa]	Ultimate strain [%]
E/AR-glass	2500-2600	1800-3500	70-75	2.0-3.5
S-glass	2500-2600	3400-4800	85-100	3.5-5.0
Carbon (HS)	1700-1800	3500-5000	200-260	1.2-1.8
Carbon (HM)	1800-2000	2500-4000	350-700	0.4-0.8
Aramid (HM)	1400-1450	2700-4500	115-130	2.5-3.5
PBO	1540-1560	5800	180-270	2.5-3.5
Steel reinforcement	7500	500-600	200	3.5-7.5
Prestressing steel	7500	1680	195	3.5

Glass fibre is produced by extruding liquid glass through a small opening followed by stretching, resulting in a fibre which is between 5-25 µm in diameter. At this stage this inorganic fibre have a poor abrasion resistance and is very surface active, therefore the fibres undergo sizing to improve the protection against wear and ensure sufficient cohesion with the matrix. Glass fibres are divided into several groups, where the most widely used is E-glass, however S- and AR-glass are also common. The abbreviations stand for electric, strength and alkali-resistant, respectively. Although the fibre possesses many desirable properties, such as high tensile strength and good thermal resistance, glass fibre display poor performance with respect to creep and long term loading and is known to degrade when exposed to water, acid and alkaline solutions (Zoghi, 2014). The inability to withstand long term loading make glass fibre composites unsuitable for prestressing (Täljsten, Blanksvärd and Sas, 2016).

Aramid fibre is an organic fibre more commonly known as Kevlar™. The fibre is produced from para-phenylene-terephthalamide which, much like glass fibre, is pressed through a nozzle and pulled out to obtain a diameter of 12-15 µm (Zoghi, 2014). The fibre is known for its high energy absorption and toughness, but the material characteristics also include high tensile strength, low creep, good fatigue resistance and good resistance against elevated temperatures (Täljsten, Blanksvärd and Sas, 2016). However, it is sensitive to moisture and UV radiation which need to be considered when selecting an appropriate matrix (Zoghi, 2014).

Carbon fibre is an inorganic fibre and is by far the most widely used in strengthening applications (Täljsten, Blanksvärd and Sas, 2016). The fibre comes in a number of different types, where high-modulus and high-strength carbon fibres are more relevant as FRP reinforcement. These fibres are manufactured from polyacrylonitrile, PAN, or liquid crystalline pitch and consist of heat treatment, fibre stretching and oxidation. Carbon fibres are typically coated with a sizing agent, usually epoxy, to enhance the cohesion interaction with the matrix and improve the abrasion resistance. The fibres have high tensile strength and is superior most fibres with its high modulus of elasticity. Moreover, they are very resistant against creep and fatigue as well as exhibit very good chemical, UV radiation and moisture resistance (Zoghi, 2014).

PBO fibre is a newly developed organic fibre which display better energy absorption than aramid fibre while the modulus of elasticity and tensile strength correspond to or is slightly higher than that of high-strength carbon fibres. Furthermore, the fibre have high creep and fire resistance (Wu et al., 2003).

The fibres can either be continuous or discontinuous, however using continuous lengths will result in a more efficient composite as the load is not required to be transferred to another fibre after a certain distance (Zoghi, 2014).

With the exception of glass, the fibres previously described are anisotropic and will therefore exhibit different properties in longitudinal and transverse direction. In order to obtain anything other than anisotropic behaviour for the composite, the fibres must be arranged and distributed in different angles. FRP is usually orthotropic but the isotropic behaviour that steel exhibits may be possible in theory, however at best a quasi-isotropic behaviour can be achieved in practice (Zoghi, 2014).

The fibre amount of FRP is normally limited by the manufacturing or handling process, but within the limits more fibres result in better properties. At high levels the fibres can be so closely packed that the matrix cannot properly enclose the fibres and thus may become exposed to the surroundings. The recommended maximum fibre amount by volume is 70% for pultruded products, such as rods and bars, and 35% for hand-lay up applications (Nordin, 2003). Pultrusion and hand layup are common manufacturing techniques which are described in Section 3.5.

3.3 Behaviour and properties of FRP

As stated previously, the properties of FRP highly depend on its constituents and the volume fraction, orientation and length of the fibres. This allow FRP to be customised to fit the requirements of a certain application.

The density of FRP elements ρ_f depend on the volume fraction of the materials used to form the composite. As these quantities generally are known, the density can be determined as the sum of the constituents density multiplied by its volume fraction, i.e.

$$\rho_f = \sum \rho_i v_i \tag{3.1}$$

where ρ_i and v_i is the density and volume fraction of constituent i. This is commonly known as the rule of mixtures and can be used to estimate various properties of composites with continuous unidirectional fibres. Common material properties of various FRP types are shown in Table 3.3 (Zoghi, 2014).

Table 3.3 Material properties of Aramid, Carbon and Glass FRP (Zoghi, 2014).

	Coefficient of thermal expansion [$10^{-6}/°C$]		Tensile strength	Modulus of elasticity	Ultimate
Material	Longitudinal	Transverse	[MPa]	[GPa]	strain [%]
AFRP	≈ -2	≈ 30	600-2500	30-125	1.8-4.0
CFRP	≈ 0	≈ 25	600-3000	80-500	0.5-1.8
GFRP	≈ 5	≈ 25	400-1600	30-60	1.2-3.7

It is well known that steel and concrete has approximately the same coefficient of thermal expansion, CTE, of $10 \cdot 10^{-6}/°C$. This result in an insignificant thermal strain difference between steel reinforcement and concrete at the bond interface of reinforced concrete when the member is exposed to temperature changes. As shown in Table 3.3, all FRPs have a CTE which deviates slightly or significantly from that of steel and concrete depending on which axis is studied. When FRP is used as internal reinforcement this may have negative effects on the bond between the FRP and the concrete, however for externally bonded reinforcement the difference is of minor importance and can be neglected since there is no restraint (Zoghi, 2014).

The glass transition temperature T_g is, contrary to the CTE, of much more importance regardless of application. It describes at which temperature the boundary between an amorphous materials viscous and hard state lies. The matrix has a lower glass transition temperature than the fibres and therefore governs the composites mechanical properties at high temperatures. Prefabricated composites commonly have a T_g in between 130-140°C, while composites based on polymers that cure in ambient air can have a T_g as low as 50°C. As a result, external reinforcement may need a fire protection system while internal reinforcement must be protected by sufficient concrete cover (Zoghi, 2014).

3.3.1 Short term loading

The fibres are the main contributor to axial stiffness and strength of FRP and therefore governs its response. As the fibres have a linear elastic behaviour up to failure so will the composite. However, it is difficult to perfectly align and straighten the fibres during manufacturing and as a result FRP exhibits a stiffening response when subjected to increasing tensile load, see Figure 3.2. This is because when the fibres are straightened they become better utilised and in turn yield a stiffer behaviour (Zoghi, 2014).

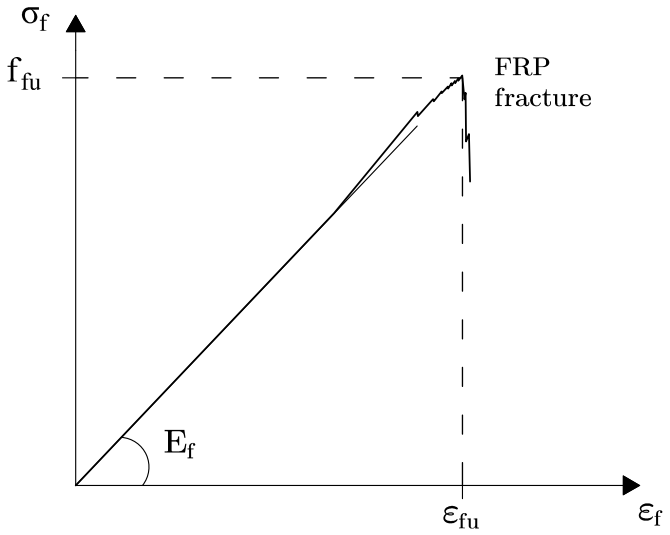

Figure 3.2 Actual stress-strain behaviour of FRP.

Figure 3.2 also show that the stiffness decrease as the FRP approaches its ultimate load. This behaviour is caused by the fracture of individual fibres, however as the matrix allows load to be continuously transferred within the FRP the material can still carry additional load before the member fails. The tensile strength and modulus of elasticity of FRP is

less than that of the used fibre, since the properties are also affected by the significantly less stiffer matrix. To obtain an estimation of, for instance, the tensile strength, modulus of elasticity and Poisson's ratio, the rule of mixtures can be applied (Zoghi, 2014).

The chemical resistance of FRP depend on its constituents and each components resistance against chemicals. The behaviour of common matrices and fibres subjected to chemicals is described in Section 3.1 and Section 3.2. Carbon shows much greater resistance against all forms of chemicals compared with aramid and glass fibres, whereas epoxy resin react very little to chemicals in comparison with vinyl esters and polyesters. Thus will a FRP consisting of carbon fibre and epoxy resin, CFRP, result in a material which have superior chemical properties over AFRP and GFRP (Zoghi, 2014).

UV radiation can affect the tensile strength of aramid and glass fibres, while carbon fibres and the resins remain unaffected. The concrete cover provide a protection for internal FRP reinforcement, thus this may be an issue for external reinforcement. However, this issue can be solved using resin additives or protective paint (Zoghi, 2014).

3.3.2 Long term loading

The creep behaviour of FRP is governed by the matrix and occur due to debonding of the fibre-matrix interface and microcracks forming within the resin. Though, since the fibres provide most of the FRPs stiffness the tensile force carried by the FRP will be transferred by the fibres and thus only loading the matrix to a lesser extent. Since the fibres show very low creep and the matrix, which is more prone to creep, only is subjected to very low stress levels the creep effects in FRP can generally be neglected. There are however a significant difference on how sustained stresses affect the short term tensile strength of different type of FRP. Studies have shown that this phenomena, known as creep rupture, allow for stress levels up to 80% of the short term strength for CFRP, whereas AFRP and GFRP can withstand 50% and 30%, respectively (Zoghi, 2014).

In applications where the FRP is prestressed is it important to consider relaxation. Neither carbon or glass fibres exhibit any pronounced relaxation, however aramid fibres show a significant amount. Thus, fibre relaxation can be avoided by choice, which is not the case for the matrices. Irrespective of choice, the viscoelastic matrix will always display relaxation. Table 3.4 compare the relaxation factor for low relaxation prestressing steel according to CEN (2004) with estimated ranges for FRP, where CFRP is shown to be considerably lower than the other materials (Zoghi, 2014).

Table 3.4 Relaxation factor comparison between different FRPs and prestressing steel (Zoghi, 2014).

Material	χ [%]
AFRP	5.0-8.0
CFRP	0.5-1.0
GFRP	1.8-2.0
Prestressing steel	2.5 (low relaxation)

Members used in buildings are normally not designed against cycling loading, yet the fatigue strength of FRP may in certain applications be of importance. AFRP and

CFRP show greater fatigue strength than prestressing steel, while GFRP exhibit lower resistance. Furthermore, CFRP exceed the values of AFRP. Similarly to creep, damages to the matrix or the fibre-matrix interface normally governs fatigue failure (Zoghi, 2014).

3.4 Adhesive layer

In applications where the FRP is externally bonded to an existing structural member the bond is established using an adhesive layer. It usually consist of a paste, which when applied to the structure can fill cavities. All resins discussed in Section 3.1 are also used as adhesives, where the most commonly used is epoxy. The adhesive may differ from the resin used as a matrix, however choosing an adhesive which has poorer properties than the used matrix would weaken the design and is thus not recommended.

Different types of epoxy allow for curing to occur at either room temperature, under elevated temperature or when exposed to UV radiation. Full strength is obtained after 4-7 days of curing, even though most of the strength is gained during the first 24 hours (Täljsten, Blanksvärd and Sas, 2016).

3.5 Manufacturing process

FRP is most frequently manufactured using pultrusion or hand layup, where pultrusion is used for large quantity orders of constant cross-sections and hand layup for more limited quantities (Zoghi, 2014).

Pultrusion is a continuous process that in principle consist of the steps shown in Figure 3.3. The continuous material, either single fibres or woven fabrics, are pulled through a resin tank in order to be covered with resin. In the following preforming fixture, excess resin and air is removed and the fibres are collected to roughly resemble the desired cross-section before entering a heated die where the final cross-section is shaped and continuously cured. The cross-section is then cut in to desired lengths or collected on a reel, depending on its shape (Zoghi, 2014).

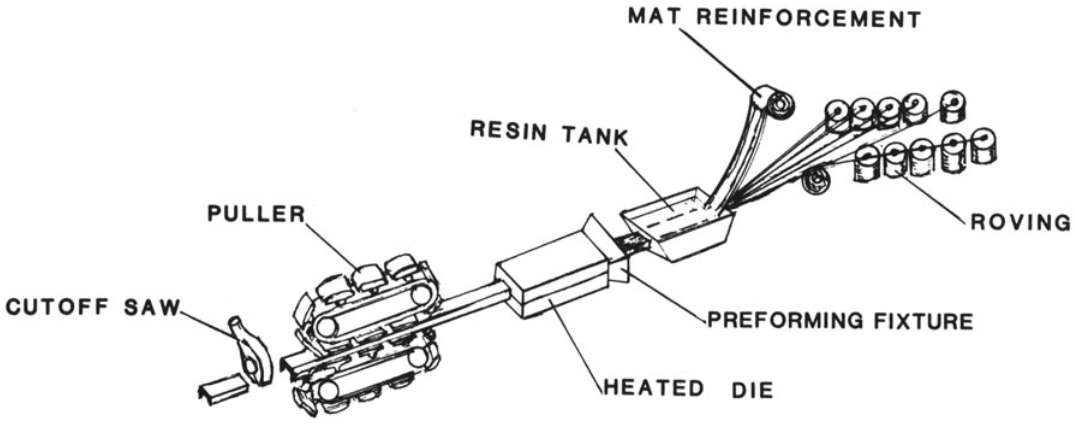

Figure 3.3 Principal steps of pultrusion manufacturing (Meyer, 1985).

Hand layup is an open moulding process and the original technique for manufacturing composites. The desired cross-section is shaped using a mould, in which fabrics are manually placed one by one and covered by resin, see Figure 3.4. Hand rollers are used on each layer to ensure proper wetting of the fibres and to improve compaction. More

layers are added until the desired thickness is reached. Curing of the finished mould can occur at either room or elevated temperature, depending on the resin type. The resin also governs what materials the mould can consist of, since for instance the shape of a wooden mould may change due to drying if it is subjected to elevated temperatures. Moulds can for instance also be fabricated in metal, concrete or ceramic if it is required (Zoghi, 2014).

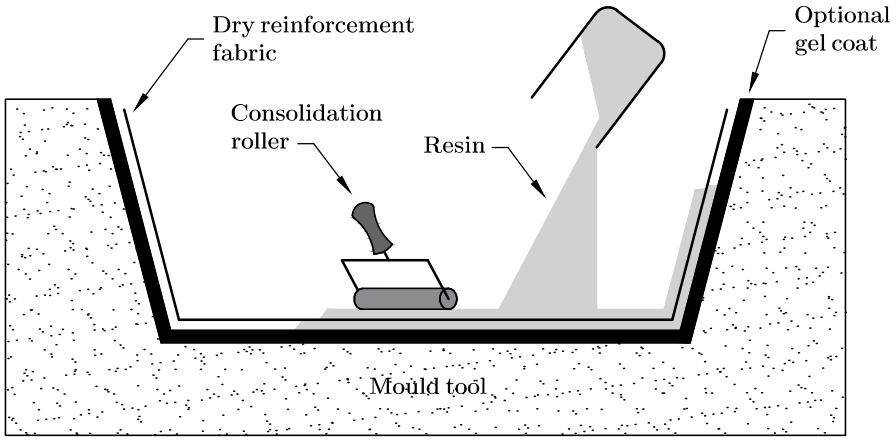

Figure 3.4 Principal procedure for hand layup manufacturing.

4 Concrete strengthened with CFRP

This chapter will focus on how CFRP can be used in order to strengthen existing concrete structures in flexure. Strengthening of concrete structures with CFRP can be used for a number of reasons even though the most common purpose is to increase the moment capacities (Täljsten, Blanksvärd and Sas, 2016). Concrete strengthening using CFRP can basically be performed either with or without a prestressing of the CFRP, both which will be described in the following sections.

4.1 Non-prestressed CFRP

Strengthening of concrete structures using non-prestressed CFRP can be made using different types of techniques and geometrical designs. Most techniques are based on using NSM CFRP-rods, CFRP laminates and CFRP fabrics, where NSM stands for near surface mounted. Regardless of which one is used, preparations of the concrete are needed and are vital to obtain the desired effect from the strengthening system. Removal of loose parts together with a vacuum cleaned and dried concrete surface before the adhesives is applied are of great importance during the preparatory work (Täljsten, Blanksvärd and Sas, 2016).

NSM CFRP-rods is a system where rods are glued or cast in pre-sawn grooves. It is important that these grooves are not sawn deeper than the concrete cover in order to not damage the steel. Rods and adhesive are placed into the grooves after the grooves have been cleaned and provided with a primer. The adhesive can also be replaced with a high quality cement mortar, in that case rods provided with quartz sand should be used. Different types of NSM-rods can be seen in Figure 4.1a) and strengthening work being performed using NSM-rods can be seen Figure 4.1b) (Täljsten, Blanksvärd and Sas, 2016).

a) *b)*

Figure 4.1 a) NSM-rods with (i) quartz sand compared to (ii) ordinary NSM-rods. b) Work performed using NSM-rods (Täljsten, Blanksvärd and Sas, 2016).

CFRP laminates systems implies laminates which are glued to the concrete surface using epoxy adhesive. Grinding and cleaning of the surface should be performed before a primer can be applied. Application of a primer is recommended to avoid disturbance in the glueing, which can be caused due to a possible suction effect from the concrete. Since CFRP laminates are composites consisting of carbon fibres and matrix, are they preferably used on flat surfaces, for example slabs and beams. The laminate product can be seen in Figure 4.2a) and when it is used in strengthening work can be seen in Figure 4.2b) (Täljsten, Blanksvärd and Sas, 2016).

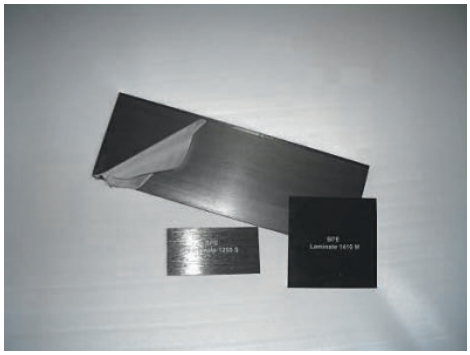

a)

b)

Figure 4.2 a) Laminates and b) strengthening work with laminates (Täljsten, Blanksvärd and Sas, 2016).

CFRP fabrics are woven fibres, which can be in several directions. The woven fibres are flexible, since they have no matrix. This flexibility makes them useful for curved surfaces, for example columns and shear strengthening of beams. A adhesive is instead applied to the surface, then the fabric is applied, followed by application of even more adhesive. The used adhesive has lower viscosity compared to systems using laminates and NSM-rods. Several layer of fabric can be applied before curing. The fabrics can be seen in 4.3a) and application of fabrics during strengthening work can be seen in Figure 4.3b) (Täljsten, Blanksvärd and Sas, 2016).

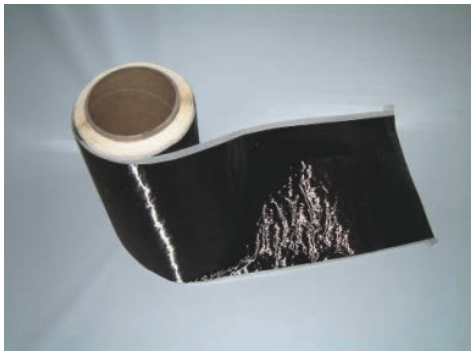

a)

b)

Figure 4.3 a) Fabric and b) strengthening work with fabrics (Täljsten, Blanksvärd and Sas, 2016).

Using fabrics or laminates are the most used methods while NSM-rods is considered to be a newer method. One risk with using laminates that can be avoided if NSM-rods are used is the creation of air voids underneath the laminates, which will affect the effect of the added CFRP. For cases where the strengthened structure is subjected to an environment where the CFRP material needs to be protected, using NSM-rods is beneficial (Nordin and Täljsten, 2006). The concept is the same independently of which of the different techniques that is used, where adding non-prestressed CFRP material results in a increased ultimate load carrying capacity. A sectional drawing of the final work of a concrete member strengthened using laminates or fabrics can be seen in Figure 4.4a) and using NSM-rods in Figure 4.4b) (Nordin, 2003).

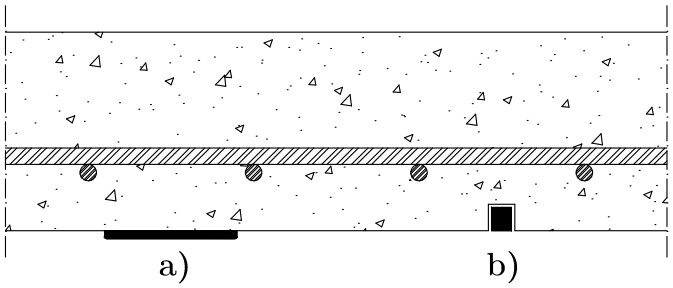

Figure 4.4 Concept of placing different types of CFRP, a) laminates or fabrics and b) NSM-rods.

4.2 Prestressed CFRP

Prestressing the CFRP when strengthening an existing concrete member results in the same principle effect as when prestressing concrete, which has been described in Chapter 2. By prestressing the CFRP an additional negative moment is introduced, which cambers the member and reduces the deformations. Due to the negative moment, the tensile zone is reduced and as it is decreased or even eliminated, cracking of the concrete can be avoided. The most efficient way is to place the CFRP at the bottom surface as seen in Figure 4.5a), since the longest possible lever arm is desired. However, this is not always possible due to the geometry, an alternative for those cases is placing the CFRP at the sides, as seen in Figure 4.5b).

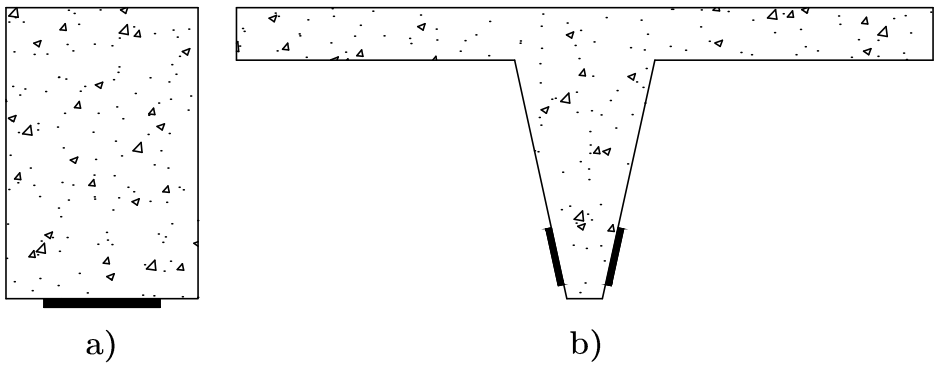

Figure 4.5 CFRP placed on a) the bottom surface and b) on the sides of the web.

If the CFRP is prestressed it is possible to get a higher utilisation of the CFRP (Nordin and Täljsten, 2006). According to Nordin (2003) four main reasons exists why prestressed CFRP can be beneficial compare to non-prestressed:

- Better utilisation of the CFRP
- Unloading of the steel reinforcement
- Higher steel yielding loads
- Decreased crack size and mean crack distance

One of the most advantageous benefits is the increase of yielding load of the steel reinforcement. This increase can be up to 50% compared to unstrengthen structures and up to 25% compared to structures strengthened with non-prestressed CFRP, as the load-deflection curve in Figure 4.6 implies. Since prestressing the CFRP decreases the strain in the steel reinforcement, the CFRP can be utilised to a higher extent compared

to the case of using non-prestressed CFRP, where the strain in the steel reinforcement becomes the limited factor due to the current loading. Prestressing the CFRP also results in about twice the cracking load compared to non-prestressed CFRP, where no increase in cracking load is possible, as seen in Figure 4.6 (Nordin, 2003).

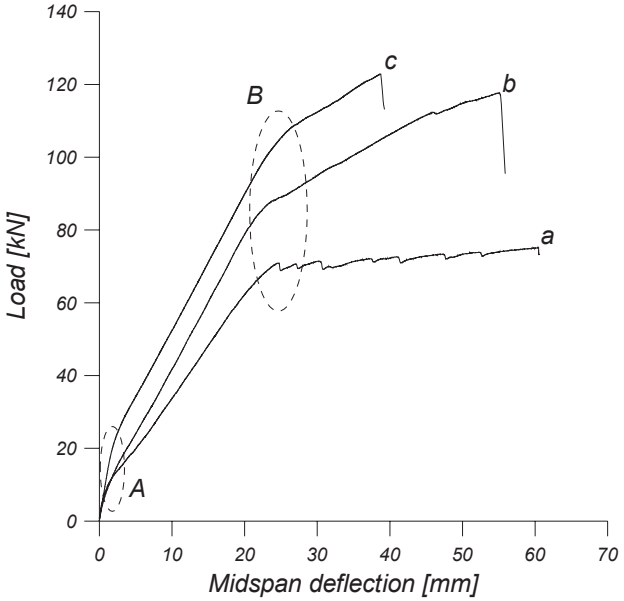

Figure 4.6 A) Cracking and B) yielding. a) Unstrengthened member, b) strengthened with non-prestressed CFRP and c) strengthened with prestressed CFRP (Nordin, 2003).

Non-prestressed CFRP has been used during a relatively long period of time compared to prestressed CFRP. There has been research on prestressed CFRP and there is no doubt about its benefits, the main issues have been how to apply it in the field. Due to accessibility and the design of the structural system, methods used in laboratories can be more or less useless in the field. As for the non-prestressed, preparation work is also very important when using prestressed CFRP since the quality of the system is highly dependant on the surface which it is applied on. The surface is therefore sandblasted or grinded and cleaned before application of the CFRP to achieve the best bond between the materials. It is also important that the original structure is assessed to verify that strengthening is possible due to its condition and also in order to know which techniques that will be applicable. If the conditions are too poor, strengthening with prestressed CFRP might not be possible (Nordin, 2005).

4.2.1 Prestressing techniques

Prestressing of CFRP can be achieved with different techniques, the most common ones are prestressed NSM CFRP, externally prestressed CFRP tendons and prestressed externally bonded CFRP, which all are described in the proceeding sections.

4.2.1.1 Near surface mounted CFRP

The prestressed NSM CFRP are very similar to the method using NSM CFRP describe in Section 4.1, where CFRP-rods are placed into sawn grooves in the concrete cover. The

difference is that they are prestressed after they have been placed into the grooves together with the adhesive, and then pulled using hydraulic jacks to achieve the prestressing. The prestressing force is kept until the adhesive has cured, then released and the force is then transferred via the adhesive to the concrete. Since the NSM technique involves placing the rods in the concrete cover, it is more suitable for outdoor structures like bridges than for indoor structures, which usually has less concrete cover (Nordin, 2005).

The NSM technique is more beneficial if the CFRP needs to be protected, since the rods are placed into grooves. However, they cannot be placed too close to each other, since problems might arise and failure can occur due to interaction between two rods. For real structures has the NSM-technique only been used as non-prestressed, since no practical useful method has been developed. Laboratory test has however been performed with a prestressing of the NSM-rods, where external supports were used to prestress against, as can be seen in Figure 4.7. This type of arrangement will in many cases not be possible when a real structure is to be strengthened, therefore further research is needed (Nordin, 2005).

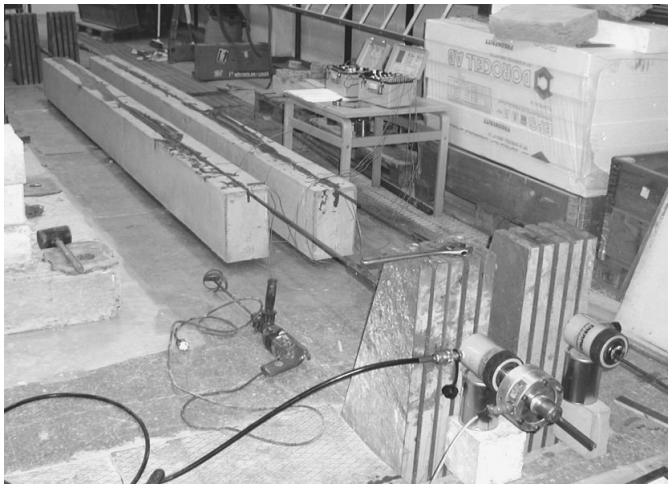

Figure 4.7 Laboratory test on a reinforced concrete beam strengthened with prestressed NSM CFRP-rods (Nordin, 2005).

4.2.1.2 External prestressing with CFRP tendons

The concept of this technique is defined by unbonded tendons, which are placed and prestressed outside the strengthened member and anchored at the ends. External tendons is a common technique to use in order to prestress concrete, where steel is the most commonly used material, although FRP materials can also be used (Nordin, 2005).

CFRP tendons for use during external prestressing are available as rods, cables, rectangular strips, braided rods and multi-wire strands. External prestressing with CFRP tendons will result in the desired effects from the prestressing concept, although, one existing problem with external prestressing tendons is anchorage. Mainly two types of anchors are used, wedge anchor and grout-potted anchor. For a wedge anchor the tendon is placed in a cone and through a wedge which is pushed to anchorage the tendon, see Figure 4.8a). Local damage to the tendon can occur when using this type of anchorage. For a grout-potted anchorage the tendon is placed in a cone which is filled with resin or grout, see Figure 4.8b). Pull-out from the cone is one problem with this type of anchorage

(Nordin, 2005).

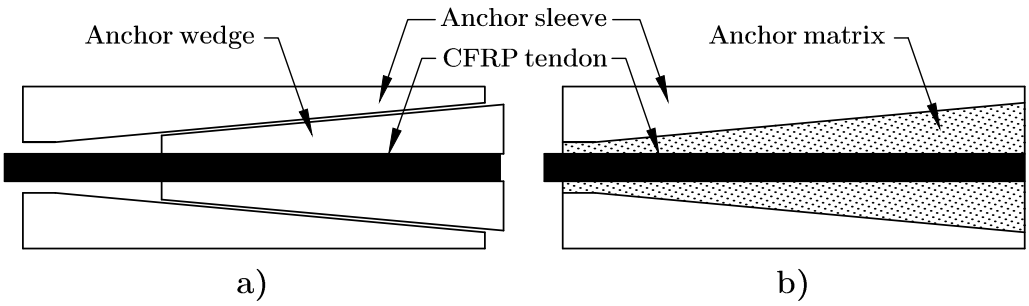

Figure 4.8 Principle design of a) wedge and b) grout-potted anchor.

4.2.1.3 Prestressed externally bonded CFRP

There has been a relatively large number of tests performed on externally bonded prestressed CFRP. The most investigated are laminates and sheets, where end peeling has been shown to be a problem for pultruded composite laminates (Nordin, 2005).

The principle of externally bonded prestressed CFRP can be seen in Figure 4.9, where grinding an cleaning of the concrete surface is the first thing which needs to be done in order to remove loose pieces and to ensure maximum bond, since the bond is essential for this prestressing technique. As soon as a clean and dry concrete surface is obtained the adhesive can be applied on the CFRP, which then are placed on the tension side of the concrete. When the CFRP has been placed on the concrete surface, it is prestressed as a prestressing force is applied, a force that has to be sustained during curing of the adhesives. The force is later released when a sufficient curing has been reached and the CFRP is then cut (Nordin, 2005).

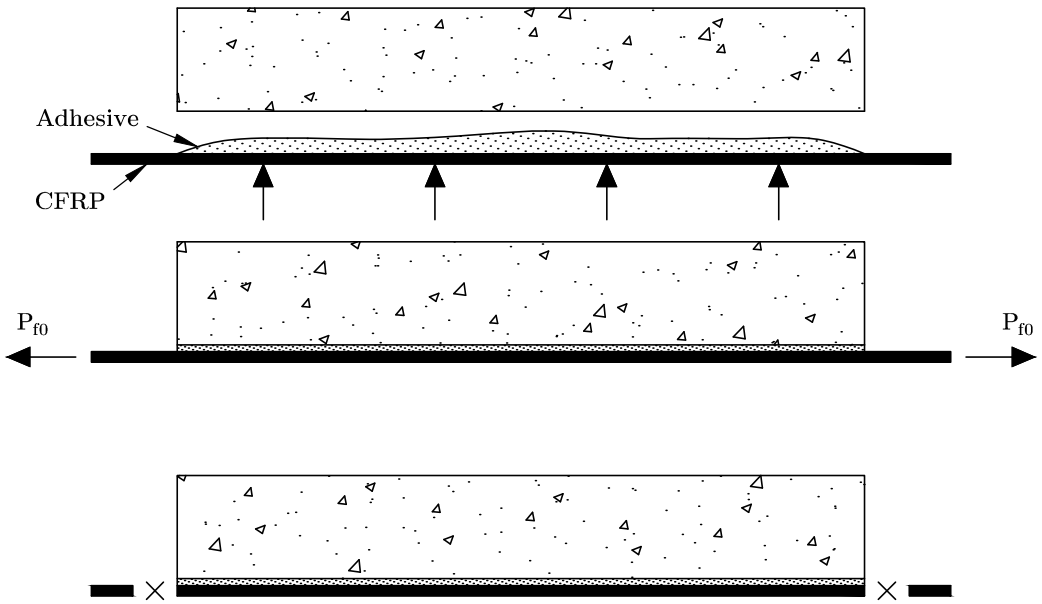

Figure 4.9 Principle for applying externally bonded CFRP-laminates.

In order to increase the capacities of concrete members by using prestressed externally

bonded CFRP, several systems have been developed to introduce a prestress in the laminate. These systems generally fall into three categories: cambered beam system, tensioning against an external reaction frame and tensioning against the strengthened beam itself.

Cambered beam system

The concept of the cambered beam system is to unload the beam which is to be strengthened. The CFRP laminates are not directly prestressed, instead an indirect prestressing is applied by cambering the beam upwards using hydraulic jacks at midspan. The beam is held cambered during the application of the laminates and as soon as the adhesive has cured, the hydraulic jacks are removed and the prestress is then introduced. The procedure can be seen in Figure 4.10 (El-Hacha, Wight and Green, 2001).

The main drawback of using this system is that only a low prestressing level can be introduced, which makes it an inefficient way of using the material, since the required effort in field applications is large. During the process there is also a risk of damaging and overstressing the strengthened beam, which can result in cracking of the concrete (El-Hacha, Wight and Green, 2001).

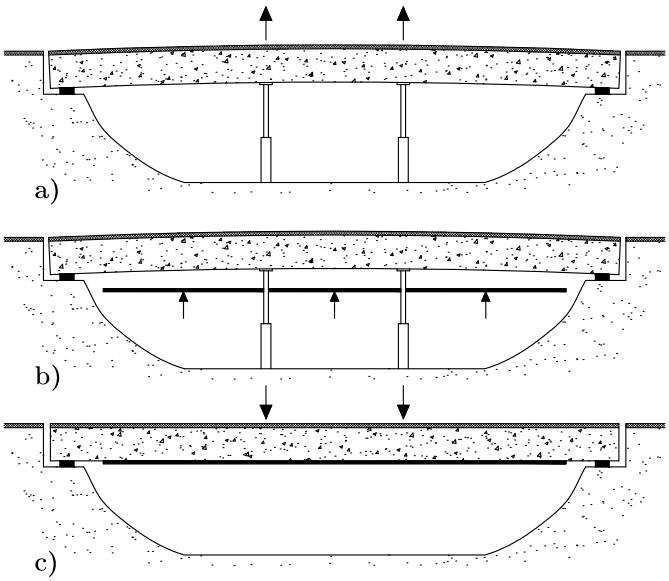

Figure 4.10 Field application with cambered beam system, a) cambering of the beam using hydraulic jacks, b) application of prestressed CFRP-laminates, c) after the hydraulic jacks has been removed.

Tensioning against an external reaction frame

This system involves tensioning the laminates against an independent system. As shown in Figure 4.11, the CFRP ends are bonded to steel plates which are connected to an external steel frame, independent from the strengthened beam. On the steel frame the laminates can be tensioned with hydraulic jacks. As the laminates are tensioned, the steel frame is raised and the CFRP is bonded to the concrete surface using an adhesive. After the adhesive has cured, the prestressing system is released and the prestress is gradually transferred to the beam (El-Hacha, Wight and Green, 2001).

Tensioning against an independent beam system is well studied for small beams in laboratory test. 6 m long T-beams has shown to get an increase of 32% in flexural strength with a prestressing level of 50% of the CFRP ultimate strength. Using this

method can include different types of anchorage systems but it is also possible to perform without anchorage. When the laminate has been tensioned and is applied to the concrete surface, heating elements are placed in the midspan and moved towards the ends of the CFRP laminate and the prestressing level of the laminate is reduced. The adhesive is cured and the CFRP are fully bonded for a short part of the laminate. This procedure is then repeated in several steps until the entire length of the CFRP is bonded and the prestressing level is at the ends are reduced to a low level. This leads to no need for anchorage and reduced shear stresses between the adhesive and the concrete at the end of the laminate (El-Hacha, Wight and Green, 2001).

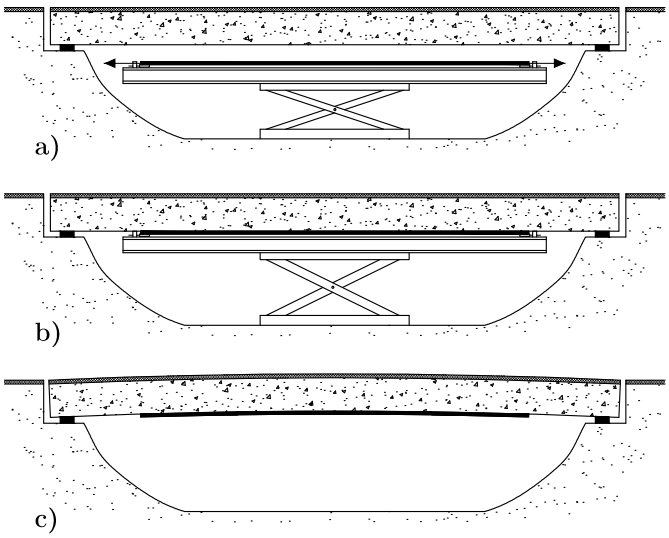

Figure 4.11 Field application with tensioning against an external reaction frame, a) tensioning the CFRP-laminate against the external reaction frame, b) application of the CFRP-laminate to the beam, c) the beam after the strengthening procedure.

Tensioning against the strengthened beam itself

A commonly used technique is where the strengthened beam itself is used for tensioning the CFRP laminate, as Figure 4.12 shows. At the end, anchors are placed which the laminate is bonded to and a separate anchorage is fixed to the beam. The laminate is tensioned using hydraulic jacks at one or two ends, which are pulling the laminate anchors and reacting against the separate anchorage mounted on the beam (El-Hacha, Wight and Green, 2001).

It is beneficial to tension against the beam itself, since the technique can be applied in many situations. The required equipment is less compared to the other techniques as well as the needed space is less, which is beneficial since the access to the strengthened beam often is limited (El-Hacha, Wight and Green, 2001).

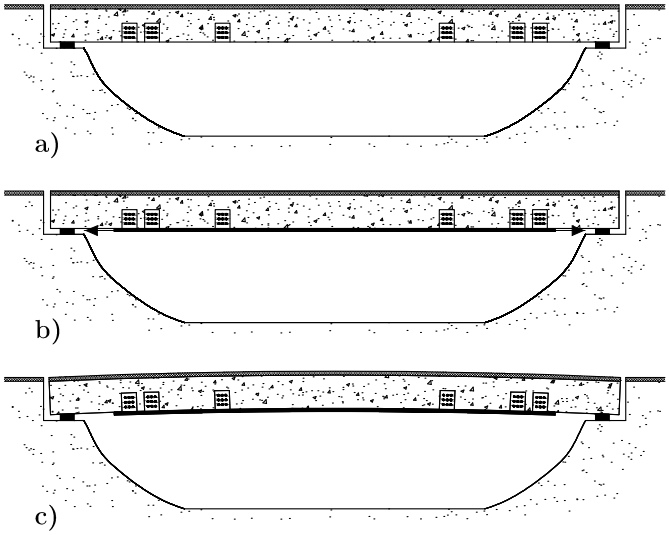

Figure 4.12 Field application with tensioning against the strengthened beam itself, a) application of anchors to the strengthened beam, b) prestressing of the CFRP-laminates, c) the beam after the strengthening procedure.

4.2.2 Failure modes of externally bonded CFRP

Some different failure modes can occur when the ultimate load is reached for reinforced concrete structures strengthened with externally bonded CFRP. The possible failure modes are shown in Figure 4.13 and consist of crushing of concrete, CFRP rupture, shear failure and different types of CFRP debonding (Täljsten, Blanksvärd and Sas, 2016).

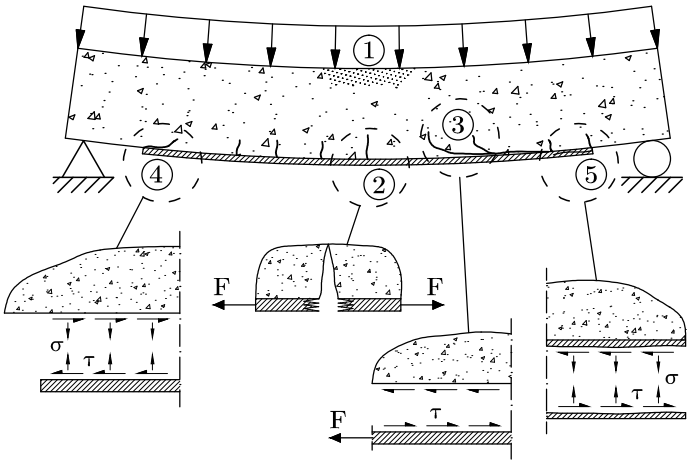

Figure 4.13 Possible failure modes of a CFRP strengthened member. 1) Concrete crushing. 2) Rupture of CFRP. 3) Flexural intermediate crack debonding. 4) Plate end and critical diagonal crack debonding. 5) Interlaminar debonding.

Crushing of concrete usually is the result of insufficient ductility, which in case of reinforced and prestressed concrete occur when either a section is provided with too much reinforcement or when a too large prestressing force is applied. Similarly, if the CFRP is prestressed too much the compressive strength of the concrete may be reached

before the steel reinforcement starts to yield which results in concrete crushing.

CFRP rupture is the only failure mode which allow the material to be fully utilised, since it occur when the tensile strength of the CFRP is reached. As the rupture is brittle this failure is normally not ideal, but as CFRP rupture normally is preceded by the more common debonding failure it rarely is a problem (Grelle and Sneed, 2013). In situations where CFRP rupture occur the steel must yield sufficiently at failure in order to ensure adequate ductility. This is achieved when the curvature is large enough at failure and is checked by calculating the ductility index as

$$\delta_\kappa = \frac{\kappa^{\mathrm{u}}}{\kappa^{\mathrm{y}}} \tag{4.1}$$

where κ^{u} is the curvature at failure and κ^{y} is the curvature at yielding. The minimum allowable value of the index depends on the steel quality and strength class of the concrete. For instance, the minimum value for steel grade S500 and concrete with strength class C35/45 or higher is 2.6 (Fédération internationale du béton, 2001).

Shear failure modes common in concrete structures, such as flexural shear and web shear cracks, may govern the design of a CFRP strengthened member. Although prestressing increases the shear resistance of the member, at certain loading levels, shear may become governing and shear strengthening is needed in order to further increase the capacity of the member.

4.2.2.1 Debonding failure

The most common failure mode in CFRP strengthened structures is debonding failure, which mainly consist of concrete cover separation, flexural intermediate crack, FIC, plate end, PE and critical diagonal crack, CDC (Grelle and Sneed, 2013). However, interlaminar debonding in the end of the composite may also occur (Täljsten, Blanksvärd and Sas, 2016).

Even though the CFRP is bonded to the concrete along its entire length the load is, similarly to welded steel connections, only transferred within a certain distance from each end, called the effective bond length, which can be seen in Figure 4.19. As the prestressed CFRP is bonded to the concrete, high interfacial shear and normal stresses develop in the adhesive layer at the end of the CFRP, which is described more later. These stresses are the cause of both *concrete cover separation*, and *PE debonding*, where the failures are initiated by a crack at the plate end. For concrete cover separation the crack then propagates to the level of the reinforcement and continues towards the middle of the member, while the crack propagates along the concrete-adhesive interface for PE debonding (Grelle and Sneed, 2013). The modes are shown in Figure 4.14 and Figure 4.15.

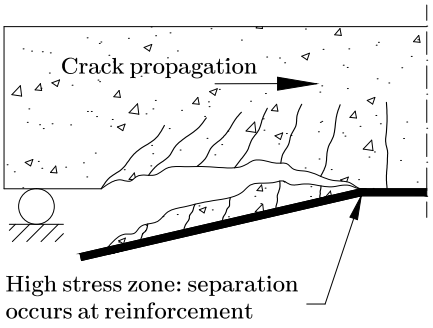

Figure 4.14 Concrete cover separation.

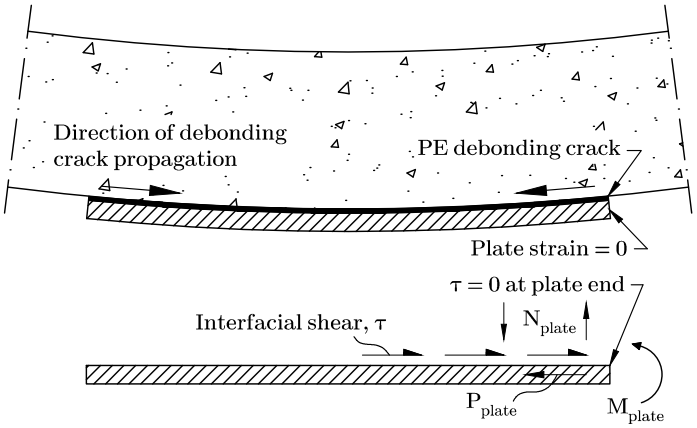

Figure 4.15 Plate end debonding mechanism.

FIC debonding, illustrated in Figure 4.16, is initiated by flexural cracks which when sufficiently developed will gradually debond the CFRP from the concrete and progress outwards (Oehlers, 2006).

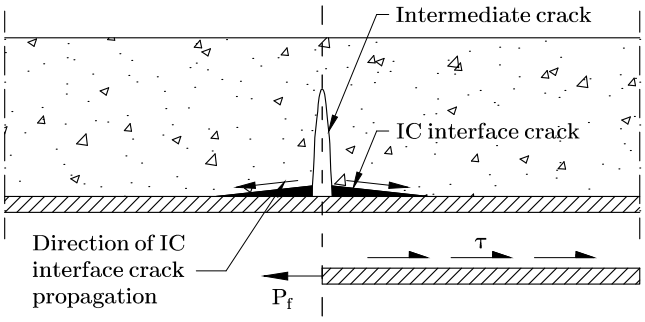

Figure 4.16 Flexural intermediate crack debonding.

CDC debonding, shown in Figure 4.17, start as a shear crack which propagates towards the end of the CFRP and since the shear cracks spread towards the middle of the member the debonding crack continue to increase as more shear cracks develop (Oehlers, 2006).

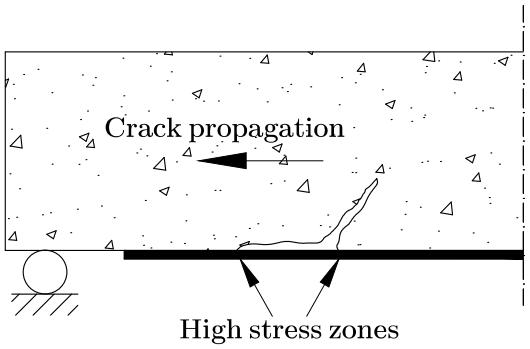

Figure 4.17 Critical diagonal crack debonding.

4.2.3 Interfacial shear and peeling stresses

Prestressed CFRP contributes to the stiffness and the strength of the structural member and will already at small deformations be activated. It is therefore necessary with a large transfer of force to the CFRP laminate in order to gain as large contribution as possible. As mentioned in Section 4.2.2.1, the force is normally transferred over a rather short distance, the effective bond length (Haghani and Al-Emrani, 2016). When a CFRP laminate is prestressed and bonded to a beam, tensile forces will develop in the bonded laminate which have to be transferred to the beam via interfacial stresses. These stresses consist of shear and normal stress, also called peeling stress. See Figure 4.18 for a principle of the interfacial stresses (Yang and Ye, 2002).

Shear stresses appear due to the difference in deformation between the CFRP and the concrete (Yang and Ye, 2002). Studies has shown that material properties such stiffness of adhesive and laminate as well as dimensions of the laminate have a clear effect on the magnitude of the maximum shear stress in the composite member (Al-Emrani and Kliger, 2006).

Peeling stresses is a result of the moment caused by the eccentric prestressing force in the CFRP, since the moment wants to bend the laminate but this is prevented by the adhesive resulting in peeling stresses in the adhesive. The peeling stresses are consequently dependent on the bending moment, stiffness of the laminate and the properties of the adhesive (Yang and Ye, 2002).

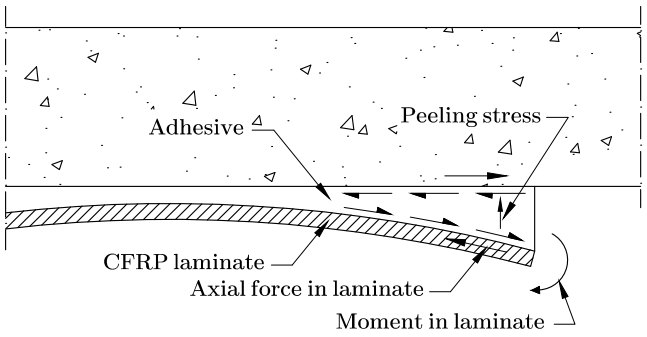

Figure 4.18 Shear and peeling stresses at the end of the laminate.

The prestressing force in the laminate will build up increasingly over the laminates length, as seen in Figure 4.19. The effective bond length is where the axial force in the laminate

is developed before it has reached the full prestressing force. The force will be transferred simultaneously as it increases and after the effective bond length, the force has completely been transferred. As the prestressing force is transferred over the effective bond length, high interfacial shear stresses will appear at this area, as seen in Figure 4.19.

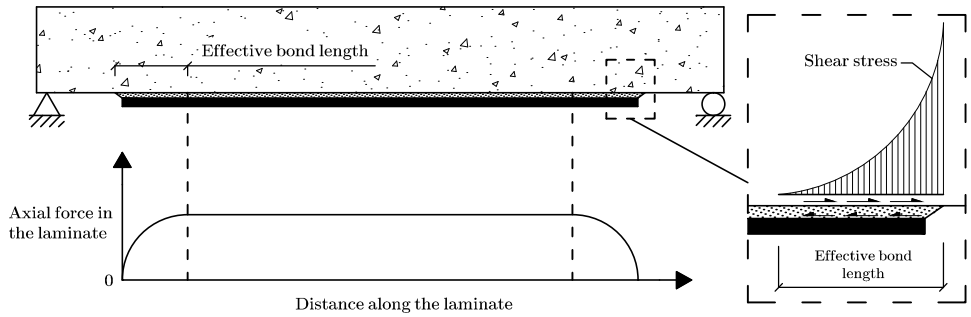

Figure 4.19 Development of axial force in the laminate and the interfacial shear stresses at the end of the laminate.

The interfacial stresses are influenced by a number factors as material properties, prestressing force and loading. How different laminates and adhesives influence the interfacial stresses are of interest since an amount of different product exist. Some parameters which can be used to affect the interfacial stresses is therefore described.

A very stiff laminate is not preferable for a prestressed laminate, since the stiffer laminate loses more prestressing in case of creep. The prestressing of the laminate is what creates the strengthening effective, independently of the laminate stiffness, and therefore is the use of a high stiffness laminate only resulting in higher costs.

The elastic modulus of the adhesive affects the interfacial stresses in a way that if it is decreased, the shear stresses generated by the prestressing force will also decrease. Since the shear stress decreases, an increased effective bond length is needed in order to transfer the same prestressing force, resulting in a more gradual transfer of the prestressing force. This will in turn give a more uniformly distribution of the shear stress and thus also decrease the maximum shear stress. The axial force at the end of the laminate will also decrease due to the decreased effective bond length and there will consequently also be a decreased bending moment. This will in turn reduce the peeling stresses (Al-Emrani and Kliger, 2006).

The geometry of the laminate can be changed in order to decrease the interfacial shear stresses by increasing the cross-sectional area of the laminate. The peeling stresses will decrease due to the increased cross-sectional area. For a constant initial stress, the maximum interfacial stresses are decreased if the width of the laminate is increased and the thickness is decreased. Regarding the maximum shear and peeling stresses at the ends of the laminate, a wider and thinner laminate is beneficial (Al-Emrani and Kliger, 2006).

The interfacial stresses are also affected by the magnitude of the prestressing force and external loading. Since a decreased prestressing force will give a lower axial force in the laminate and therefore also decreased shear and peeling stresses. Although, the prestressing force will cause initial interfacial stresses, there will also be interfacial stresses created by the loading as the beam is put in use (Täljsten, 1997). The interfacial

stresses at the end of the laminate due to loading are relatively small compared to the interfacial stresses caused by the prestressing force and these are normally already to high. Some sort of anchorage is therefore usually needed.

Different calculation models of how to estimate the interfacial stresses exist, where it normally is assumed that the material is linear elastic and the shear and peeling stresses is constant through the thickness of the adhesive layer, since the thickness is small (Yang and Ye, 2002). Al-Emrani and Kliger (2006) have derived an analytical model for calculating the maximum shear stress at the end of a prestressed laminate, as shown in Equation (4.2). Equation (4.3) can according to Täljsten, Blanksvärd and Sas (2016) be used to calculating the interfacial stresses due to loading. These models can be applied for any beam with arbitrary cross-section and material properties. The bending moment in the laminate has been neglected since the bending stiffness of the laminate normally is relatively small compared to the strengthened beam due to the fact that the laminate is thin and relatively flexible.

$$\tau_{\max} = \frac{P_{\mathrm{f0}}}{A_{\mathrm{f}} E_{\mathrm{f}}} \cdot \frac{G_{\mathrm{a}}}{t_{\mathrm{a}}} \cdot \frac{\tanh\left(\frac{\omega L_{\mathrm{f}}}{2}\right)}{\omega} \tag{4.2}$$

$$\tau_{\max} = \frac{qG_{\mathrm{a}}}{2t_{\mathrm{a}} E_{\mathrm{c}} W_{\mathrm{c}}} \cdot \frac{(a^2 + al_0)\lambda + 0.5l_0}{\lambda^2} \tag{4.3}$$

where P_{f0} is the initial prestressing force in the laminate, A_{f} the cross-sectional area, E_{f} the modulus of elasticity of the laminate, G_{a} the shear modulus of the adhesive, t_{a} the thickness of the adhesive layer, L_{f} the length of the laminate, l_0 is the length of the span, E_{c} the modulus of elasticity of the strengthened beam, W_{c} the section modulus of the strengthened beam, q is the uniformly distributed load after strengthening a the distance between the support and the end of the laminate, ω and λ are constants which are defined as

$$\omega^2 = \frac{G_{\mathrm{a}} b_{\mathrm{f}}}{t_{\mathrm{a}}} \cdot \left(\frac{1}{A_{\mathrm{f}} E_{\mathrm{f}}} + \frac{1}{A_{\mathrm{c}} E_{\mathrm{c}}} + \frac{h^2}{4 I_{\mathrm{c}} E_{\mathrm{c}}}\right) \tag{4.4}$$

$$\lambda^2 = \frac{G_{\mathrm{a}} b_{\mathrm{f}}}{t_{\mathrm{a}}} \cdot \left(\frac{1}{A_{\mathrm{f}} E_{\mathrm{f}}} + \frac{1}{A_{\mathrm{c}} E_{\mathrm{c}}} + \frac{z_0}{E_{\mathrm{c}} W_{\mathrm{c}}}\right) \tag{4.5}$$

where h is the total height of the member and z_0 the internal lever arm.

4.2.4 Anchorage of externally bonded CFRP

Debonding is a very unfavourable failure mode, since it usually takes place before the ultimate strength of the CFRP is reached. Due to the development of high interfacial stresses at the effective bond length, a decrease in efficiency of the strengthening occurs and experiments have shown that a prestressing force of maximum 15-20% of the CFRPs ultimate strength would be manageable if no anchors are used. Anchorage systems at the ends of the laminate can therefore be used in order to postpone the debonding and higher loads can then be transferred to the CFRP, resulting in an overall efficiency of the strengthening system. A number of different types

of anchorage systems exists, which can be sorted into two principle categories, either mechanical anchorage or non-mechanical anchorage (Haghani and Al-Emrani, 2016).

4.2.4.1 Mechanical anchorage

The most common way of anchoring the CFRP is by using a mechanical anchorage system. The mechanical anchorage systems are used to transfer the high prestressing force from the laminate to the strengthened member.

The purpose of the anchorage system can be different depending on the specific case. They can be used to improve interfacial shear stress transfer, provide a stress transfer mechanism if no bond length is available beyond the critical section or it can be used to prevent or delay interfacial cracking, which is the most common purpose when debonding or failure of the concrete surface starts due to peeling stresses. It is normally only needed to place anchors at the ends, which can be done in a variety of ways. Some examples are the use of spike anchors, transverse wrapping and plate anchor, which are described briefly below (Grelle and Sneed, 2013).

Spike anchors are strands of bundled fibres where one end is embedded in the matrix and the other in the concrete. Since the same material as the externally bonded FRP can be used for the spike anchors, corrosion problem can be eliminated. Spike anchors can be installed in different orientations but are normally installed orthogonal to or in-plane with the CFRP, named as 90° and 180° spike anchors. The 90° spike anchors can be used throughout the CFRP length or near the end, as shown in Figure 4.20a). The 180° anchors are usually used to anchor the laminate, when the geometry of the concrete member is complex and the CFRP has to be discontinued, for example as Figure 4.20b) is showing (Grelle and Sneed, 2013).

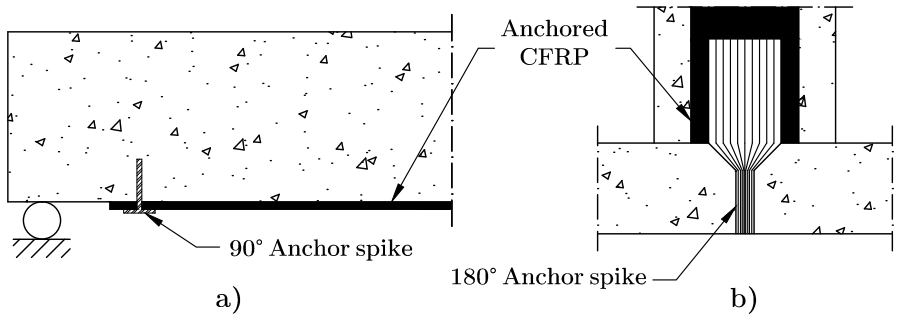

Figure 4.20 The use of a) 90° and b) 180° spike anchors.

Transverse wrapping is an anchorage system where a material is wrapped around the concrete member and the bonded CFRP to create a clamping effect. The wrapping material can also be U-shaped due to the geometry of the strengthened member as seen in Figure 4.21. CFRP is preferably used as wrapping material to avoid corrosion problem with using dissimilar materials. The strips used for wrapping can be located at the end of the CFRP or continuous along the length. To get effectiveness in the anchorage, a certain level of stress in the wraps is needed. Prestressing the wraps are therefore favourable to get a higher clamping force, although it can be hard to perform in practice for some cases (Grelle and Sneed, 2013).

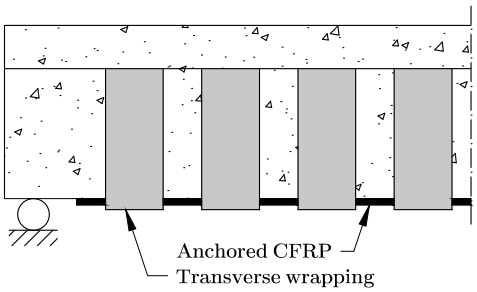

Figure 4.21 CFRP laminates anchored with the transverse wrapping system on a concrete T-beam.

Plate anchors has been used in many studies where they appear as metallic or composite plates. The general concept is the same, where the laminate which is being anchored is bonded to a plate, which in turn is bolted or bonded to the concrete member. Shear stresses are transferred at the interface of the CFRP and the plate since the CFRP typically is bonded to the plate. The stress is then transferred to the concrete member through the plates connection, which can consist of bolts through the plate into the concrete, or areas of the plate outside of the CFRP which are glued to the concrete (Grelle and Sneed, 2013).

4.2.4.2 Non-mechanical anchorage

When prestressed externally bonded CFRP has been used in order to strengthen concrete members, some sort of mechanical anchorage is usually used to increase the efficiency of the strengthening system. However, some problems can arise with the use of mechanical anchorages. These problems are the need for extra maintenance, decreased long term performance and higher costs as there is a need for installation of mechanical parts and extra time for preparatory work. This has led to the development of alternative methods without mechanical anchorage (Haghani and Al-Emrani, 2016).

The principle of these anchorage systems are that the high interfacial shear stress is decreased instead of providing an increased force transfer which is the principle of the mechanical anchorage systems. For a beam strengthened with prestressed CFRP laminates it has been shown that the magnitude of the shear stress along the effective bond length is related to the rate at which the axial force develops in the laminate, i.e. the slope of the axial force-distance curve in Figure 4.22. The shear stress is proportional to the first derivative of the axial force in the laminate and it can be shown that

$$\tau(x) = \beta \cdot \frac{d P_{\mathrm{f}}(x)}{dx} \tag{4.6}$$

where τ is the interfacial shear stress, P_{f} is the axial force in the laminate and β is a function of the material and geometrical properties. According to Equation (4.6) can the magnitude of the shear stress be controlled by changing the distribution of the axial force along the effective bond length (Haghani and Al-Emrani, 2016).

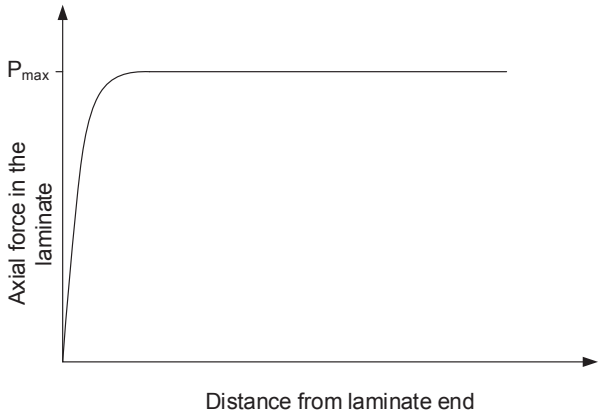

Figure 4.22 Development of axial force in the laminate.

Gradient anchorage method

The principle of this method is to gradually reduce the prestressing force in the laminate to control the magnitude of the interfacial shear stress. The method has a purely epoxy-based connection between the concrete and the CFRP laminate. The principle of the method is based on the fact that epoxy has an ability to cure faster under higher temperature and therefore can be able to carry shear loads after a short time span.

Epoxy is applied to the concrete surface and the CFRP is prestressed. The anchorage is achieved by heating the epoxy in segments at the strip end. For every segment being heated, a partial release in the prestress force follows. The procedure is completed when the the prestressing force has reached zero at the very end of the CFRP laminate. By using this process, the total prestressing force can be spread over several segments. A schematic illustration of the process can be seen in Figure 4.23 (Michels and Czaderski, 2012).

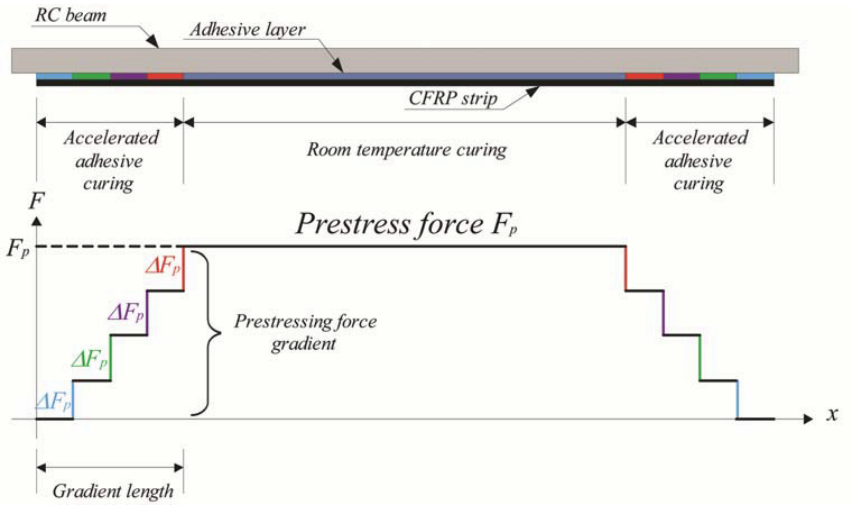

Figure 4.23 Schematic illustration of a decreasing prestressing force for the gradient anchorage method (Michels and Czaderski, 2012).

The heating and force releasing procedure can be seen in Figure 4.24, which consists of heating of the first segment for about 25 minutes followed by a five minutes cooling period and then after the cooling, the force is released in segment one. The procedure is repeated until the end. Total duration needed to create a sufficient anchorage is greatly

shortened compared to mechanical anchors (Michels and Czaderski, 2012).

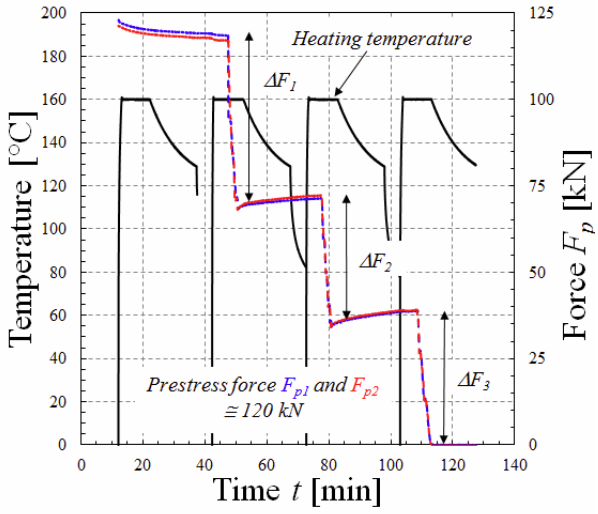

Figure 4.24 Heating and force release procedure for Gradient anchorage method (Michels and Czaderski, 2012).

Tenroc method

A new method has recently been developed at Chalmers University of Technology and is here denoted as the Tenroc method. This method is based on stepwise introduction of the prestressing force in the laminate, rather than gradual release of the prestressing force (Haghani and Al-Emrani, 2016).

The gradually introduction of the prestressing force is used in order to achieve a smoother force distribution, as the one shown in Figure 4.25. The effective bond length is divided into several steps, where the magnitude of the axial stress in the laminate is increased for each step. By keeping the difference between the magnitudes of the axial force in each step at a minimum level, the development of high interfacial shear stresses could be prevented. Since this force transfer mechanism is used, the shear and peeling stresses are reduced to levels which can be tolerated by the concrete and the adhesive in a way that results in that no mechanical anchorage system is needed (Haghani and Al-Emrani, 2016).

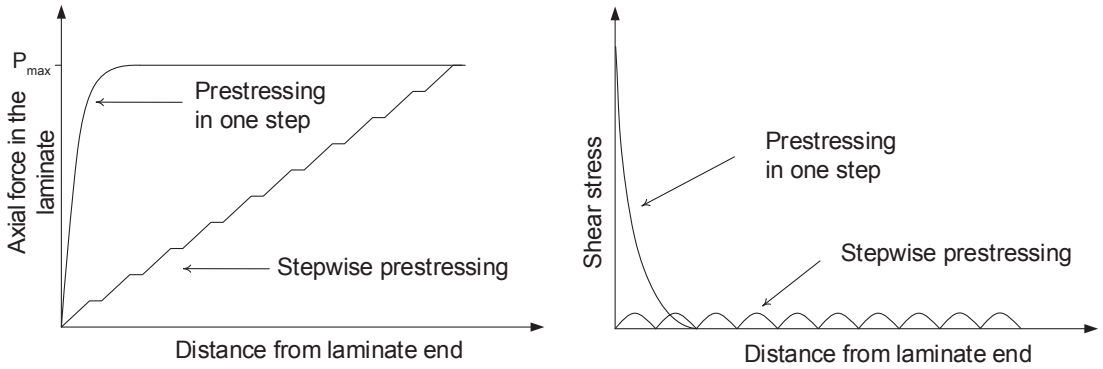

Figure 4.25 a) Axial force in the laminate and b) the corresponding interfacial shear stress along the effective bond length.

The transfer of the prestressing force to the laminate is achieved by using a special device, which can be seen in Figure 4.26 and 4.27. It consists of a number of tabs, which are mechanically fastened to the CFRP laminate and connected to each other with a series of springs. Figure 4.28 is showing a principle of how the prestressing is divided by designing the stiffness of the springs in a way that each tab will deliver a certain and equal part of the total prestressing force to the CFRP laminate. As can be seen in Figure 4.26, ten tabs are connected to each other with the use of metallic rods. For the case in 4.26, the stiffness of the springs is designed with an introduction of 10% of the total prestressing force in each tab and eventually to the concrete. For the connection of the CFRP laminate to the device, a GFRP plate is used as a medium. The GFRP plate is screwed to the device and the CFRP is then bonded to the surface of the GFRP (Haghani and Al-Emrani, 2016).

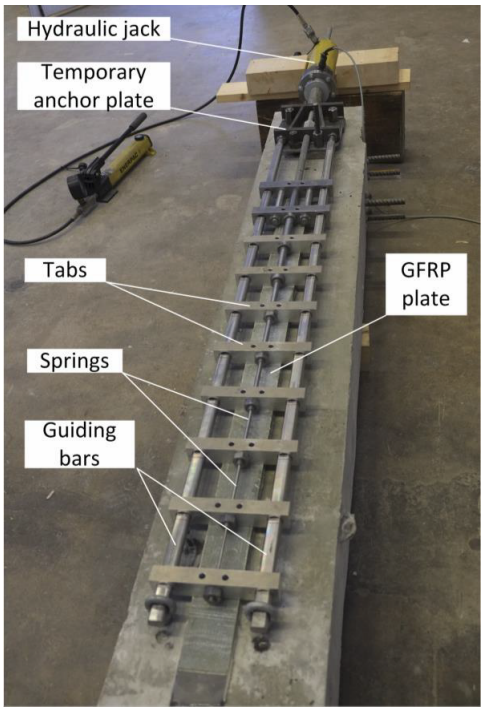

Figure 4.26 The prestressing device and setup during prestressing.

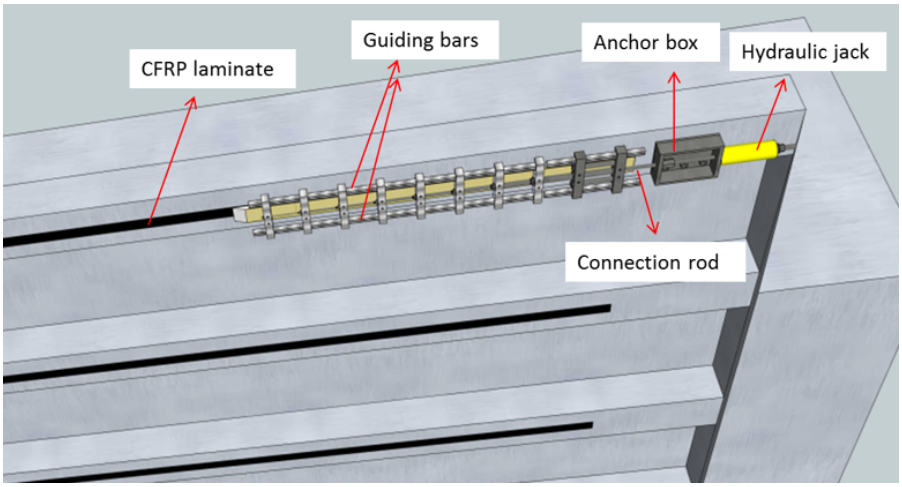

Figure 4.27 The prestressing device placed on the strengthened beam.

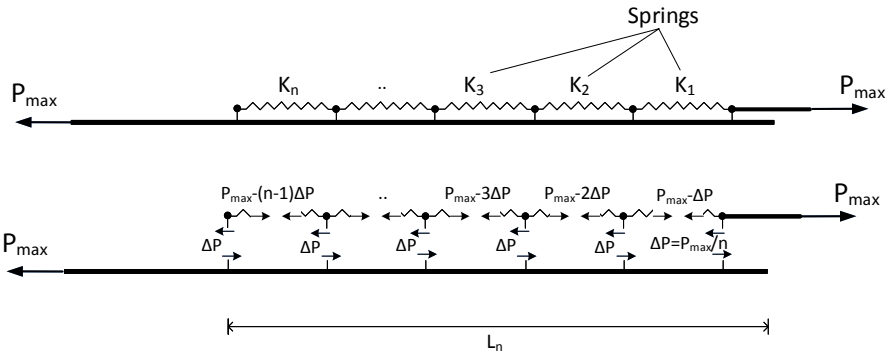

Figure 4.28 Principle of distributing the prestressing force over the FRP strengthening laminate using a spring system.

4.3 Working environment

Strengthening of concrete structures with non-prestressed or prestressed CFRP, involves a certain amount of labour containing for example sandblasting, grinding and handling of uncured epoxy adhesives. For this kind of work, it is important to have a good working environment as well as proper waste disposal.

Epoxy adhesives are the most used adhesive for bonding CFRP to concrete when strengthening work is carried out. It is also used as an epoxy filler when the concrete has too high roughness and needs reparation before the CFRP is applied. Therefore, clear instructions for how to handle and mix the epoxy adhesives should be available as well as theoretical education to the workers. Epoxy is allergenic and should not get in contact with the skin, which is why it is very important with proper safety clothing while handling uncured epoxy. People with allergic skin problems are therefore not allowed to work with uncured epoxy. Working with cured epoxy do not imply any health threats though (Täljsten, Blanksvärd and Sas, 2016).

There is ongoing research on more environmental friendly alternatives of bonding FRP to concrete at Chalmers University of Technology. The research aim to replace the current adhesives so that these only are used in controlled environments, i.e. during manufacturing. The proposed solution, which is still to be tested, comes from FRP stay-in-place formwork systems where bond to concrete is improved by adding coarse silica sand in the bottom of the mould (R. Goyal, Mukherjee and S. Goyal, 2016) and consists of instead coating the FRP with coarse silica sand and thereafter achieve bond to the concrete using cement.

5 Prestressed concrete strengthened with prestressed CFRP

The behaviour of prestressed concrete strengthened with prestressed CFRP subjected to increased loading has to the extent of the authors' knowledge not been been discussed in any literature. However, since adding CFRP means to add a linear elastic material the behaviour most likely is similar to that of prestressed concrete beams, described in Section 2.2, but with the cracking state further delayed thus resulting in a stiffer response. The strengthening will in practice be performed while a certain amount of loading is acting on the member. Therefore, the initial state is somewhere along the moment-curvature diagram of the prestressed concrete beam - ideally prior to cracking.

The prestressing force introduced in the CFRP will after strengthening be transferred to the member and result in a compressive force acting with an eccentricity and results in a negative moment contribution which reduces the curvature. A previously cracked beam may therefore return to its uncracked state and recover a part of its lost stiffness if the prestressing is sufficient to close developed cracks.

A comparison between the principal moment-curvature relationship of an unstrengthened and strengthened prestressed concrete beam is shown in Figure 5.1. The behaviour of the uncracked strengthened beam is linear up to the cracking moment. As described in Section 2.2, cracking will reduce the stiffness of the member and as more sections becomes cracked the behaviour gradually transforms towards that of a fully cracked beam, i.e. state II.

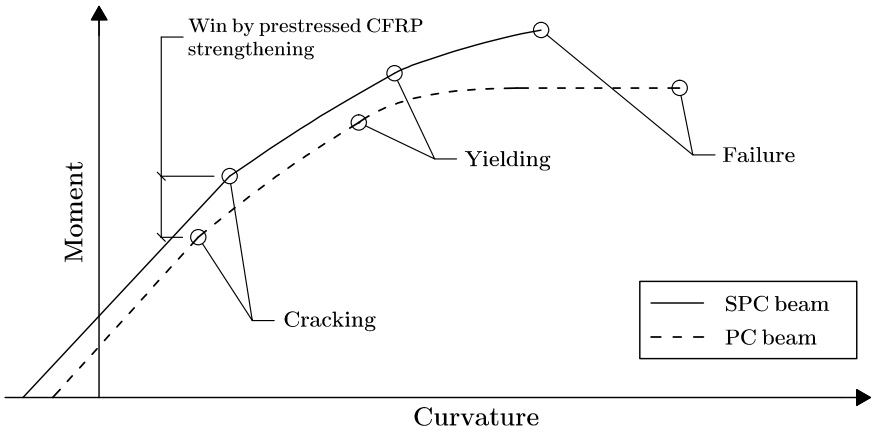

Figure 5.1 Principal moment-curvature diagram for a prestressed concrete beam, unstrengthened and strengthened with prestressed CFRP laminates.

As the load continues to increase, the prestressing steel reaches yielding, however since its stress-strain relationship normally is described with an inclined yielding branch the load can be further increased until its ultimate strain is reached.

Failure will occur either when the top fibre reaches the concrete compressive strength resulting in concrete crushing or when the ultimate strain of the CFRP is reached resulting in CFRP rupture. As was described in Section 3.3.1, the stress-strain relationship will be linear up to failure for the CFRP, see Figure 3.2.

If the strengthened member is unloaded to levels less than the applied loading during

strengthening, the curvature will decrease proportional to the moment and follow the same inclination as between the state after CFRP application and prior to cracking, as the principal curve in Figure 5.1 shows.

The stress in the concrete, the steel and the CFRP need to be limited in order to prevent damage in the service state. According to Fédération internationale du béton (2001) the stresses should fulfil the following conditions:

$$\sigma_{cc} \leq 0.45 f_{ck} \tag{5.1}$$

$$\sigma_{s} \leq 0.8 f_{yk} \tag{5.2}$$

$$\sigma_{f} \leq \eta f_{fuk} \tag{5.3}$$

where σ_{cc} is the stress in the top concrete fibre, f_{ck} the characteristic compressive strength of the concrete, σ_{s} the stress in the steel reinforcement, f_{yk} the characteristic yield strength of the steel reinforcement, σ_{f} the stress in the CFRP, f_{fuk} the ultimate tensile strength of the CFRP and η is the FRP stress limitation coefficient, which depends on the type of FRP and is suggested to be 0.8 for carbon. The main focus of Fédération internationale du béton (2001) is strengthening of reinforced concrete structures and a stress limitation for prestressing steel is not given, however the condition given by Equation (5.2) is also reasonable for prestressing steel as neither steel should be yielding in the service state.

There has been a large amount of research performed on concrete members strengthened with prestressed CFRP laminates, though most research on prestressed CFRP laminates considers strengthening of reinforced concrete members. Experiments on RC beams strengthened with prestressed CFRP laminates has according to Rezazadeh, Barros and Costa (2015) showed an increase in cracking load by 82% and by 42% in failure load, for 1.4x20 mm laminates. According to Pellegrino and Modena (2009) can the cracking load be increased by 195% and the failure load by 79%, where 1.2x80 mm laminates were used. Since anchorage of prestressed CFRP laminates can be problematic can the prestressing force be a limiting factor. By using a non-mechanical anchorage system, where the prestressing force is gradually introduced, Michels and Czaderski (2012) has successfully anchored a prestressing force of 120 kN using the gradient method and Haghani and Al-Emrani (2016) has successfully anchored 110 kN using the Tenroc method.

6 Analytical approach

In this chapter the analytical approach is described. The approach is adopted using Mathcad for which the complete code is found in Appendix B.

6.1 Theory

The flexural behaviour of the prestressed concrete beam is simplified by refining the analytical approach presented by Rezazadeh, Barros and Costa (2015). This approach was developed for short term response of reinforced concrete beams with both tensile and compressive steel reinforcement and describes the relationship between moment and curvature at distinct points along the curve. In between these points the relation is assumed to be linear.

6.1.1 Safety concept

The material parameters are reduced in the design to increase the safety margin and take production variations and defects into account. The partial factors for concrete and steel are chosen in accordance with CEN (2004) while the factors for CFRP are taken from Westerberg (2007). In addition, the design modulus of elasticity of the CFRP laminate E_{fd} is used in the failure state. In all states until failure the mean value E_f is used. The recommended partial factors are listed in see Table 6.1.

Table 6.1 List of recommended partial factors for concrete, steel and CFRP.

Material	Value
Concrete, γ_c	1.5
Steel reinforcement, γ_s	1.15
Prestressing steel, γ_p	1.15
CFRP	
Strength, γ_f	1.25
Modulus of elasticity, γ_{fE}	1.1

According to Nordin (2005) the CFRP prestressing should not exceed 65% of the ultimate strength of the CFRP f_f as higher levels may have unfavourable effects on the service life and lead to creep rupture.

6.1.2 Effects of long term loading

Strengthening of members normally occur after being used for a long time, therefore it is assumed that the long term effects of prestressed concrete; steel relaxation, shrinkage and creep deformations, are fully developed.

Relaxation of the prestressing steel is considered by reducing the initial prestressing force

P_{0i} according to

$$P_{0\infty} = (1 - \chi) \cdot P_{0i} \tag{6.1}$$

where χ is the relaxation factor and $P_{0\infty}$ is the final prestressing force after long time which is used in the calculations. *Concrete shrinkage* results in shortening of the member which is described by a concrete deformation ε_{cs}. This value is normally provided by the manufacturer of the member and is therefore not estimated. The effects of this deformation is considered by subtracting the shrinkage strain from the steel reinforcement and the prestressing steel strain and therefore shortening the steel parts by the same amount as the concrete.

Creep is a stress dependent deformation which is complex to model accurately when the load varies in time. This is because each load-change influences the concrete stress and therefore the resulting creep deformation. To simplify calculations it is assumed that the chosen long term loading has been constant and that the final deformation remain when the short term response of the unstrengthened and strengthened member is studied. Therefore a creep modulus of elasticity $E_{c,\varphi}$ is introduced as

$$E_{c,\varphi} = \frac{E_{cm}}{\varphi} \tag{6.2}$$

where φ is the creep coefficient of concrete. $E_{c,\varphi}$ is used to consider the creep deformation in the deflection calculations described in Section 6.1.8.

6.1.3 Stress-strain relationship for steel

According to CEN (2004), the stress-strain diagram of steel can be chosen to have either a horizontal branch or an inclined branch, see Figure 6.1.

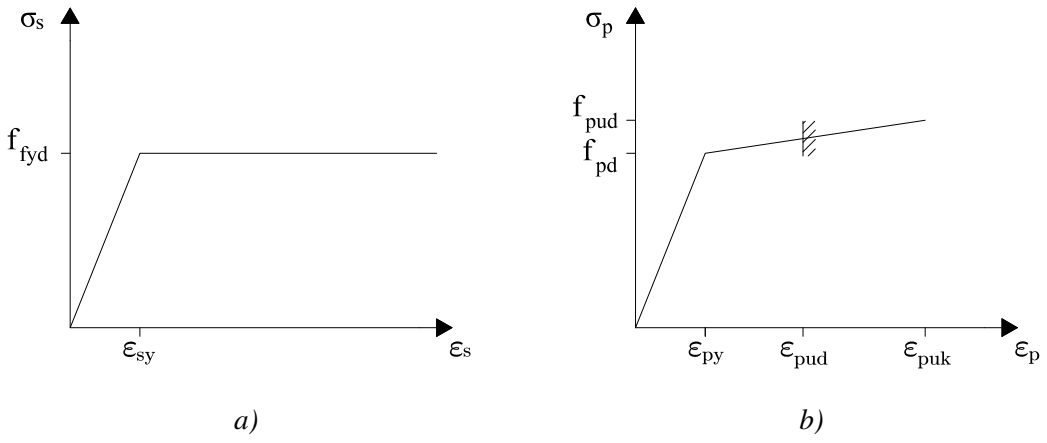

Figure 6.1 Alternative stress-strain curves for design according to CEN (2004), with a) a horizontal branch and b) an inclined branch after yielding.

The behaviour of hot rolled or heat treated steel, i.e. steel reinforcement, is best represented by Figure 6.1a) while the behaviour of cold worked steel, i.e. prestressing steel, is best represented by Figure 6.1b). The original simplified approach is therefore adjusted so that the tensile steel is described using an inclined branch which allows an initial stress

to be specified to better model the prestressing steel. The stress-strain relationship for the steel reinforcement is thus described as

$$\sigma_{\mathrm{s}}\left(\varepsilon_{\mathrm{s}}\right)=\begin{cases} E_{\mathrm{s}}\cdot\varepsilon_{\mathrm{s}}, & \varepsilon_{\mathrm{s}}<\varepsilon_{\mathrm{sy}} \\ f_{\mathrm{yd}}, & \varepsilon_{\mathrm{s}}\geq\varepsilon_{\mathrm{sy}} \end{cases} \tag{6.3}$$

and for the prestressing steel as

$$\sigma_{\mathrm{p}}\left(\varepsilon_{\mathrm{p}}\right)=\begin{cases} E_{\mathrm{p}}\cdot\varepsilon_{\mathrm{p}}, & \varepsilon_{\mathrm{p}}<\varepsilon_{\mathrm{py}} \\ f_{\mathrm{pd}}+\frac{f_{\mathrm{pud}}-f_{\mathrm{pd}}}{\varepsilon_{\mathrm{puk}}-\varepsilon_{\mathrm{py}}}\cdot\left(\varepsilon_{\mathrm{p}}-\varepsilon_{\mathrm{py}}\right), & \varepsilon_{\mathrm{sy}}<\varepsilon_{\mathrm{p}}\leq\varepsilon_{\mathrm{pud}} \end{cases} \tag{6.4}$$

6.1.4 Effects of a non-rectangular cross-section

When studying non-rectangular cross-sections, such as double-T slabs, the neutral axis can be positioned in such a way that a simplified compressive block cannot be used due to a resulting non-rectangular compressive zone. For double-T slabs, this occur when the neutral axis is positioned in the web but it is normally not the case for prefabricated members. However, when a member is strengthened the added compressive force applied near the tensile edge will shift the neutral axis downwards in order to keep equilibrium and may fall within the web. Furthermore, when studying numerous states prior to failure the location of the neutral axis will most likely at some point be positioned so that a non-rectangular compressive zone is obtained.

Engström (2015) describes an iterative method for handling a non-rectangular compressive zone. By guessing the location of the neutral axis, dividing the compressive zone into smaller segments and summing the contribution from each segment to the horizontal equilibrium the correct position of the neutral axis can be determined. The approach is a simplification of the general approach where the concretes force contribution is calculated as

$$F_{\mathrm{c}}=\int\sigma_{\mathrm{c}}\left(\varepsilon_{\mathrm{c}}(z)\right)\cdot b(z)\,dz \tag{6.5}$$

which can be used in computer software, such as Mathcad, to obtain more accurate results. Here, $\sigma_{\mathrm{c}}(\varepsilon_{\mathrm{s}})$ is the stress-strain relationship for concrete, $\varepsilon_{\mathrm{c}}(z)$ is the strain distribution for the cross-section, z is the distance from the top concrete fibre and $b(z)$ is the width in section z. The integral should only be evaluated over the height of the concrete which is active, i.e. for uncracked sections where $-\varepsilon_{\mathrm{cu}}\leq\varepsilon_{\mathrm{c}}\leq\varepsilon_{\mathrm{ct}}$ and for cracked sections where $-\varepsilon_{\mathrm{cu}}\leq\varepsilon_{\mathrm{c}}\leq 0$. The integration over the area of the cross-section is illustrated in Figure 6.2.

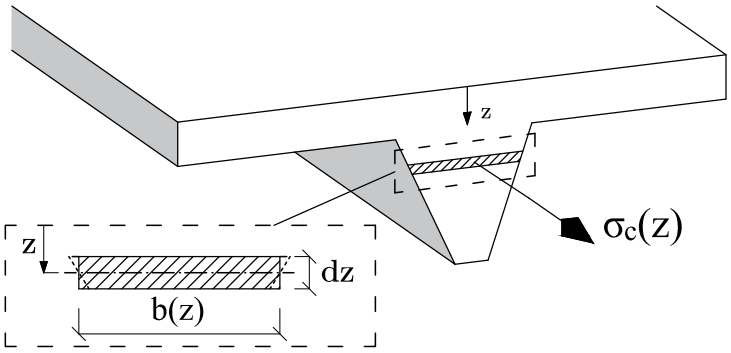

Figure 6.2 Integration over the area of the cross-section.

According to CEN (2004), the stress-strain relationship for concrete can be taken as

$$\sigma_c(\varepsilon_c) = \begin{cases} f_{cd} \cdot \left[1 - \left(1 - \frac{\varepsilon_c}{\varepsilon_{c2}}\right)^n\right], & 0 \leq \varepsilon_c < \varepsilon_{c2} \\ f_{cd}, & \varepsilon_{c2} \leq \varepsilon_{\mathbf{c}} \leq \varepsilon_{cu2} \end{cases} \tag{6.6}$$

where $n = 2$ and $\varepsilon_{c2} = 2‰$ for $f_{ck} \leq 50$ MPa. By using the generalised approach, i.e. based on Equation (6.5), the neutral axis can be determined directly from the horizontal equilibrium equation. When the position is known, the concretes contribution to the moment resistance can be determined using

$$M_c = \int \sigma_c(\varepsilon_c(z)) \cdot b(z) \cdot z \, dz \tag{6.7}$$

which is evaluated over the same height as when the horizontal equilibrium was obtained.

6.1.5 Shear and peeling stresses

The prestressing introduced into the CFRP and the load applied after strengthening result in interfacial shear and peeling stresses in the adhesive layer. These form principal stresses which could exceed the tensile strength of the concrete and lead to cover separation. The maximum shear stress in the adhesive is calculated by superposition of the results obtained from two different equations, where the contribution from the prestressing force and external loading after CFRP application is taken into account. However, even moderate levels of prestressing result in high interfacial stresses which require mechanical anchorage or a gradual introduction of the prestressing to avoid concrete separation.

6.1.6 Prestressed concrete, PC

To evaluate the effectiveness of the strengthening the unstrengthened member is assessed in a number of states, i.e. initial camber, prior to CFRP application, cracking, yielding and failure. The latter may either be due to concrete crushing or rupture of the prestressing steel. Based on the known information in each state, two generalised scenarios can be identified.

Scenario 1. Assume that the concrete strain ε_{cz} at a distance d_z [m] from the top is known,

see Figure 6.3a). The strain in the top concrete fibre ε_{cc}^{i} can then be expressed as

$$\varepsilon_{cc}^{i}(x^{i}) = \varepsilon_{cz} + \frac{0 - \varepsilon_{cz}}{d_z - x^{i}} \cdot d_z = \varepsilon_{cz} \cdot \left(1 - \frac{d_z}{d_z - x^{i}}\right) \tag{6.8}$$

where x^{i} [m] is the location of the neutral layer and i denotes the studied state. The strain distribution, see Figure 6.3b), can then be expressed as

$$\varepsilon_{c}^{i}(z, x^{i}) = \varepsilon_{cc}^{i}(x^{i}) + \frac{\varepsilon_{cz} - \varepsilon_{cc}^{i}(x^{i})}{d_z} \cdot z \tag{6.9}$$

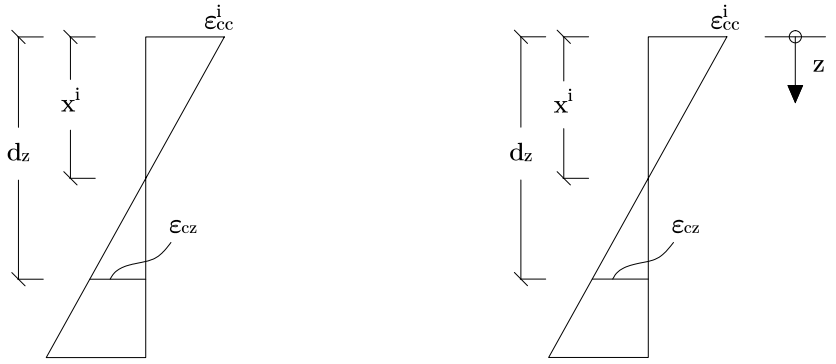

Figure 6.3 Illustration of strain relationships to determine a) the top concrete fibre and b) the strain distribution.

Subsequently, the strain in the steel reinforcement and prestressing steel becomes $\varepsilon_{s}^{i}(x^{i}) = \varepsilon_{c}^{i}(d_s, x^{i}) - \varepsilon_{cs}$ and $\varepsilon_{p}^{i}(x^{i}) = \varepsilon_{p0\infty} - \varepsilon_{cs} + \varepsilon_{c}^{i}(d_p, x^{i})$, respectively. Since Equation (6.9) only contain one unknown, horizontal equilibrium can be used to determine the strain distribution, i.e. by using iteration solve when

$$\sum F = 0 \tag{6.10}$$

The external moment M^{i} [Nm] needed to counteract the moment caused by the internal forces is then obtained from moment equilibrium.

Scenario 2. Assume that the external moment M^{i} is known. The strain distribution described by Equation (6.9) then becomes a function of two unknown variables, x^{i} and ε_{cz}, and where ε_{cc}^{i} becomes a function of the two unknowns, i.e.

$$\varepsilon_{c}^{i}(z, x^{i}, \varepsilon_{cz}) = \varepsilon_{cc}^{i}(x^{i}, \varepsilon_{cz}) + \frac{\varepsilon_{cz} - \varepsilon_{cc}^{i}(x^{i}, \varepsilon_{cz})}{d_z} \cdot z \tag{6.11}$$

Subsequently, the strain in the steel reinforcement and prestressing steel is expressed as $\varepsilon_{s}^{i}(x^{i}, \varepsilon_{cz}) = \varepsilon_{c}^{i}(d_s, x^{i}, \varepsilon_{cz}) - \varepsilon_{cs}$ and $\varepsilon_{p}^{i}(x^{i}, \varepsilon_{cz}) = \varepsilon_{p0\infty} - \varepsilon_{cs} + \varepsilon_{c}^{i}(d_p, x^{i}, \varepsilon_{cz})$, respectively. In order to determine the two unknowns in Equation (6.11) both horizontal and moment equilibrium must be used.

At initial camber and prior to CFRP application, the external moment is known which

allows the strain distribution to be determined using Scenario 2. For cracking, yielding and failure the concrete strain is known in a certain location in the strain distribution and is therefore solved using Scenario 1. In the latter states, the external moment is used to determine a corresponding uniformly distributed load q^{i} [N/m], which is calculated according to

$$q^{\mathrm{i}} = \frac{8 \cdot M^{\mathrm{i}}}{l_0^2} \tag{6.12}$$

where l_0 is the length of the span. The conditions used to determine the strain distribution for the different states are listed in Table 6.2.

Table 6.2 List of known strain or moment used in each state to determine the strain distribution for the unstrengthened prestressed reinforced concrete member.

State (notation, i)	$\varepsilon_{\mathrm{cz}}$	d_{z}	M^{i}
Initial camber (ci)	-	-	0
Prior to CFRP application (pca)	-	-	Any
Cracking (cr)	$\frac{f_{\mathrm{ctk0,05}}}{E_{\mathrm{cm}}}$	h	-
Yielding (y)	$\varepsilon_{\mathrm{py}} - \varepsilon_{\mathrm{p0}\infty}$	d_{p}	-
Concrete failure (u,cc)	$-\varepsilon_{\mathrm{cu}}$	0	-
Rupture of prestressing steel (u,rp)	$\varepsilon_{\mathrm{pud}} - \varepsilon_{\mathrm{p0}\infty}$	d_{p}	-

- $\varepsilon_{\mathrm{cz}}$, d_{z} and M^{i} are input variables for Equation (6.8), (6.9) and (6.11).
- $f_{\mathrm{ctk0,05}}$ [Pa] is the lower characteristic tensile strength of concrete.
- E_{cm} [Pa] is the mean modulus of elasticity of concrete.
- h [m]is the total height of the member.
- d_{p} [m] is the distance from the top concrete fibre to the prestressing steel.
- $\varepsilon_{\mathrm{py}}$ [-] is the yield strain of the prestressing steel.
- $\varepsilon_{\mathrm{p0}\infty}$ [-] is the prestrain the prestressing steel after long time.
- $\varepsilon_{\mathrm{pud}}$ [-] is the design ultimate strain of the prestressing steel.
- $\varepsilon_{\mathrm{cu}}$ [-] is the ultimate compressive strain of the concrete.

The governing failure mode depends on if the cross-section is under- or over-reinforced. This is determined by calculating the critical prestressing steel area which result in simultaneous concrete crushing and rupture of the prestressing steel. Thus, the strain in the top concrete fibre is

$$\varepsilon_{\mathrm{cc}}^{\mathrm{crit}} = -\varepsilon_{\mathrm{cu}} \tag{6.13}$$

and the concrete strain at the level of the prestressing steel is

$$\varepsilon_{\mathrm{cp}}^{\mathrm{crit}} = \varepsilon_{\mathrm{pud}} - \varepsilon_{\mathrm{p0}\infty} - \varepsilon_{\mathrm{cs}} \tag{6.14}$$

resulting in a concrete strain distribution according to

$$\varepsilon_{\mathrm{c}}^{\mathrm{crit}}(z) = \varepsilon_{\mathrm{cc}}^{\mathrm{crit}} + \frac{\varepsilon_{\mathrm{cp}}^{\mathrm{crit}} - \varepsilon_{\mathrm{cc}}^{\mathrm{crit}}}{d_{\mathrm{p}}} \cdot z \tag{6.15}$$

from which the strain in the steel reinforcement is determined as $\varepsilon_{\mathrm{s}}^{\mathrm{crit}} = \varepsilon_{\mathrm{c}}^{\mathrm{crit}}(d_{\mathrm{s}}) - \varepsilon_{\mathrm{cs}}$ and the location of the neutral axis x^{crit} is solved. In the horizontal equilibrium equation the only unknown is the critical prestressing steel area $A_{\mathrm{p}}^{\mathrm{crit}}$. Concrete crushing occur if the prestressing steel area A_{p} exceeds $A_{\mathrm{p}}^{\mathrm{crit}}$, i.e. the cross-section is over-reinforced, otherwise rupture of the prestressing steel governs the failure and the cross-section is said to be under-reinforced.

From the strain distribution, the curvature at each state is calculated as

$$\kappa^{\mathrm{i}} = \frac{\varepsilon_{\mathrm{cp}}^{\mathrm{i}} - \varepsilon_{\mathrm{cc}}^{\mathrm{i}}}{d_{\mathrm{p}}} \tag{6.16}$$

where $\varepsilon_{\mathrm{cp}}^{\mathrm{i}}$ is the concrete strain at the level of the prestressing steel and $\varepsilon_{\mathrm{cc}}^{\mathrm{i}}$ is the strain in the top concrete fibre.

6.1.7 CFRP strengthened prestressed concrete, SPC

The approach described in Section 6.1.6 is extended to also describe the states involving the strengthened member, i.e. after CFRP application and the strengthened cracking, yielding and failure states. Since the ultimate strain of prestressing steel greatly exceed that of CFRP laminate, rupture of the prestressing steel is no longer a plausible failure mode and is disregarded – instead concrete crushing and rupture of the CFRP laminate may govern the members ultimate capacity.

For the state after CFRP application the external moment is known and equal to the external moment prior to CFRP application, i.e. the state can be calculated according to Scenario 2. Similarly as for the unstrengthened member the concrete strain is known in a certain point of the strain distribution for the cracking, yielding and failure states and is therefore handled according to Scenario 1.

When the CFRP is applied to the concrete a strain difference is introduced between the concrete and the CFRP. When the strengthened member is loaded this difference is influenced by the shearing of the adhesive, see Figure 6.4.

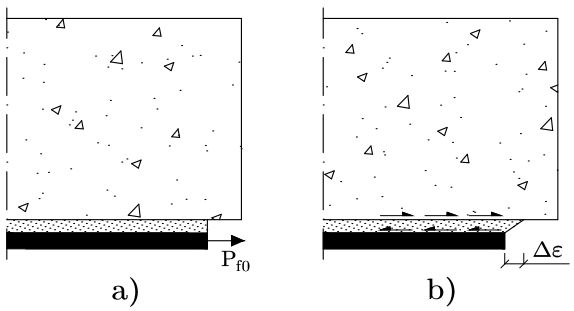

Figure 6.4 The change in strain difference $\Delta\varepsilon$ between concrete and the CFRP laminate a) before and b) after the prestressing P_{f0} is applied.

However, to simplify the calculations this effect is neglected and strain compatibility is assumed between the CFRP and the concrete. From this assumption the strain in the concrete on the level of the CFRP ε_{cf}^{pca} becomes the strain for which the prestressing force in the CFRP is known. This is equivalent to P_{0i} in prestressed concrete. Contrary to prestressed concrete, the strain value is most often non-zero and therefore must be accounted for in the different states. Two situations can occur, where either the total CFRP strain ε_f^i is known and the concrete strain at the level of the CFRP ε_{cf}^i is sought – or vice versa. The relationship can be derived from Figure 6.5 and becomes

$$\varepsilon_f^i = \varepsilon_{f0} + \varepsilon_{cf}^i - \varepsilon_{cf}^{pca} \tag{6.17}$$

or

$$\varepsilon_{cf}^i = \varepsilon_f^i - \varepsilon_{f0} + \varepsilon_{cf}^{pca} \tag{6.18}$$

where ε_{f0} is the prestrain of the CFRP.

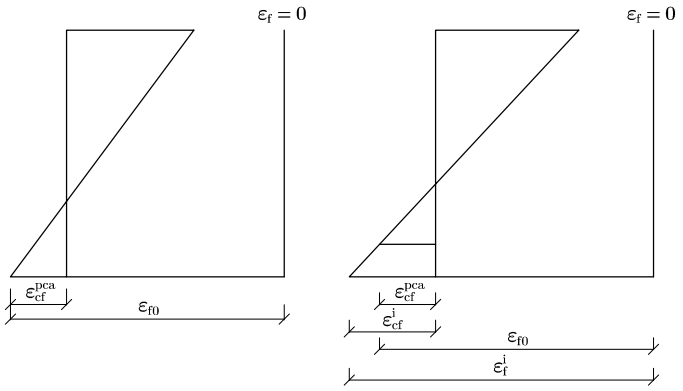

Figure 6.5 Strain difference relationship between the concrete and the CFRP laminate.

The conditions used to determine the strain distribution for the different states are listed in Table 6.3.

Table 6.3 List of known strain or moment used in each state to determine the strain distribution for the CFRP strengthened prestressed reinforced concrete member.

State (notation, i)	ε_{cz}	d_z	M^i
After CFRP application (aca)	-	-	M^{pca}
Cracking (cr)	$\frac{f_{ctk0,05}}{E_{cm}}$	h	-
Yielding (y)	$\varepsilon_{py} - \varepsilon_{p0\infty}$	d_p	-
Concrete failure (u,cc)	$-\varepsilon_{cu}$	0	-
Rupture of CFRP laminate (u,rc)	$\varepsilon_{fud} - \varepsilon_{f0} + \varepsilon_{cf}^{pca}$	d_f	-

- ε_{cz}, d_z and M^i are input variables for Equation (6.8), (6.9) and (6.11).
- M^{pca} [Nm] is the moment applied prior to CFRP application
- $f_{ctk0,05}$ [Pa] is the lower characteristic tensile strength of concrete.
- E_{cm} [Pa] is the mean modulus of elasticity of concrete.
- h [m] is the total height of the member.
- d_p [m] is the distance from the top concrete fibre to the prestressing steel.
- d_f [m] is the distance from the top concrete fibre to the CFRP laminate.
- ε_{py} [-] is the yield strain of the prestressing steel.
- $\varepsilon_{p0\infty}$ [-] is the prestrain the prestressing steel after long time.
- ε_{fud} [-] is the ultimate strain of the CFRP laminate.
- ε_{f0} [-] is the prestrain applied to the CFRP laminate.
- ε_{cu} [-] is the ultimate compressive strain of the concrete.

After CFRP application the compressive stress in the top concrete fibre σ_{cc}^{aca} may be reduced so that tensile stresses appear. For double-T slabs with thin flanges, the deck may crack during strengthening and thus lead to a reduction of the stiffness. Of this reason, the stress is limited to

$$\sigma_{cc}^{aca} \leq 0 \tag{6.19}$$

The governing failure mode depend on if the cross-section is under- or over-reinforced. This is determined by calculating the critical CFRP laminate area which results in simultaneous concrete crushing and rupture of the CFRP laminate. Thus, according to Table 6.3 the strain in the top concrete fibre is

$$\varepsilon_{cc}^{crit} = -\varepsilon_{cu} \tag{6.20}$$

and the concrete strain at the level of the CFRP laminate is

$$\varepsilon_{cf}^{crit} = \varepsilon_{fud} - \varepsilon_{f0} + \varepsilon_{cf}^{pca} \tag{6.21}$$

The concrete strain distribution is obtained as

$$\varepsilon_c^{crit}(z) = \varepsilon_{cc}^{crit} + \frac{\varepsilon_{cf}^{crit} - \varepsilon_{cc}^{crit}}{d_f} \tag{6.22}$$

from which the strain in the steel reinforcement and the prestressing steel is determined as $\varepsilon_s^{crit} = \varepsilon_c^{crit}(d_s) - \varepsilon_{cs}$ and $\varepsilon_p^{crit} = \varepsilon_{p0\infty} - \varepsilon_{cs} + \varepsilon_c^{crit}(d_p)$, respectively. Since the location of the neutral axis x^{crit} also can be solved from the concrete strain distribution, the only

unknown in the horizontal equilibrium equation is the critical CFRP laminate area $A_{\mathrm{f}}^{\mathrm{crit}}$, which can thus be determined. Concrete crushing occur if the CFRP laminate area A_{f} exceeds $A_{\mathrm{f}}^{\mathrm{crit}}$, i.e. the cross-section is over-reinforced, otherwise rupture of the CFRP laminate governs the failure and the cross-section is said to be under-reinforced.

To establish the complete moment-curvature relationship and since the behaviour up to cracking is linear, a fictitious initial camber is calculated by interpolating the results obtained for after CFRP application and cracking.

Similarly to the unstrengthened member, the cracking, yielding and failure load is calculated according to Equation (6.12) and corresponding curvature according to Equation (6.16).

6.1.8 Deflection

The general formulation of global deformations described in Engström (2015) is used to estimate the deflections up to the cracking load. Since the material has a linear elastic response until cracking the flexural rigidity EI is assumed to be constant along the member and the curvature distribution $\kappa(x)$ is expressed as

$$\kappa(x) = \frac{M(x)}{EI} \tag{6.23}$$

where $M(x)$ is the moment distribution for the studied load, E is the long term or short term modulus of elasticity and I is the moment of inertia of the transformed concrete section. The moment distribution of a uniformly distributed load q is described as

$$M_{\mathrm{q}}(x) = \frac{q \cdot x \cdot (l_0 - x)}{2} \tag{6.24}$$

and for an axial force P acting with an eccentricity e as

$$M_{\mathrm{P}} = P \cdot e \tag{6.25}$$

The acting loads considered are presented in Table 6.4 together with the used moment distribution, modulus of elasticity and moment of inertia.

Table 6.4 Loads and corresponding moment distribution, modulus of elasticity and moment of inertia used when calculating deflection. The long term load refers to the estimated load which has been applied on the member during it's current life span, prior to CFRP application.

Load	Moment distribution	Modulus of elasticity	Moment of inertia
Loag term load	$M_{\mathrm{q}}(x, q_{\mathrm{l}})$	$E_{\mathrm{c},\varphi}$	$I_{\mathrm{I,ef}}^{\mathrm{pc}}$
Shrinkage force	$F_{\mathrm{cs,s}} \cdot e_{\mathrm{s}}$	$E_{\mathrm{c,ef}}$	$I_{\mathrm{I,ef}}^{\mathrm{pc}}$
Prior to CFRP application	$M_{\mathrm{q}}(x, q^{\mathrm{pca}})$	E_{cm}	$I_{\mathrm{I,ef}}^{\mathrm{pc}}$
Cracking load			
Unstrengthened, PC	$M_{\mathrm{q}}(x, q^{\mathrm{cr}})$	E_{cm}	$I_{\mathrm{I,ef}}^{\mathrm{pc}}$
Strengthened, SPC			$I_{\mathrm{I,ef}}^{\mathrm{spc}}$
Prestressing force			
Steel	$(P_{0\infty} - F_{\mathrm{cs,p}}) \cdot e_{\mathrm{p}}$	$E_{\mathrm{c,ef}}$	$I_{\mathrm{I,ef}}^{\mathrm{pc}}$
CFRP laminate	$P_{\mathrm{f0}} \cdot e_{\mathrm{f}}$	E_{cm}	$I_{\mathrm{I,ef}}^{\mathrm{spc}}$

The deflection δ is obtained by considering the change of slope along the beam according to Figure 6.6 which can be expressed as

$$\delta(x_1) = \theta_{\mathrm{A}} \cdot x_1 - \int_0^{x_1} \kappa(x)(x_1 - x)\, dx \tag{6.26}$$

where θ_{A} is the adjacent support rotation and x_1 is the studied section.

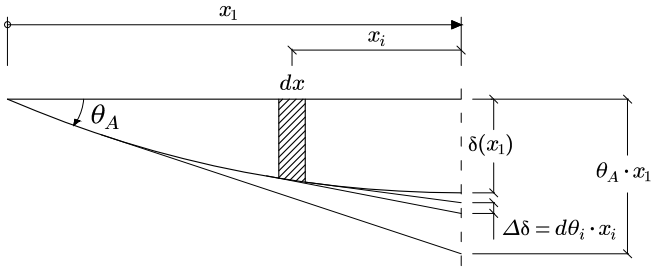

Figure 6.6 Calculation of the deflection in section x_1 considering the adjacent support rotation and the continuous change of slope along the beam.

For a simply supported span the support rotation is determined by

$$\theta_{\mathrm{A}} = \int_0^{\frac{l_0}{2}} \kappa(x)\, dx \tag{6.27}$$

The deflection from each load acting in the studied state is calculated from Equation (6.26) and summarised in order to obtain the total deflection. The contributions included in each state is shown in Table 6.5.

Table 6.5 Deflection contributions included when calculating the total deflection in each studied state.

Load	Prior to CFRP application	After CFRP application	Cracking	
			PC	SPC
Long term load	☒	☒	☒	☒
Shrinkage force	☒	☒	☒	☒
Load prior to CFRP application	☒	☒	☐	☐
Cracking load				
Unstrengthened	☐	☐	☒	☐
Strengthened	☐	☐	☐	☒
Prestressing force				
Steel	☒	☒	☒	☒
CFRP	☐	☒	☐	☒

6.2 Verification

To validate the analytical approach the short term results obtained for an unstrengthened rectangular cross-section is compared with the results obtained from StruSoft PRE-Stress version 6.5.005. The comparison was conducted on a beam provided by COWI AB which was designed for another project. The geometry of the beam is shown in Figure 6.7.

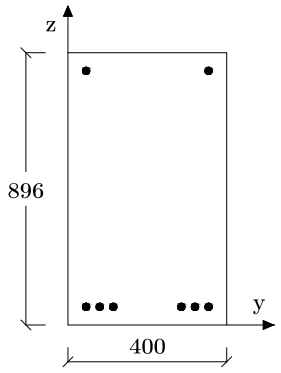

Figure 6.7 Geometry of rectangular cross-section used for unstrengthened verification.

The geometry parameters are implemented to work for a double-T slab and in order to describe a rectangular cross-section the parameters listed in Table 6.6 are used.

Table 6.6 Geometry settings used to describe the rectangular cross-section used for verification.

Parameter	Value [mm]
Total height, h	896
Flange thickness, t_{f}	100
Flange width, b_{f}	400
Web top width, $b_{\mathrm{w,t}}$	400
Web bottom width, $b_{\mathrm{w,b}}$	400
Web height, h_{w}	796

The material properties used in PRE-Stress are, when available, translated to the corresponding parameter in the approach which all are presented in Appendix A. The results obtained from PRE-Stress and the analytical approach are compared in Table 6.7.

Table 6.7 Comparison between the cracking and failure moment [kNm] obtained from the analytical approach and StruSoft PRE-Stress.

Moment	PRE-Stress	Analytical approach	Difference
M^{cr}	623.5	601.8	3.61%
M^{u}	776.5	776.1	0.05%

The difference in results between PRE-Stress and the analytical approach are insignificant for the ultimate moment, while there is a negligible difference for the cracking moment. According to StruSoft AB (2016) the cracking moment is determined from f_{ctm}, however its value is not presented in the program. In the analytical approach, which is based on concrete strain, the cracking moment is determined when the bottom concrete fibre $\varepsilon_{\mathrm{ct}}^{\mathrm{cr}}$ reaches

$$\varepsilon_{\mathrm{ct}}^{\mathrm{cr}} = \frac{f_{\mathrm{ctm}}}{E_{\mathrm{cm}}} \tag{6.28}$$

Due to the similarity in results between the two calculations, the analytical approach is considered accurate for unstrengthened calculations. As mentioned in Chapter 1 there is no commercial software available which can help validate the results of the strengthened beam and the result is instead validated by comparing how the curvature, stresses and the position of the neutral axis change between the different studied states.

After CFRP application the eccentric compressive CFRP prestressing force should result in a reduced curvature as well as a more compressed concrete and steel compared to what is obtained prior to CFRP application. For an increasing prestressing level the reduction should increase.

For the strengthened cracking state the neutral axis is expected to move downwards and the concrete and steel reinforcement to become more compressed compared to the same unstrengthened state. This is due to the added compressive force in the lower part of the member. Both these characteristics are expected in all latter states. As the prestressing

force in the steel will be reduced by the introduction of the CFRP prestressing force it is uncertain if the expected moment increase and the change in curvature will result in a larger or smaller prestressing force in the steel in the latter states compared to the unstrengthened member.

To verify that the deformation calculation performed, the mid-span deflection for an eccentric axial force and a uniformly distributed load is compared with the deformation calculated from the corresponding elementary case, i.e. for an eccentric axial force

$$\delta_{\mathrm{P}} = \frac{Pel_0^2}{8EI} \tag{6.29}$$

and for a uniformly distributed load

$$\delta_{\mathrm{q}} = \frac{5ql_0^4}{384EI} \tag{6.30}$$

Both equations yield the exact same result as the calculation performed based on the analytical approach. This is expected since the elementary cases are derived from the general formulation used in the approach.

7 Case study and results

In the present chapter, the double-T slab included in the case study is presented and assessed. Furthermore, the results obtained by adopting the analytical approach described in Section 6.1 on a series of strengthening cases are presented and evaluated.

7.1 Case study

The double-T slabs that constitute the concrete roof of Frölunda kulturhus have different geometries and lengths. The studied member was chosen by COWI AB based on length, location and accessibility to the area above and beneath the member. Basic information on the 14.4 m long member was obtained from a data sheet provided by its manufacturer Strängbetong AB. The failure load due to bending and shear is limited to 6.5 kN/m^2 and 8.0 kN/m^2, respectively, however the cracking load is unknown. The cross-section, placement of the steel reinforcement and the prestressing steel as well as provided steel areas can be seen in Figure 7.1.

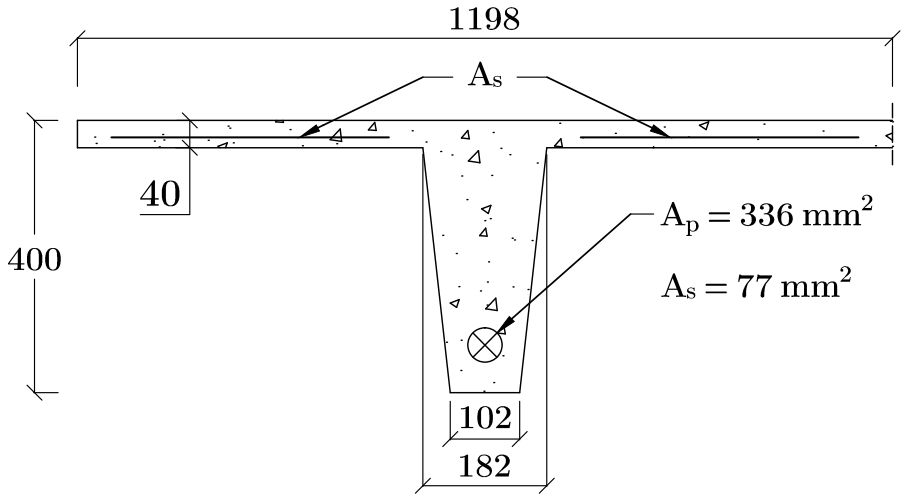

Figure 7.1 Cross-section of the studied double-T slab at Frölunda Kulturhus. Dimensions in mm.

The member was manufactured in the late 1970s when the old Swedish design code Svensk Bygg Norm 1975, SBN 75, was valid (Statens planverk, 1975) and contain concrete and steel according to old standards. The concrete is class K60 and the steel reinforcement is of type Ps50 while the prestressing steel consist of 2 mm wires with steel quality according to Swedish Standard SS1757-05. The concrete and steel reinforcement is assumed equivalent to class C50/60 and K500B, respectively. The prestressing steel was initially prestressed with 1450 MPa, which is higher than what is commonly used today. This was possible since thin wires in general have higher ultimate stress than steel strands due to its smaller diameter. Since no information on the material properties of the prestressing steel was found, it was instead approximated from a stress-strain relationship for 2.11 mm wire manufactured in accordance with the same standard, see Figure 7.2.

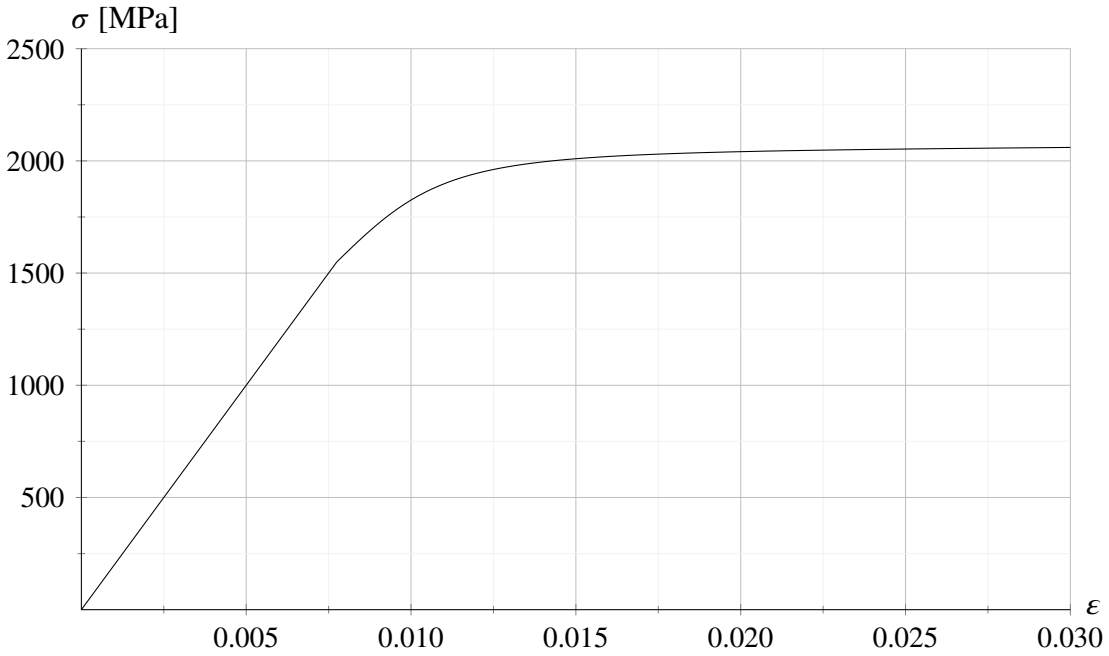

Figure 7.2 Stress-strain relationship for 2.11 mm wire.

According to Statens planverk (1969), a supplement to SBN 75, the prestressing should be limited to the lesser of 80% of $f_{\mathrm{p0,2k}}$ and 65% of f_{puk}, which for the 2 mm wire result in

$$f_{\mathrm{p0.2k}} = \frac{1450\ \mathrm{MPa}}{0.8} = 1813\ \mathrm{MPa}; \qquad f_{\mathrm{puk}} = \frac{1450\ \mathrm{MPa}}{0.65} = 2231\ \mathrm{MPa} \tag{7.1}$$

Since the 2.11 mm wire according to Figure 7.2 has an ultimate stress of 2060 MPa it is unreasonable to expect the ultimate stress to increase to 2231 MPa for such a small change in diameter. Therefore it is assumed that the prestressing was limited by $f_{\mathrm{p0,2k}}$. Furthermore, the stress-strain relationship for the 2 mm wire is assumed to have a similar shape as the relationship for the 2.11 mm wire. The known relationship is therefore used to approximate the $f_{\mathrm{p0,1k}}$- and f_{puk}-values for the 2 mm wire by using the ratio between $f_{\mathrm{p0,2k}}$, $f_{\mathrm{p0,1k}}$ and f_{puk} for the 2.11 mm wire. From Figure 7.2 the following is obtained

$$\frac{\sigma(0.02)}{\sigma(0.01)} = \frac{2041\ \mathrm{MPa}}{1825\ \mathrm{MPa}} = 1.118 \ \Rightarrow\ \frac{f_{\mathrm{p0.2k}}}{1.118} = \frac{1813\ \mathrm{MPa}}{1.118} = 1621\ \mathrm{MPa} \tag{7.2}$$

$$\frac{\sigma(0.02)}{\sigma(0.03)} = \frac{2041\ \mathrm{MPa}}{2060\ \mathrm{MPa}} = 0.991 \ \Rightarrow\ \frac{f_{\mathrm{p0.2k}}}{0.991} = \frac{1813\ \mathrm{MPa}}{0.991} = 1829\ \mathrm{MPa} \tag{7.3}$$

The 0.1%-proof stress for the 2 mm wire then become

$$f_{\mathrm{p0.1k}} = \frac{f_{\mathrm{p0.2k}}}{\gamma_{\mathrm{p}} \cdot 1.118} = \frac{1813\ \mathrm{MPa}}{1.15 \cdot 1.118} = 1410\ \mathrm{MPa} \tag{7.4}$$

where γ_{p} is the partial safety factor for prestressing steel. The calculated value is lower than the prestress given by the manufacturer and consequently cannot be accurate. On

the safe side, the 0.1%-proof stress is therefore assumed to be

$$f_{\mathrm{p0.1k}} = \sigma_{\mathrm{p0i}} \cdot \gamma_{\mathrm{p}} = 1450\ \mathrm{MPa} \cdot 1.15 = 1668\ \mathrm{MPa} \tag{7.5}$$

The characteristic ultimate stress is taken from the approximation, i.e.

$$f_{\mathrm{puk}} = 1829\ \mathrm{MPa} \tag{7.6}$$

Since the ultimate strain of the 2 mm wire is unknown, yet according to Strängbetong AB the 2 mm wire is less ductile than the 2.11 mm wire, the value is taken as 90% of the ultimate strain of the 2.11 mm wire

$$\varepsilon_{\mathrm{pud}} = 0.9 \cdot 3\% = 2.7\% \tag{7.7}$$

All these approximated values are considered to be on the safe side.

7.1.1 Strengthening cases

The studied double-T slab allows a CFRP laminate to be placed either on the bottom surface of the web or on its sides. Placement on the bottom maximises the lever arm but limits the possible laminate width to 80 mm due to the web geometry. Applying the CFRP to the sides of the web results in a reduced lever arm, however it allows wider laminates to be used as well as placing laminates on each side of the web resulting in a larger total CFRP area.

The studied strengthening cases are listed in Table 7.1, where the position and the area of the CFRP laminate as well as the applied load during strengthening varies. The latter is referred to as the state prior to CFRP application.

Table 7.1 Strengthening cases used for the case study.

Case	b_{frp}	t_{frp}	n_{f}	d_{f}	q_{l}	q^{pca}
1	80	1.4	1	400.7	4.7	3.85
2	100	1.4	2	340.0	4.7	3.85
3	120	1.4	2	330.0	4.7	3.85
4	80	1.4	1	400.7	4.7	3.07
5	100	1.4	2	340.0	4.7	3.07
6	120	1.4	2	330.0	4.7	3.07
7	80	1.4	1	400.7	4.7	2.35
8	100	1.4	2	340.0	4.7	2.35
9	120	1.4	2	330.0	4.7	2.35

- b_{frp} [m] is the width of the laminate.
- t_{frp} [m] is the thickness of the laminate.
- n_{f} [-] is the number of applied laminates.
- d_{f} [m] is the distance from the top concrete fibre to the laminate.
- q_{l} [N/m] is the long term load.
- q^{pca} [N/m] is the load prior to CFRP application.

Since the load history is unknown, the long term load is chosen close to the determined unstrengthened cracking load to include as large creep deformations as possible without cracking. The studied loads prior to CFRP application consist of two chosen loads, based on rough estimates of which load may be acting on the double-T slab during strengthening and one if only the self-weight of the double-T slab were acting. The latter one is only used to evaluate the analytical approach, as it is not feasible for a roof member.

Each case was studied up to a CFRP prestressing level of 50% of the ultimate strength, the resulting prestressing force per laminate for the used laminate widths are listed in Table 7.2.

Table 7.2 Resulting prestressing force per laminate [kN] for studied widths and prestressing levels.

	Laminate width		
Prestressing	80 mm	100 mm	120 mm
10%	27.8	34.7	41.7
20%	55.6	69.4	83.3
30%	83.3	104.2	125.0
40%	111.1	138.9	166.7
50%	138.9	173.6	208.3

Table 7.2 shows that prestressing the 80, 100 and 120 mm laminate above 40%, 30% and 20%, respectively, result in a high prestressing force which may be difficult to anchor according to the literature described in Chapter 5. In order to provide sufficient space for anchoring devices, a distance of 2 m is assumed between the support and the laminate end.

7.1.2 Evaluation criteria

The vision described in Chapter 1 results in a set of loading conditions from which the strengthening cases are evaluated. The considered loads are listed in Table 7.3.

Table 7.3 List of loads used in the load combinations for the double-T slab.

Load	Value	
Permanent		
Double-T slab	1.96	kN/m^2
Installations	0.3	kN/m^2
Insulation/membrane	0.06	kN/m^2
Protective layer[1]	0.025	kN/m^2
Sedum	0.5	kN/m^2
Soil[2]	1.6	kN/m^2
Variable		
Imposed[3]	3.0	kN/m^2
Snow[4]	1.2	kN/m^2

[1] 50 mm isodrän-board, 50 kg/m^3.

[2] 100 mm, 16 kN/m^3.

[3] Category C3.

[4] Gothenburg, $s_k = 1.5$ kN/m^2, $\mu = 0.8$.

On the basis of CEN (2002) and Boverket (2013), two load combinations are chosen to evaluate the strengthening cases. These are based on two of the additional loading scenarios which are expected if the vision is realised. The load combinations are listed in Table 7.4 and are limited to represent plantings with snow and a crowd load without snow. These are considered to be the most critical combinations, but there are additional ones which need to be considered in further design - such as crowd load with snow.

Table 7.4 Load combinations and combination factors for loads.

	Permanent load			Variable load	
Combination	*General roof components*[1]	*Sedum*	*Soil*	*Imposed*[2]	*Snow*[3]
Serviceability limit state					
SLS 1	1		1		1
SLS 2	1	1		1	
Ultimate limit state					
ULS 1: Eq 6.10a	1.35		1.35		$1.5 \cdot 0.6$
ULS 1: Eq 6.10b	1.20		1.20		1.5
ULS 2: Eq 6.10a	1.35	1.35		$1.5 \cdot 0.7$	
ULS 2: Eq 6.10b	1.20	1.20		1.5	

[1] Double-T slab, installations, insulation/membrane and protective layer.

[2] $\psi_0 = 0.7$ for ULS 6.10a.

[3] $\psi_0 = 0.6$ for ULS 6.10a.

The design load obtained from each load combination is presented in Table 7.5 and are used to evaluate the obtained cracking moment for each strengthening case.

Table 7.5 Design loads obtained from the load combinations.

	Design loads	
Combination	[kN/m^2]	[kN/m]
Serviceability limit state		
SLS 1	5.15	6.16
SLS 2	5.85	7.00
Ultimate limit state		
ULS 1: Eq 6.10a	6.41	7.67
ULS 1: Eq 6.10b*	6.53	7.83
ULS 2: Eq 6.10a	6.99	8.37
ULS 2: Eq 6.10b*	7.91	9.48

* Governing ULS design equation.

According to Chapter 5 the stress in the steel and concrete should in serviceability limit state not exceed certain values. The limits are listed in Table 7.6 and based on the material parameters presented in Appendix C.

Table 7.6 Stress limitations.

Material	Stress limit [MPa]
CFRP	2480
Concrete in compression	22.5
Steel reinforcement	400
Prestressing steel	1334

In addition, the stress in the top concrete fibre should fulfil the condition:

$$\sigma_{cc}^{aca} \leq 0 \tag{7.8}$$

after CFRP application to limit the risk of loosing stiffness. Lastly, the midspan deflection is chosen to not exceed

$$\frac{l_0}{400} = 36 \text{ mm} \tag{7.9}$$

to ensure sufficient stiffness in the strengthened double-T slab.

7.2 Results

Throughout the presented results, unstrengthened beams are denoted as PC and strengthened as SPC followed by the applied prestressing level as a percentage of the CFRP ultimate design strain. The following states are investigated; initial camber, prior to CFRP application, after CFRP application, cracking, yielding of the prestressing steel and failure. All used material properties are found in Appendix C and the raw result data in Appendix D.

7.2.1 Moment-curvature relationships

Adopting the analytical approach presented in Section 6.1 results in a series of moment-curvature relationships describing the behaviour of the beams for each strengthening case. The strengthened moment-curvature relationships are compared to the unstrengthened relationship and presented for each studied case in Figure 7.3-7.11.

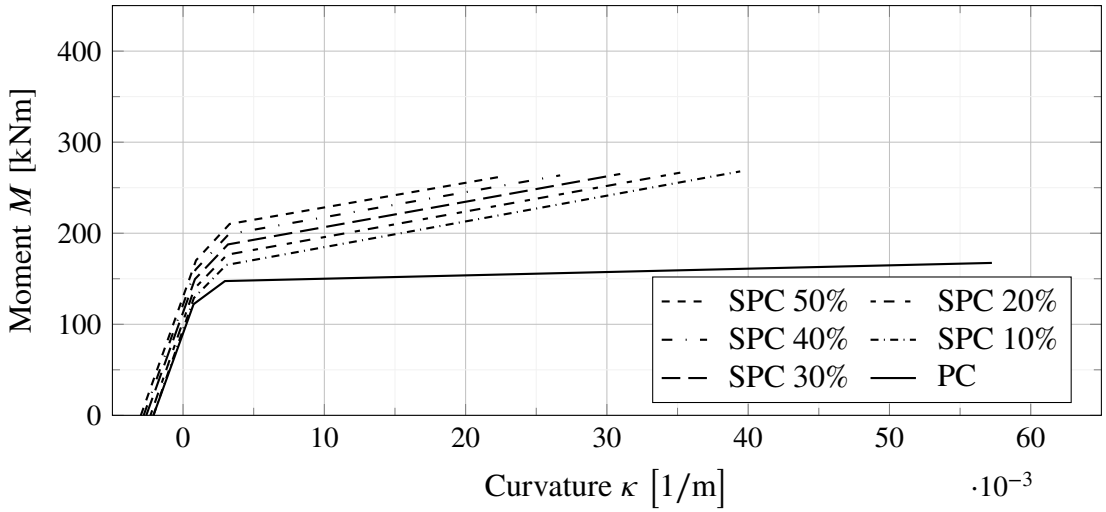

Figure 7.3 Moment-curvature relationships for various levels for CFRP prestressing according to case 1 compared with the unstrengthened double-T slab.

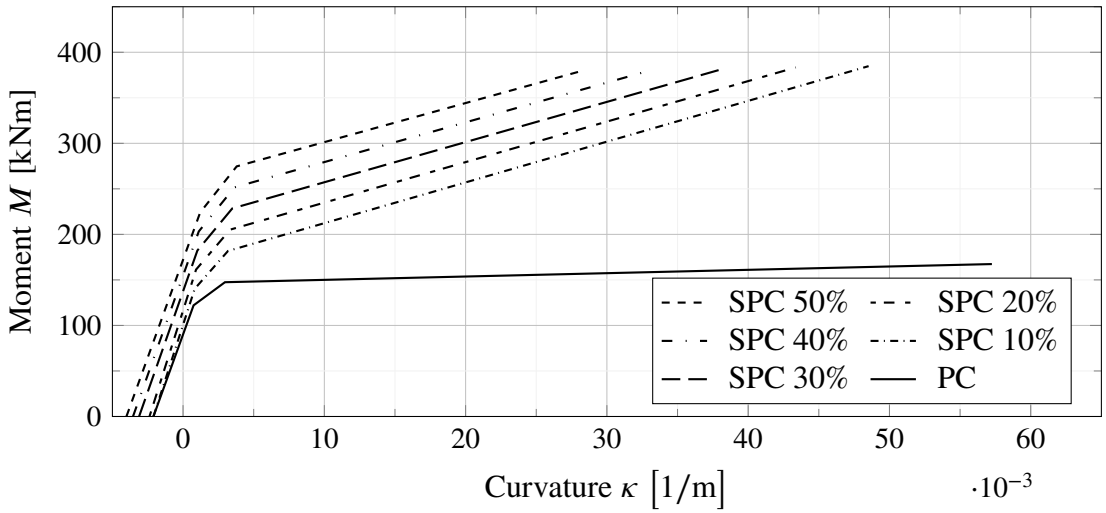

Figure 7.4 Moment-curvature relationships for various levels for CFRP prestressing according to case 2 compared with the unstrengthened double-T slab.

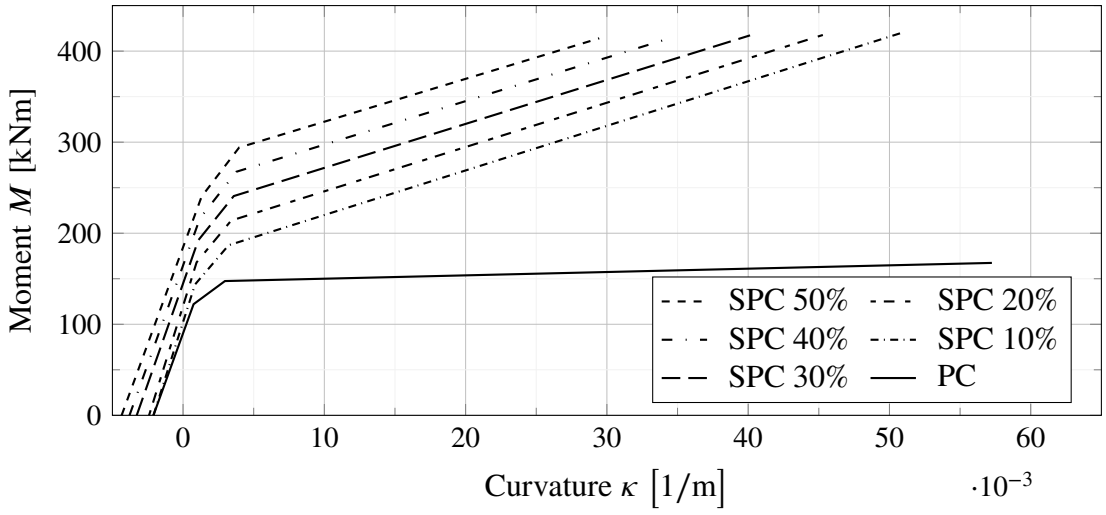

Figure 7.5 Moment-curvature relationships for various levels for CFRP prestressing according to case 3 compared with the unstrengthened double-T slab.

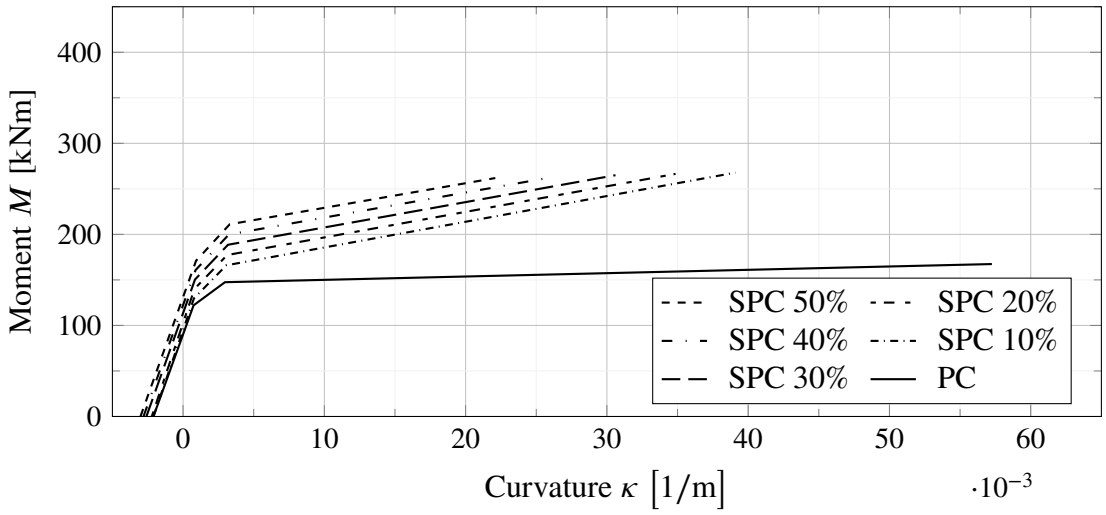

Figure 7.6 Moment-curvature relationships for various levels for CFRP prestressing according to case 4 compared with the unstrengthened double-T slab.

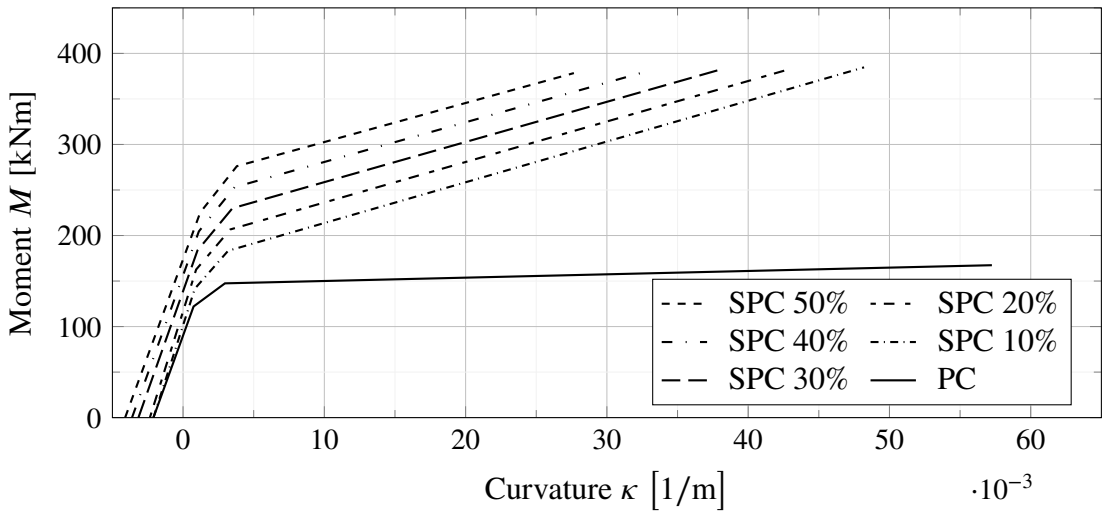

Figure 7.7 Moment-curvature relationships for various levels for CFRP prestressing according to case 5 compared with the unstrengthened double-T slab.

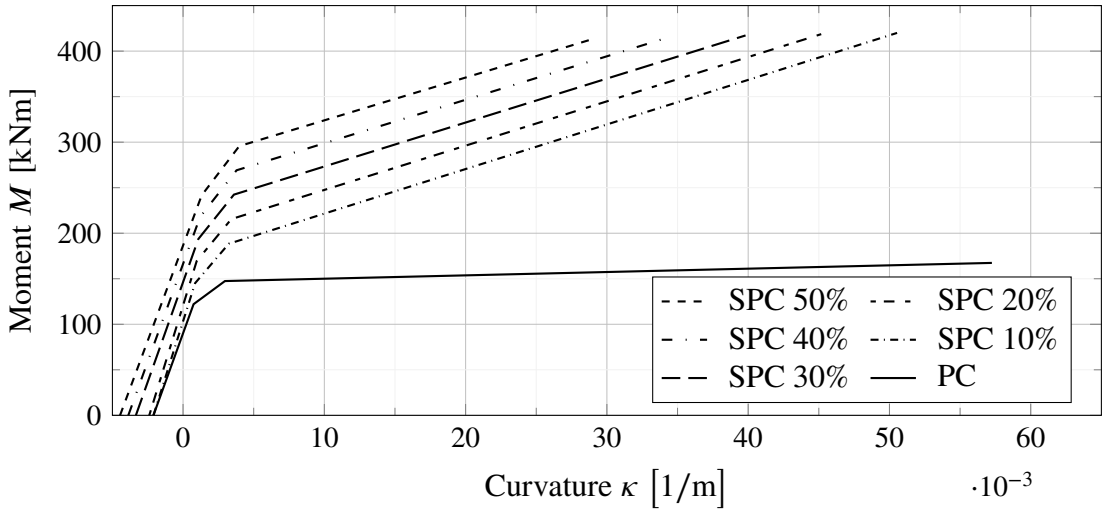

Figure 7.8 Moment-curvature relationships for various levels for CFRP prestressing according to case 6 compared with the unstrengthened double-T slab.

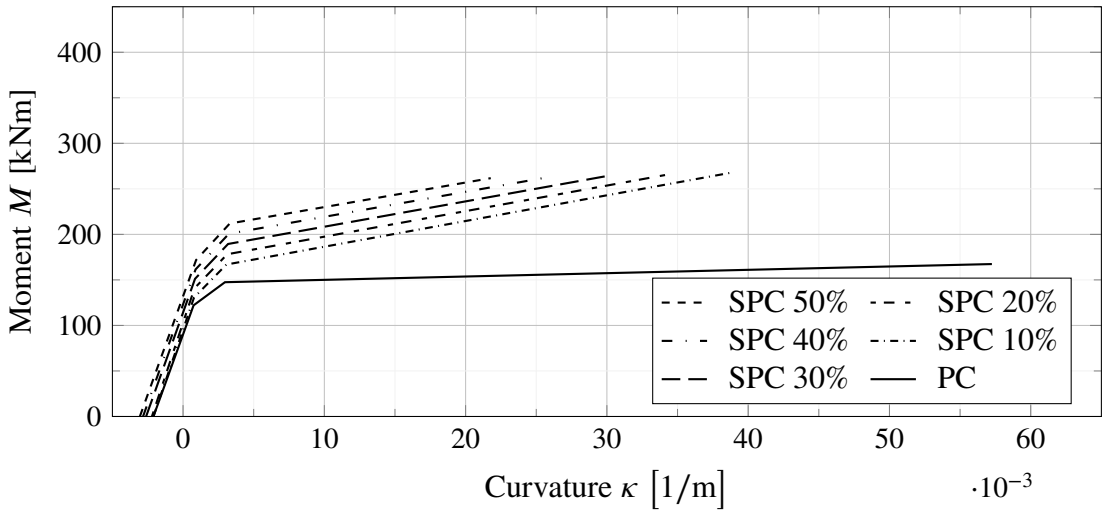

Figure 7.9 Moment-curvature relationships for various levels for CFRP prestressing according to case 7 compared with the unstrengthened double-T slab.

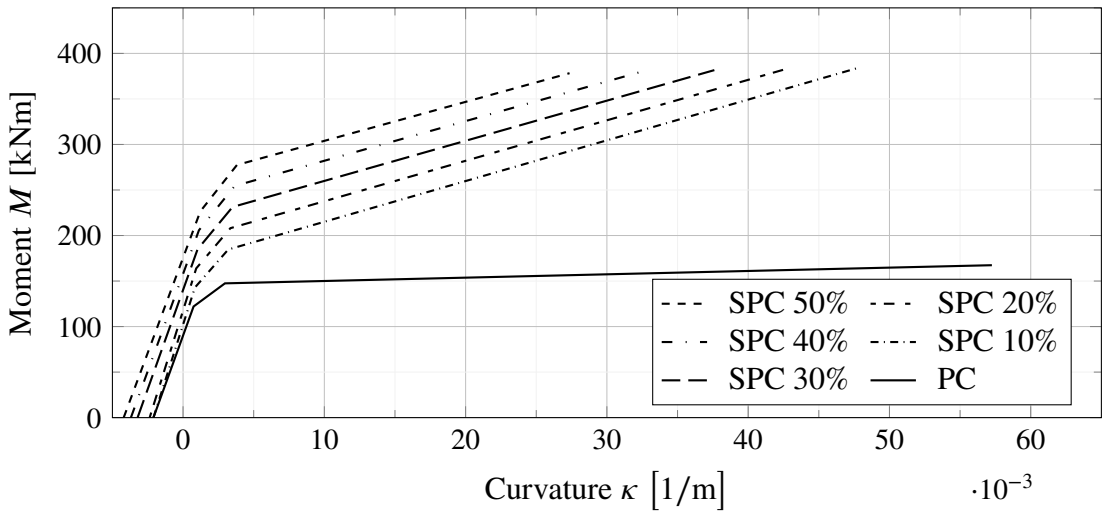

Figure 7.10 Moment-curvature relationships for various levels for CFRP prestressing according to case 8 compared with the unstrengthened double-T slab.

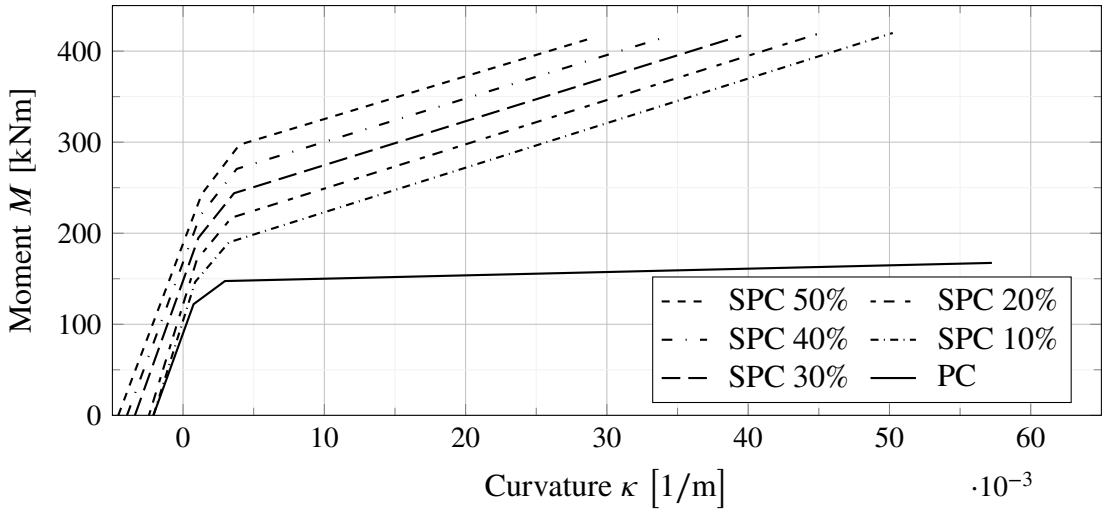

Figure 7.11 Moment-curvature relationships for various levels for CFRP prestressing according to case 9 compared with the unstrengthened double-T slab.

From the moment-curvature relationship determined for the unstrengthened double-T slab, the cracking and failure moment is calculated to 122.1 and 167.4 kNm, respectively. The failure moment is greatly underestimated as the capacity obtained from the data sheet provided by the manufacturer is 203 kNm, however this is explained by the roughly estimated material properties of the prestressing steel. The moment-curvature relationships of the studied strengthening cases are considered reasonable as all strengthened beams within a case result in about the same failure moment. Furthermore, the curvature is reduced for an increase in CFRP prestressing together with an increase in cracking and yielding moment. Since this holds irrespective of the load prior to CFRP application, only the feasible strengthening cases are studied further – i.e. strengthening case 1-6.

As CFRP rupture governs the capacity, the ductility index described in Section 4.2.2 is calculated and presented for each studied case in Table 7.7.

Table 7.7 Ductility index for the studied strengthening cases.

Beam type	Case 1	Case 2	Case 3	Case 4	Case 5	Case 6
SPC 10%	12.9	15.2	15.8	12.8	15.1	15.6
SPC 20%	11.3	13	13.4	11.2	12.9	13.2
SPC 30%	9.7	11	11.2	9.6	10.8	11.1
SPC 40%	8.2	9.1	9.2	8.1	9	9.1
SPC 50%	6.8	7.4	7.4	6.7	7.3	7.3

As Table 7.7 shows, all strengthening cases and studied levels of prestressing are well above the recommended minimum ductility index of 2.6 - which ensures that the strengthened member has adequate ductility.

7.2.2 Stress distribution

Each studied strengthening case results in a unique stress distribution in each studied state and the stress in the top concrete fibre, the steel reinforcement, the prestressing steel

and the CFRP laminate for all studied cases can be found in Appendix D. The tendencies illustrated by Figure 7.12 and 7.13 are similar for all studied cases and prestressing levels.

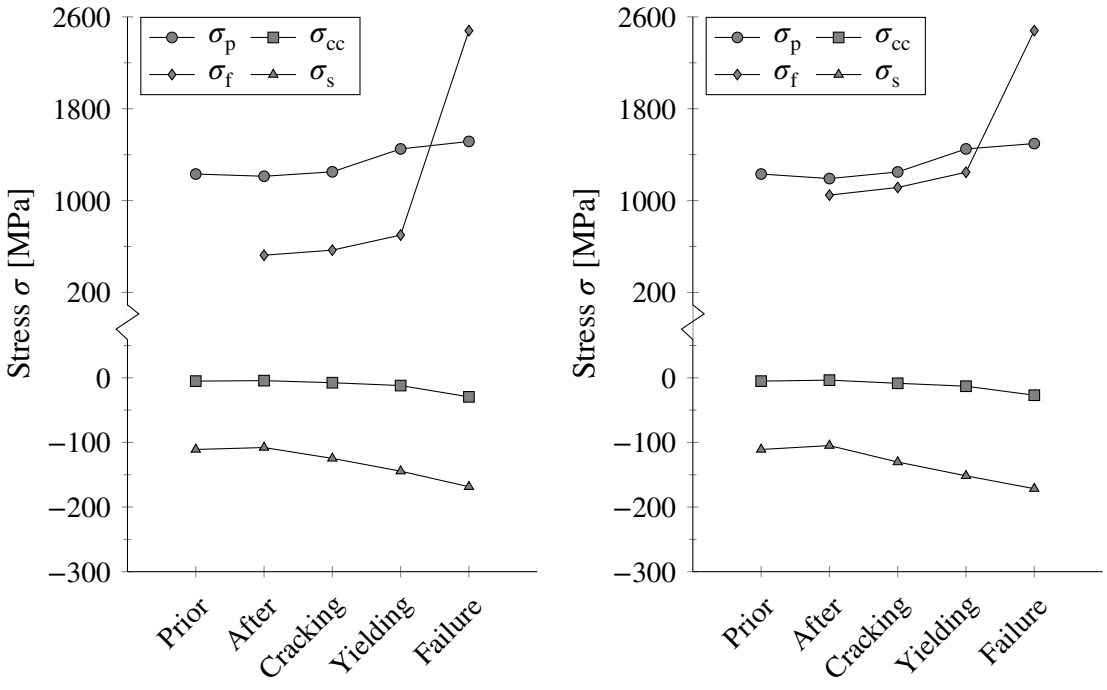

a) Case 1, 20% CFRP prestressing. *b) Case 1, 40% CFRP prestressing.*

Figure 7.12 Stress change in the CFRP laminate, prestressing steel, top concrete fibre and steel reinforcement from prior to CFRP application to failure

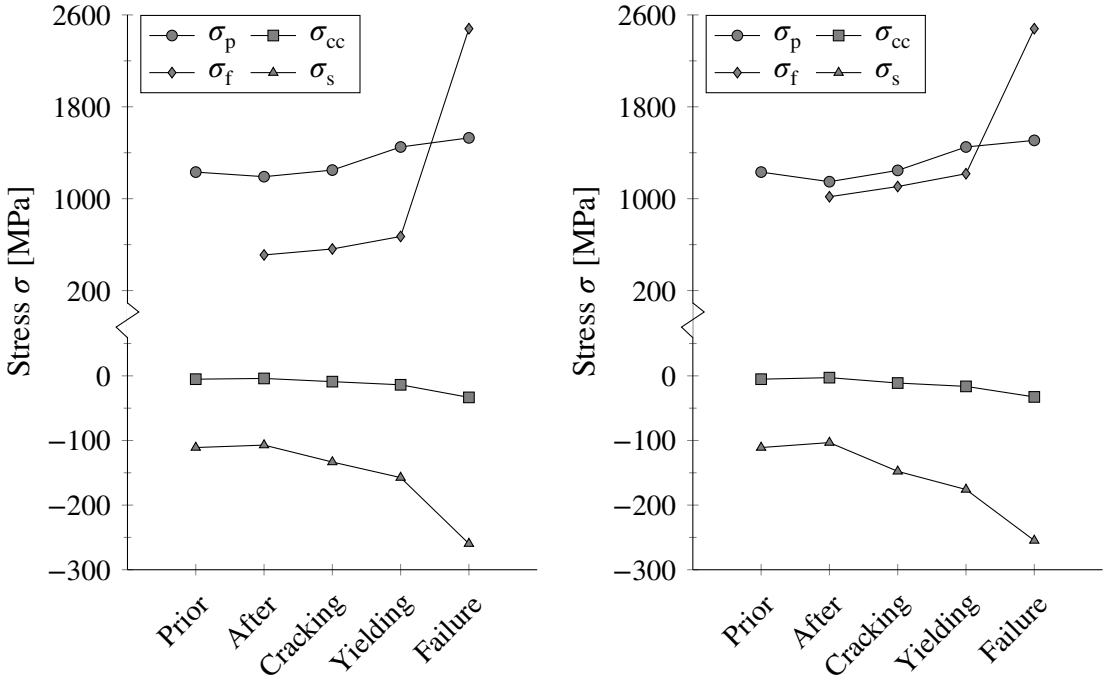

a) Case 2, 20% CFRP prestressing. *b) Case 2, 40% CFRP prestressing.*

Figure 7.13 Stress change in the CFRP laminate, prestressing steel, top concrete fibre and steel reinforcement from prior to CFRP application to failure.

Both Figure 7.12 and 7.13 shows that the stresses develop as expected and is well below the stress limits listed in Table 7.6. Figure 7.14 show a comparison of the steel reinforcement stresses at failure for the same cases.

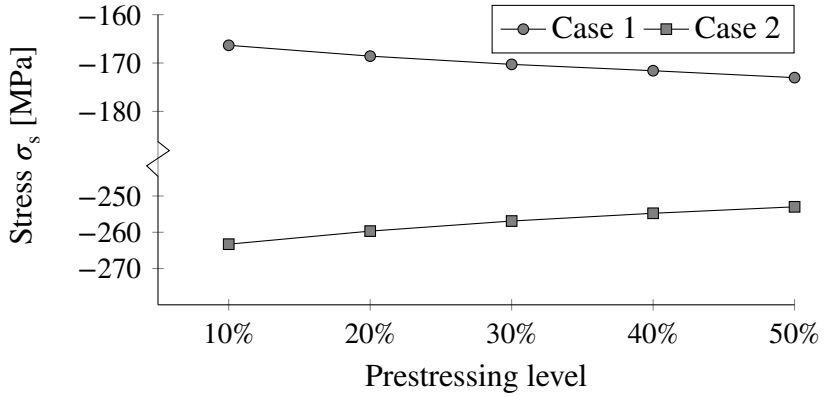

Figure 7.14 Comparison of change in steel reinforcement stress at failure for increasing CFRP prestressing between case 1 and 2.

For case 2, Figure 7.14 shows a decrease in compressive stress for an increasing prestressing level – which is an unexpected result. The stress in the top concrete fibre after CFRP application for each case are listed in Table 7.8.

Table 7.8 Top concrete stress [MPa] after CFRP application.

Beam type	Case 1	Case 2	Case 3	Case 4	Case 5	Case 6
SPC 10%	-4.78	-4.59	-4.55	-3.12	-2.92	-2.88
SPC 20%	-4.40	-4.01	-3.92	-2.73	-2.31	-2.21
SPC 30%	-4.02	-3.4	-3.26	-2.33	-1.67	-1.51
SPC 40%	-3.63	-2.77	-2.56	-1.92	-1.00	-0.77
SPC 50%	-3.23	-2.10	-1.82	-1.51	-0.29	0.03

Table 7.8 shows that most cases and prestressing levels meet the condition of obtaining compressive stresses in the top after strengthening.

The location of the neutral axis for each case and state are presented in Table 7.9-7.11 and clearly show that an increased prestressing level results in a downward shifted neutral axis – which is expected.

Table 7.9 The neutral axis position [mm] from the top concrete fibre at cracking, yielding and failure for various levels of CFRP prestressing according to case 1 and 2 compared with the unstrengthened double-T slab.

	Case 1			Case 2		
Beam type	Cracking	Yielding	Failure	Cracking	Yielding	Failure
PC	295	118	24	295	118	24
SPC 10%	298	125	36	305	132	44
SPC 20%	303	128	38	315	141	46
SPC 30%	307	132	40	323	149	48
SPC 40%	311	136	42	330	157	51
SPC 50%	315	139	46	335	164	56

Table 7.10 The neutral axis position [mm] from the top concrete fibre at cracking, yielding and failure for various levels of CFRP prestressing according to case 3 and 4 compared with the unstrengthened double-T slab.

	Case 3			Case 4		
Beam type	Cracking	Yielding	Failure	Cracking	Yielding	Failure
PC	295	118	24	295	118	24
SPC 10%	307	135	48	298	125	36
SPC 20%	318	145	49	303	129	38
SPC 30%	327	154	52	307	132	40
SPC 40%	334	163	55	311	136	42
SPC 50%	340	171	60	315	139	46

Table 7.11 The neutral axis position [mm] from the top concrete fibre at cracking, yielding and failure for various levels of CFRP prestressing according to case 5 and 6 compared with the unstrengthened double-T slab.

	Case 5			Case 6		
Beam type	Cracking	Yielding	Failure	Cracking	Yielding	Failure
PC	295	118	24	295	118	24
SPC 10%	306	133	44	308	135	48
SPC 20%	315	142	46	319	146	50
SPC 30%	323	150	48	327	155	52
SPC 40%	330	157	52	335	163	56
SPC 50%	336	164	56	341	171	61

7.2.3 Interfacial shear stresses from prestressing

The estimated maximum shear stress obtained in each studied case is shown in Table 7.12. Since the contribution is independent of the external load the shear stress is equal for cases with the same amount of CFRP area.

Table 7.12 Maximum shear stress [MPa] for the studied cases and prestressing levels.

Prestressing	Case 1 & 4	Case 2 & 5	Case 3 & 6
SPC 10%	17.6	24.6	24.5
SPC 20%	35.3	49.2	49.0
SPC 30%	52.9	73.8	73.5
SPC 40%	70.5	98.4	98.0
SPC 50%	88.2	123.0	122.5

As the stresses listed in Table 7.12 are higher than the concrete tensile strength, the principal stress will without the contribution from external load also exceed this value and anchorage is therefore required.

7.2.4 Increase of load-carrying capacity

Table 7.13-7.14 show the increase in cracking and failure moment for each case in percentage of the corresponding moment for the unstrengthened double-T slab. In all studied cases the governing failure mode was rupture of the CFRP laminate.

Table 7.13 Percentage increase in cracking and failure moment of the unstrengthened double-T slab for case 1-3.

	Case 1		Case 2		Case 3	
Beam type	Cracking	Failure	Cracking	Failure	Cracking	Failure
SPC 10%	5.6	60.0	14.9	129.9	17.7	150.9
SPC 20%	14.1	59.2	32.2	129.0	37.6	150.1
SPC 30%	22.5	58.4	49.3	128.1	57.4	149.3
SPC 40%	31.0	57.4	66.5	127.1	77.1	148.4
SPC 50%	39.4	56.5	83.5	126.1	96.8	147.3

Table 7.14 Percentage increase in cracking and failure moment of the unstrengthened double-T slab for case 4-6.

	Case 4		Case 5		Case 6	
Beam type	Cracking	Failure	Cracking	Failure	Cracking	Failure
SPC 10%	6.3	60.0	16.0	129.8	18.9	150.9
SPC 20%	14.8	59.2	33.2	129.0	38.8	150.1
SPC 30%	23.2	58.3	50.4	128.0	58.6	149.2
SPC 40%	31.7	57.4	67.5	127.1	78.3	148.3
SPC 50%	40.1	56.4	84.6	126.0	97.9	147.3

Comparing the determined moment capacities of the strengthening cases with the design loads determined in Section 7.1.2 results in the utilisation ratios in Table 7.15-7.17.

Table 7.15 Utilisation ratios in percentage of the governing design loads for various levels of CFRP prestressing in case 1-2.

	Case 1				Case 2			
Beam type	SLS 1	SLS 2	ULS 1	ULS 2	SLS 1	SLS 2	ULS 1	ULS 2
SPC 10%	124	141	76	92	114	129	53	64
SPC 20%	115	130	76	92	99	112	53	64
SPC 30%	107	121	77	93	88	100	53	64
SPC 40%	100	113	77	93	79	89	53	65
SPC 50%	94	107	77	94	71	81	54	65

Table 7.16 Utilisation ratios in percentage of the governing design loads for various levels of CFRP prestressing in case 3-4.

	Case 3				Case 4			
Beam type	SLS 1	SLS 2	ULS 1	ULS 2	SLS 1	SLS 2	ULS 1	ULS 2
SPC 10%	114	129	53	64	111	126	48	59
SPC 20%	99	112	53	64	95	108	48	59
SPC 30%	88	100	53	64	83	94	49	59
SPC 40%	79	89	53	65	74	84	49	59
SPC 50%	71	81	54	65	67	76	49	59

Table 7.17 Utilisation ratios in percentage of the governing design loads for various levels of CFRP prestressing in case 5-6.

	Case 5				Case 6			
Beam type	SLS 1	SLS 2	ULS 1	ULS 2	SLS 1	SLS 2	ULS 1	ULS 2
SPC 10%	111	126	48	59	123	140	76	92
SPC 20%	95	108	48	59	114	130	76	92
SPC 30%	83	94	49	59	106	121	77	93
SPC 40%	74	84	49	59	99	113	77	93
SPC 50%	67	76	49	59	93	106	77	94

Table 7.15-7.17 shows that only a few strengthening cases fulfil both design loads in serviceability limit state, while most fulfil the design loads in ultimate limit state with a sizable margin.

The midspan deflection upon cracking for the studied cases are presented in Table 7.18. As an increased prestressing level lead to an increased cracking moment it is reasonable that the deflection at cracking increase, yet all cases fulfil the condition of being less than 36 mm.

Table 7.18 Estimated midspan deflection [mm] at cracking for various levels of CFRP prestressing and cases compared with the unstrengthened double-T slab.

Beam type	Case 1	Case 2	Case 3	Case 4	Case 5	Case 6
PC	23.9	23.9	23.9	23.9	23.9	23.9
SPC 10%	23.0	24.0	24.3	23.3	24.5	24.9
SPC 20%	23.6	25.5	26.7	23.9	26.0	27.2
SPC 30%	24.1	27.7	28.8	24.4	28.2	29.3
SPC 40%	24.7	29.5	30.9	25.0	30.0	31.4
SPC 50%	25.9	31.2	32.9	26.2	31.7	33.4

8 Discussion

In this chapter the results obtained from adopting the analytical approach on the studied member in the case study is discussed with respect to validation and possible improvements.

The results obtained from the case study are analysed with respect to a number of different parameters in order to confirm the developed analytical approach. From the moment-curvature relationships the cracking and failure is observed to increase with an increased prestressing level as well as for a decreased loading prior to CFRP application. The location of the neutral axis changes as expected in each studied state, where an increased prestressing level shifts the position downwards. By studying the position when the prestressing level is kept constant within the strengthening case, the neutral axis is observed to move upwards when the external load increases. This indicates that the results obtained by adopting the approach are reasonable, yet experimental tests or FE modelling are required for a more comprehensive validation.

The presented approach only considers the mid-section of the member where the moment due to external load is the highest. In order to obtain more accurate results for curvature along the entire length of the beam more sections need to be studied. With respect to the top concrete fibre, the critical section of a prestressed beam commonly appear close to the support where the load effects of the external load is less. This result in a higher risk for tensile stresses to appear in the top concrete fibres of sections other than the mid-section after CFRP application. To determine the maximum allowable prestressing force for which the double-T slab remains uncracked in all sections directly after strengthening, these critical sections must be identified.

High interfacial shear stresses appear between the CFRP laminate and the concrete when prestressing is transferred to the concrete, these stresses needs to be treated with an anchorage system. Mechanically anchoring the prestressing force with bolts drilled into the concrete may be problematic since a large amount of thin and closely spaced prestressing wires are used in the double-T slab. This make gradual step-wise prestressing a more suitable method. Due to the limited width of the web it may be difficult to apply the required strengthening equipment on the bottom surface of the web, thus placing the CFRP laminate on its sides is preferred.

Placement and cross-sectional area of the laminate has shown to influence how the stresses in the steel reinforcement changes with increasing prestressing level. It has been observed that for each position of the CFRP laminate, there exists a certain area where the stress at failure changes from increasing to decreasing with an increased prestressing level. The reason to this phenomenon has not been further investigated.

When the strengthened double-T slab reach failure, the prestressing steel will be below its ultimate strain. The contribution from the prestressing steel to the moment capacity of the member is reduced for an increasing CFRP prestressing level and it is believed that by evaluating laminates with different ultimate strength and strain parameters an optimum condition can be determined where the prestressing steel contributes the most. However, the reduction is most apparent in the failure state and therefore not a considerable problem if the member should remain uncracked in the service state.

The failure moment determined for the unstrengthened beam in the case study is substantially lower than the capacity provided according to the manufacturer. This is explained

by the assumptions made for the prestressing steel, i.e. the approximated yielding stress and ultimate strain, which are chosen to be on the safe side. Determining the actual material properties of the prestressing steel would result in an increase of the cracking and failure moment for both the unstrengthened and strengthened double-T slab.

The case study has shown that for an equal amount of totally applied prestressing force in the CFRP a prestressed concrete member will result in a lower percentage increase in cracking load compared with a reinforced concrete member. This is explained by the fact that the cracking load already has been increased by the initial prestressing of the member and in order to achieve an equal increase in cracking load for the prestressed member, an increased prestressing force in the CFRP is needed. Thus, strengthening of prestressed concrete members are less economical to strengthen than reinforced concrete members.

A prestressing force up to 120 kN per laminate has in previous research successfully been anchored with non-mechanical methods, which together with the recommended stress limitations results in a possible increase of cracking load. The predicted additional loading associated with the suggest development of the roof limit which of the studied strengthening cases that provide sufficient moment capacity. Three studied cases consisting of two 30% prestressed 100x1.4 mm^2 laminates placed on each side of the web are shown to fulfil the demands. These are performed at a load prior to CFRP application of 3.85, 3.07 and 2.35 kN/m^2, where only the 3.85 and 3.07 kN/m^2 cases are considered to be feasible at Frölunda kulturhus. The two strengthening cases results in an increase of the cracking load by 49.3% and 50.4%, respectively, while the failure load is increased by 128.1% and 128.0%, respectively. Since a higher load prior to CFRP application results in a lower percentage increase in cracking load, a load of 3.07 kN/m^2 during strengthening is suggested to maximise the possible load increase. The design load in serviceability limit state is 5.85 kN/m^2 which may exceed the existing shear capacity of the deck support neglected in the study, thus shear strengthening may be required.

The studied load cases only assume a very limited amount of soil to be acting on the roof structure, which in practice cannot be used for other than small plantings. It is suggested that if plantings are to be used the roof area should be divided into different sections where thicker soil depths can be located near supports. However, this must be studied separately.

9 Conclusions

The following conclusions are drawn based on the results and the discussion:

- The results obtained when adopting the analytical approach are found reasonable, however experimental tests or FE modelling is required to further confirm the approach.
- To ensure that no tensile stresses appear in the top concrete fibres along the beam directly after strengthening more sections must be studied.
- A non-mechanical anchoring system is recommended in order to limit the interfacial shear stresses induced by the prestressed CFRP laminate.
- Evaluating laminates with different ultimate strain and strength parameters, the strain reduction in the prestressing steel may be limited and thus utilising more of the original prestressing at failure, however for members which should remain uncracked in the service state – this effect is less prominent and may be ignored.
- Strengthening of prestressed concrete members is less economical than for reinforced concrete members, since introducing an equally large prestressing force yield a lower percentage increase of the cracking load.
- Applying a prestressing force of 120 kN per laminate may increase the cracking and failure load of the double-T slab by about 50% and 130%, respectively. Shear strengthening may be required to fully utilise the increased capacity.
- The double-T slabs in the roof structure of Frölunda kulturhus may be strengthened to a degree which enables the roof to be developed into a public and urban space.

9.1 Further research

In order to validate the analytical approach presented in this thesis, experimental tests and FE analysis are required. In addition the approach can be developed further to also include all critical sections along the strengthened beam.

Since this thesis only considers flexure strengthening in longitudinal direction, the need for flexure strengthening in transversal direction and shear strengthening must be studied.

To better understand and explain how the different parameters influence the result a parametric study may be performed, which can help determine why the steel stresses decrease or increase at failure depending on the position and cross-sectional area of the CFRP laminate.

Finally, it is suggested to study strengthening of continuous prestressed concrete members with prestressed CFRP laminates.

References

Boverket (2013) *Boverkets konstruktionsregler BFS 2013:10 EKS 9* (Boverket mandatory provisions and general recommendations BFS 2013:10 EKS 9. In Swedish), Karlskrona: Boverket.

CEN (2002) *Eurocode 0: Basis of structural design*, Brussels: European Comittee for Standardization.

CEN (2004) *Eurocode 2: Design of concrete structures - Part 1-1: General rules and rules for buildings*, Brussels: European Comittee for Standardization.

Al-Emrani, M. and Kliger, R. (2006) "Analysis of interfacial shear stresses in beams strengthened with bonded prestressed laminates", *Composites Part B: Engineering*, vol. 37, pp. 265–272.

Engström, B. (2011) *Design and analysis of prestressed concrete structures*, Report 2011:7, Gothenburg: Chalmers University of Technology.

Engström, B. (2015) *Design and analysis of continous beams and columns*, Gothenburg: Chalmers University of Technology.

Fédération internationale du béton (2001) *Externally bonded FRP reinforcement for RC structures bulletin No.14*, Stuttgart: Sprint-Digital-Druck.

Goyal, R., Mukherjee, A. and Goyal, S. (2016) "An investigation on bond between FRP stay-in-place formwork and concrete", *Construction and Building Materials*, vol. 113, pp. 741–751.

Grelle, S. V. and Sneed, L. H. (2013) "Review of Anchorage Systems for Externally Bonded FRP Laminates", *International Journal of Concrete Structures and Materials*, vol. 7, no. 1, pp. 17–33.

El-Hacha, R., Wight, R. and Green, M. (2001) "Prestressed fibre-reinforced polymer laminates for strengthening structures", *Progress in Structural Engineering and Materials*, vol. 3, no. 2, pp. 111–121.

Haghani, R. and Al-Emrani, M. (2016) "A New Method for Application of Pre-stressed FRP laminates for Strengthening of Concrete Structures".

Meyer, R. W. (1985) *Handbook of Pultrusion Technology*, Boston, MA: Springer US.

Michels, J. and Czaderski, C. (2012) "Gradient anchorage method for prestressed CFRP strips - principle and application", *Bridge Maintenance, Safety and Management - IABMAS'12: Proceedings of the Sixth International IABMAS Conference*, London: Taylor & Francis Group, pp. 1981–1986.

Nordin, H. (2003) *Fibre reinforced polymers in civil engineering*, Luleå: Luleå University of Technology.

Nordin, H. (2005) *Strengthening structures with externally prestressed tendons*, Luleå: Department of Civil and Environmental Engineering.

Nordin, H. and Täljsten, B. (2006) "Concrete Beams Strengthened with Prestressed Near Surface Mounted CFRP", *Journal of Composites for Construction*, vol. 10, no. 1, pp. 60–68.

Oehlers, D. J. (2006) "FRP plates adhesively bonded to reinforced concrete beams: Generic debonding mechanisms", *Advances in Structural Engineering*, vol. 9, no. 6, pp. 737–750.

Pellegrino, C. and Modena, C. (2009) "Flexural strengthening of real-scale RC and PRC beams with end-anchored pretensioned FRP laminates", *ACI Structural Journal*, vol. 106, no. 3, pp. 319–329.

Rezazadeh, M., Barros, J. and Costa, I. (2015) "Analytical approach for the flexural analysis of RC beams strengthened with prestressed CFRP", *Composites Part B: Engineering*, vol. 73, pp. 16–34.

Rosato, D. and Rosato, D. (2005) *Reinforced Plastics Handbook*, 3rd ed., Oxford: Elsevier B.V.

Statens planverk (1969) *Spännbetongnormer publikation nr 17 SBN S-25:21* (Prestressed concrete standards publication no. 17 SBN S-25:21. In Swedish).

Statens planverk (1975) *Svensk bygg norm 1975* (Swedish building standard 1975. In Swedish).

StruSoft AB (2016) *PRE-Stress 6.5 manual*.

Täljsten, B. (1997) "Strengthening of Beams by Plate Bonding", *Journal of Materials in Civil Engineering*, vol. 9, no. 4, pp. 206–212.

Täljsten, B., Blanksvärd, T. and Sas, G. (2016) *Kompositförstärkning av betong* (Composite strengthening of concrete. In Swedish), Halmstad: Bulls Graphics AB.

Toyobo Co. Ltd (2005) *Technical Information PBO fibre ZYLON*, [Online], Available: http://www.toyobo-global.com/ (Feb. 21, 2016).

Westerberg, B. (2007) *Förstärkning av momentkapacitet med pålimmade kolfiberband: dimensioneringsanvisning* (Strengthening of moment capacity with externally bonded carbon fibre strips: design instructions. In Swedish), Stockholm: Sika.

Wu, Z. S., Iwashita, K., Hayashi, K. and Higuchi, T. (2003) "Strengthening Prestressed-Concrete Girders with Externally Prestressed PBO Fiber Reinforced Polymer Sheets", *Journal of Reinforced Plastics and Composites*, vol. 22, no. 14, pp. 1269–1286.

Yang, J. and Ye, J. (2002) "Interfacial stresses in plated beams with cracks", *Composite Structures*, vol. 57, no. 1, pp. 125–134.

Zoghi, M. (ed.) (2014) *International Handbook of FRP Composites in Civil Engineering*, Boca Raton: Taylor & Francis/CRC Press.

A Material parameters used for verification

Steel qualities and material values are taken as the ones used in PRE-Stress.

		Variable name	
Parameter	Value	PRE-Stress	Template
Concrete, C55/67			
Partial factor	1.5	γ_c	
Characteristic compressive strength	55 MPa	f_{ck}	
Low characteristic tensile strength	2.95 MPa	$f_{ctk0,05}$	
Mean modulus of elasticity	38.214 GPa	E_{0d}	E_{cm}
Shrinkage strain	0	-	ϵ_{cs}
Creep coefficient	0	-	φ
Steel reinforcement, B500B			
Partial factor	1.15	γ_s	
Characteristic yield strength	500 MPa	f_{yk}	
Modulus of elasticity	200 GPa	E_{sk}	E_s
Area, $2\phi 12$	226 mm^2	-	A_s
Distance from bottom	846 mm	z_s	-
Distance from top	$h - z_s$	-	d_s
Prestressing steel, Y1680S7			
Partial factor	1.15	γ_p	
Characteristic yield strength	1640 MPa	f_{yk}	$f_{p0,1k}$
Ultimate strength	1860 MPa	f_{uk}	f_{puk}
Modulus of elasticity	195 GPa	E_{sk}	E_p
Ultimate strain	0.0315	ϵ_{uk}	ϵ_{puk}
Design ultimate strain	0.0315	ϵ_{ud}	ϵ_{pud}
Area, $6\phi 12.9$	600 mm^2	-	A_p
Distance from bottom	846 mm	z_s	-
Distance from top	$h - z_p$	-	d_s

B Mathcad code

B.1 Geometry

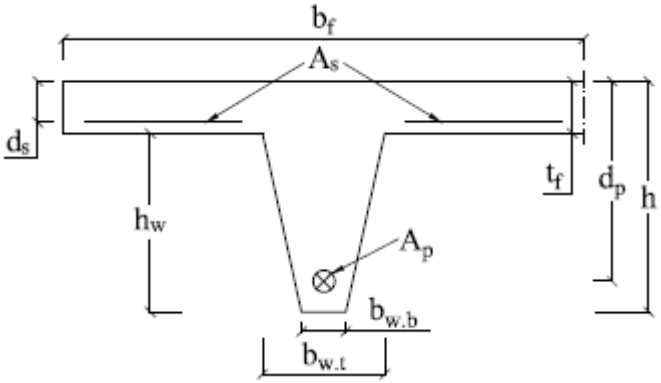

Span $l_0 := 14.4m$

Flange thickness $t_f := 40mm$

Flange width $b_f := 1198mm$

Total height $h := 400mm$

Web top width $b_{w.t} := 162mm$

Web bottom width $b_{w.b} := 102mm$

Web height $h_w := h - t_f$ $h_w = 360 \cdot mm$

Distance to prestressing steel $d_p := h - 74mm$ $d_p = 326 \cdot mm$

Distance to steel reinforcement $d_s := h - 375mm$ $d_s = 25 \cdot mm$

CFRP laminate width $b_{frp} := 100mm$

CFRP laminate thickness $t_{frp} := 1.4mm$

Thickness of adhesive layer $t_a := 2mm$

Distance to CFRP laminate $d_f := 340mm$

Number of CFRP laminates $n_f := 2$

Assumed distance from support to CFRP $a := 2m$

Effective flange width (EC2 5.3.2.1)

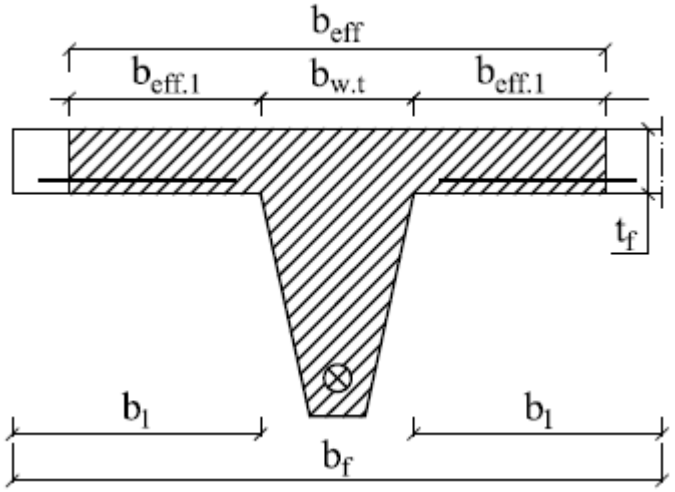

$$b_{eff.1} := \min\left(0.2 \cdot \frac{b_f - b_{w.t}}{2} + 0.1 \cdot l_0, \frac{b_f - b_{w.t}}{2}, 0.2 \cdot l_0\right) \qquad b_{eff.1} = 0.518\,m$$

Check $2 \cdot b_{eff.1} + b_{w.t} < b_f = 0$

0 = Whole flange width effective
1 = Reduced flange width effectiv

Effective flange width $b_{eff} := \min\left(2 \cdot b_{eff.1} + b_{w.t}, b_f\right)$ $b_{eff} = 1.198\,m$

Areas

Flange area $A_{c.f} := b_{eff} \cdot t_f$ $A_{c.f} = 0.048\,m^2$

Web area $A_{c.w1} := b_{w.b} \cdot h_w$ $A_{c.w1} = 0.037\,m^2$

$A_{c.w2} := \frac{\left(b_{w.t} - b_{w.b}\right) \cdot h_w}{2}$ $A_{c.w2} = 0.011\,m^2$

$A_{c.w} := A_{c.w1} + A_{c.w2}$ $A_{c.w} = 0.048\,m^2$

Gross concrete section $A_c := A_{c.f} + A_{c.w}$ $A_c = 0.095\,m^2$

CFRP laminate $A_f := n_f \cdot b_{frp} \cdot t_{frp}$ $A_f = 280 \cdot mm^2$

Function to describe section width

$$b(z) := \begin{cases} b_f & \text{if } z \le t_f \\ b_{w.t} - \frac{b_{w.t} - b_{w.b}}{h_w} \cdot \left(z - t_f\right) & \text{otherwise} \end{cases}$$

Shape of cross-section

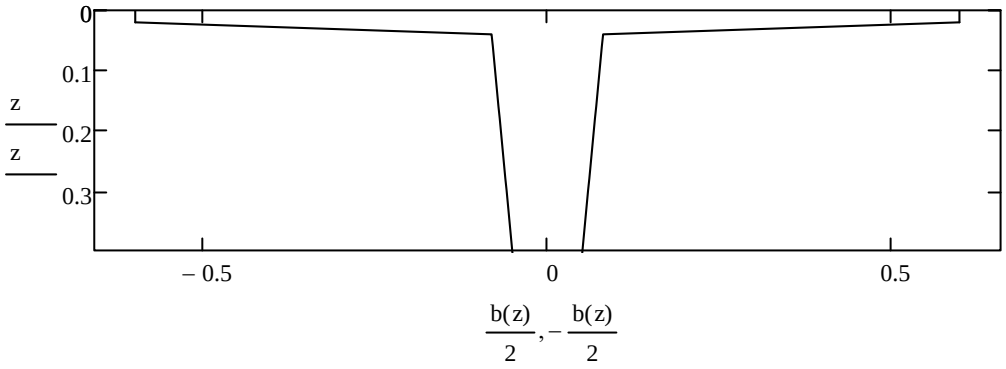

B.2 Material properties

B.2.1 Concrete

Partial factors $\gamma_c := 1.5$

$\gamma_{cE} := 1.2$

Characteristic compressive strength $f_{ck} := 50MPa$

Ultimate compressive strain $\varepsilon_{cu} := 3.5 \cdot 10^{-3}$

Characteristic tensile strength $f_{ctk0.05} := 2.9MPa$

Mean tensile strength $f_{ctm} := 4.1MPa$

Creep coefficient $\varphi := 2.5$

Shrinkage strain $\varepsilon_{cs} := 0.4 \cdot 10^{-3}$

Modulus of elasticity $E_{cm} := 37GPa$

Mean compressive strength $f_{cm} := f_{ck} + 8MPa$ $f_{cm} = 58 \cdot MPa$

Design compressive strength $f_{cd} := \frac{f_{ck}}{\gamma_c}$ $f_{cd} = 33.333 \cdot MPa$

Design tensile strength $f_{ctd} := \frac{f_{ctk0.05}}{\gamma_c}$ $f_{ctd} = 1.933 \cdot MPa$

Effective modulus of elasticity $E_{c.ef} := \frac{E_{cm}}{1 + \varphi}$ $E_{c.ef} = 10.571 \cdot GPa$

Design modulus of elasticty $E_{cd} := \frac{E_{cm}}{\gamma_{cE}}$ $E_{cd} = 30.833 \cdot GPa$

Stress-strain relationship for concrete according to EC2 3.1.7

$$n := \begin{cases} 2 & \text{if } f_{ck} \le 50MPa \\ 1.4 + 23.4 \cdot \left[\frac{\left(90 - \frac{f_{ck}}{MPa}\right)}{100} \right]^4 & \text{otherwise} \end{cases} \qquad n = 2$$

$$\varepsilon_{c2} := \min\left[\begin{cases} 2 & \text{if } f_{ck} \le 50MPa \\ 2 + 0.085 \cdot \left(\frac{f_{ck}}{MPa} - 50 \right)^{0.53} & \text{otherwise} \end{cases}, 2.8 \right] \cdot 10^{-3} \qquad \varepsilon_{c2} = 2 \times 10^{-3}$$

$$\sigma_c(\varepsilon_c) := \operatorname{sign}(\varepsilon_c) \cdot f_{cd} \cdot \begin{cases} 1 - \left(1 - \frac{|\varepsilon_c|}{\varepsilon_{c2}} \right)^n & \text{if } 0 \le |\varepsilon_c| \le \varepsilon_{c2} \\ 1 & \text{otherwise} \end{cases}$$

B.2.2 Steel reinforcement

Partial factor $\gamma_s := 1.15$

Characteristic yield strength $f_{yk} := 500MPa$

Modulus of elasticity $E_s := 200GPa$

Reinforcement area $A_s := 77mm^2$ $A_s = 77 \cdot mm^2$

Design yield strength $f_{yd} := \frac{f_{yk}}{\gamma_s}$ $f_{yd} = 434.783 \cdot MPa$

Modular ratio $\alpha_s := \frac{E_s}{E_{cm}}$ $\alpha_s = 5.405$

Modular ratio (long term) $\alpha_{s.ef} := \frac{E_s}{E_{cm}} \cdot (1 + \varphi)$ $\alpha_{s.ef} = 18.919$

Yield strain $\varepsilon_{sy} := \frac{f_{yd}}{E_s}$ $\varepsilon_{sy} = 2.174 \times 10^{-3}$

Shrinkage force at the reinforcing steel level $F_{cs.s} := \varepsilon_{cs} \cdot E_s \cdot A_s$ $F_{cs.s} = 6.16 \cdot kN$

Stress-strain diagram $\sigma_s(\varepsilon_s) := \begin{cases} \varepsilon_s \cdot E_s & \text{if } |\varepsilon_s| \le \varepsilon_{sy} \\ \text{sign}(\varepsilon_s) \cdot f_{yd} & \text{otherwise} \end{cases}$

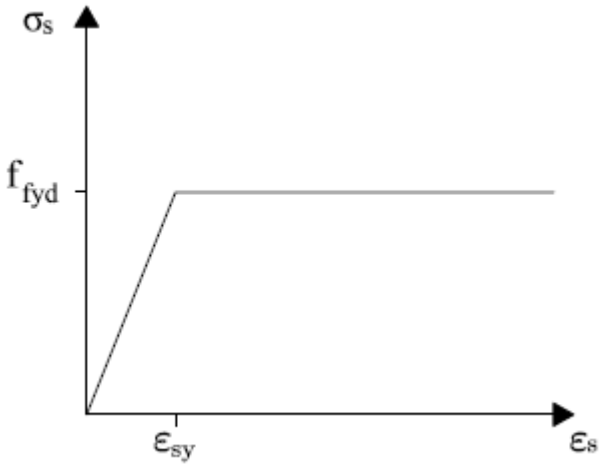

B.2.3 Prestressing steel

Partial factor $\gamma_p := 1.15$

Modulus of elasticity $E_p := 200GPa$

Characteristic 0.1% proof stress $f_{p0.1k} := 1667.5MPa$

Characteristic ultimate stress $f_{puk} := 1829MPa$

Characteristic ultimate strain $\varepsilon_{puk} := 0.027$

Total tendon area $A_p := 336mm^2$

Relaxation factor $\chi_{inf} := 8.5\%$

Applied prestressing, initial value $\sigma_{p0i} := 1450MPa$

Modular ratio $\alpha_p := \frac{E_p}{E_{cm}}$ $\alpha_p = 5.405$

Modular ratio (long term) $\alpha_{p.ef} := \frac{E_p \cdot (1 - \chi_{inf})}{E_{c.ef}}$ $\alpha_{p.ef} = 17.311$

Design yield strength $f_{pd} := \frac{f_{p0.1k}}{\gamma_p}$ $f_{pd} = 1450 \cdot MPa$

Design ultimate stress $f_{pud} := \frac{f_{puk}}{\gamma_p}$ $f_{pud} = 1590.4 \cdot MPa$

Yield strain $\varepsilon_{py} := \frac{f_{pd}}{E_p}$ $\varepsilon_{py} = 7.25 \times 10^{-3}$

Design ultimate strain $\varepsilon_{pud} := 0.9 \cdot \varepsilon_{puk}$ $\varepsilon_{pud} = 0.024$

Effective prestressing force, final valu $P_{0inf} := (1 - \chi_{inf}) \cdot \sigma_{p0i} \cdot A_p$ $P_{0inf} = 445.788 \cdot kN$

Prestrain $\varepsilon_{p0inf} := \frac{P_{0inf}}{A_p \cdot E_p}$ $\varepsilon_{p0inf} = 6.634 \times 10^{-3}$

Shrinkage force at the prestressing steel level, final value $F_{cs.p} := (1 - \chi_{inf}) \cdot \varepsilon_{cs} \cdot E_p \cdot A_p$ $F_{cs.p} = 24.595 \cdot kN$

Stress-strain diagram

$$\sigma_p(\varepsilon_p) := \begin{cases} E_p \cdot \varepsilon_p & \text{if } \varepsilon_p \le \varepsilon_{py} \\ f_{pd} + \frac{f_{pud} - f_{pd}}{\varepsilon_{puk} - \varepsilon_{py}} \cdot (\varepsilon_p - \varepsilon_{py}) & \text{otherwise} \end{cases}$$

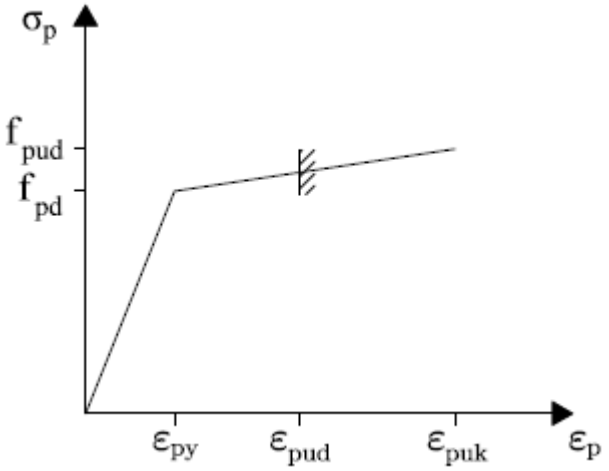

B.2.4 CFRP laminate

Partial factor $\gamma_f := 1.25$

$\gamma_{fE} := 1.1$

Ultimate tensile strength $f_{fuk} := 3100MPa$

Modulus of elasticity $E_f := 170GPa$

Design tensile strength $f_{fud} := \frac{f_{fuk}}{\gamma_f}$ $f_{fud} = 2480 \cdot MPa$

Design modulus of elasticity $E_{fd} := \frac{E_f}{\gamma_{fE}}$ $E_{fd} = 154.545 \cdot GPa$

Modular ratio $\alpha_f := \frac{E_f}{E_{cm}}$ $\alpha_f = 4.595$

Ultimate strain $\varepsilon_{fud} := \frac{f_{fud}}{E_{fd}}$ $\varepsilon_{fud} = 0.016$

B.2.5 Adhesive

Modulus of elasticity $E_a := 2GPa$

Poison's ratio $\upsilon_a := 0.3$

Shear modulus $G_a := \frac{E_a}{\left(1 + 2 \cdot \upsilon_a\right)}$ $G_a = 1.25 \cdot GPa$

B.3 Loads

Long term loading $q_l := 4.7 \frac{kN}{m}$

Loading prior to CFRP application $q_{pca} := 3.07 \frac{kN}{m}$

B.4 Analytical approach of prestressed concrete beam, PC

B.4.1 Cross-sectional constants

Transformed concrete section

Effective concrete area

$A_{I.ef} := A_c + \left(\alpha_{p.ef} - 1\right) \cdot A_p + \left(\alpha_{s.ef} - 1\right) \cdot A_s$ $A_{I.ef} = 0.102\,m^2$

Distance from the centroidal axis

$$x_{gc.pc} := \frac{A_{c.f} \cdot \frac{t_f}{2} + A_{c.w1} \cdot \left(t_f + \frac{h_w}{2}\right) + A_{c.w2} \cdot \left(\frac{h_w}{3} + t_f\right) \ldots + \left(\alpha_{p.ef} - 1\right) \cdot A_p \cdot d_p + \left(\alpha_{s.ef} - 1\right) \cdot A_s \cdot d_s}{A_{I.ef}}$$ $x_{gc.pc} = 0.123\,m$

Moment of inertia

Flange

$$I_{I.pc.f} := \frac{b_{eff} \cdot t_f^{\,3}}{12} + b_{eff} \cdot t_f \cdot \left(x_{gc.pc} - \frac{t_f}{2} \right)^2 \qquad I_{I.pc.f} = 5.151 \times 10^{-4}\,m^4$$

Rectangular web part

$$I_{I.pc.w1} := \frac{b_{w.b} \cdot h_w^{\,3}}{12} + A_{c.w1} \cdot \left(t_f + \frac{h_w}{2} - x_{gc.pc} \right)^2 \qquad I_{I.pc.w1} = 7.419 \times 10^{-4}\,m^4$$

Triangular web parts

$$I_{I.pc.w2} := 2 \frac{h_w^{\,3} \cdot \frac{b_{w.t} - b_{w.b}}{2}}{36} + A_{c.w2} \cdot \left(t_f + \frac{1}{3} \cdot h_w - x_{gc.pc} \right)^2 \qquad I_{I.pc.w2} = 9.252 \times 10^{-5}\,m^4$$

Prestressing steel

$$I_{I.pc.p.ef} := \left(\alpha_{p.ef} - 1 \right) \cdot A_p \cdot \left(d_p - x_{gc.pc} \right)^2 \qquad I_{I.pc.p.ef} = 2.258 \times 10^{-4}\,m^4$$

Reinforcement steel

$$I_{I.pc.s.ef} := \left(\alpha_{s.ef} - 1 \right) \cdot A_s \cdot \left(x_{gc.pc} - d_s \right)^2 \qquad I_{I.pc.s.ef} = 1.326 \times 10^{-5}\,m^4$$

Moment of inertia of uncracked section

$$I_{I.pc} := I_{I.pc.f} + I_{I.pc.w1} + I_{I.pc.w2} + I_{I.pc.p.ef} + I_{I.pc.s.ef} \qquad I_{I.pc} = 1.588 \times 10^{-3}\,m^4$$

4.2 Initial camber (ci)

Guess values $x_g := \frac{h}{2}$

$\varepsilon_g := -0.1 \cdot \varepsilon_{p0inf}$

Total prestressing steel strain

$$\varepsilon_{p.ci.pc}(\varepsilon_{cp}) := \varepsilon_{p0inf} - \varepsilon_{cs} + \varepsilon_{cp}$$

Concrete strain in top fibre

$$\varepsilon_{cc.ci.pc}(x_{ci}, \varepsilon_{cp}) := \varepsilon_{cp} \cdot \left(1 - \frac{d_p}{d_p - x_{ci}} \right)$$

Concrete strain distribution

$$\varepsilon_{c.ci.pc}(z, x_{ci}, \varepsilon_{cp}) := \varepsilon_{cc.ci.pc}(x_{ci}, \varepsilon_{cp}) + \frac{\varepsilon_{cp} - \varepsilon_{cc.ci.pc}(x_{ci}, \varepsilon_{cp})}{d_p} \cdot z$$

Strain in steel reinforcement

$$\varepsilon_{s.ci.pc}(x_{ci}, \varepsilon_{cp}) := \varepsilon_{c.ci.pc}(d_s, x_{ci}, \varepsilon_{cp}) - \varepsilon_{cs}$$

Horizontal equilibrium

$$F_{ci.pc}(x_{ci}, \varepsilon_{cp}) := \int_0^h \sigma_c(\varepsilon_{c.ci.pc}(z, x_{ci}, \varepsilon_{cp}))\cdot b(z)\, dz + \sigma_s(\varepsilon_{s.ci.pc}(x_{ci}, \varepsilon_{cp}))\cdot A_s \ldots + \sigma_p(\varepsilon_{p.ci.pc}(\varepsilon_{cp}))\cdot A_p$$

Moment equilibrium

$$M_{ci.pc}(x_{ci}, \varepsilon_{cp}) := \int_0^h \sigma_c(\varepsilon_{c.ci.pc}(z, x_{ci}, \varepsilon_{cp}))\cdot b(z)\cdot z\, dz \ldots + \sigma_s(\varepsilon_{s.ci.pc}(x_{ci}, \varepsilon_{cp}))\cdot A_s\cdot d_s \ldots + \sigma_p(\varepsilon_{p.ci.pc}(\varepsilon_{cp}))\cdot A_p\cdot d_p$$

Location of neutral axis and strain at the level of the prestressing steel

Given

$$F_{ci.pc}(x_g, \varepsilon_g) = 0 \qquad M_{ci.pc}(x_g, \varepsilon_g) = 0$$

$$\begin{pmatrix} x_{ci.pc} \\ \varepsilon_{cp.ci.pc} \end{pmatrix} := \text{Find}(x_g, \varepsilon_g)$$

$$x_{ci.pc} = 47.554\cdot\text{mm}$$

$$\varepsilon_{cp.ci.pc} = -5.837 \times 10^{-4}$$

Curvature

$$\kappa_{ci.pc} := \frac{\varepsilon_{cp.ci.pc} - \varepsilon_{cc.ci.pc}(x_{ci.pc}, \varepsilon_{cp.ci.pc})}{d_p} \qquad \kappa_{ci.pc} = -2.096 \times 10^{-3}\,\frac{1}{\text{m}}$$

Stress in top concrete fibre $\sigma_c(\varepsilon_{cc.ci.pc}(x_{ci.pc}, \varepsilon_{cp.ci.pc})) = 3.24\cdot\text{MPa}$

Stress in steel reinforcement $\sigma_s(\varepsilon_{s.ci.pc}(x_{ci.pc}, \varepsilon_{cp.ci.pc})) = -70.545\cdot\text{MPa}$

Stress in prestressing steel $\sigma_p(\varepsilon_{p.ci.pc}(\varepsilon_{cp.ci.pc})) = 1130.019\cdot\text{MPa}$

Stress in bottom concrete fibre $\sigma_c(\varepsilon_{c.ci.pc}(h, x_{ci.pc}, \varepsilon_{cp.ci.pc})) = -20.077\cdot\text{MPa}$

B.4.3 Prior to CFRP application (pca)

For lower loads, the position of the neutral axis can have a negative value. If a solution i not found, try changing the sign.

Guess values

$$x_g := -\frac{h}{2}$$

$$\varepsilon_g := \frac{-\varepsilon_{cu}}{8}$$

Applied moment prior to CFRP application

$$M_{pca} := \frac{q_{pca} \cdot l_0^{\,2}}{8} \qquad M_{pca} = 79.574 \cdot kN \cdot m$$

Concrete strain in bottom fibre

$$\varepsilon_{ct.pca}(\varepsilon_{cc}, x_{pca}) := \frac{\varepsilon_{cc} \cdot (x_{pca} - h)}{x_{pca}}$$

Concrete strain distribution

$$\varepsilon_{c.pca}(z, \varepsilon_{cc}, x_{pca}) := \varepsilon_{cc} + \frac{\varepsilon_{ct.pca}(\varepsilon_{cc}, x_{pca}) - \varepsilon_{cc}}{h} \cdot z$$

Strain in the steel reinforcement

$$\varepsilon_{s.pca}(\varepsilon_{cc}, x_{pca}) := \varepsilon_{c.pca}(d_s, \varepsilon_{cc}, x_{pca}) - \varepsilon_{cs}$$

Concrete strain at the level of prestressing steel

$$\varepsilon_{cp.pca}(\varepsilon_{cc}, x_{pca}) := \varepsilon_{c.pca}(d_p, \varepsilon_{cc}, x_{pca})$$

Strain the prestressing steel

$$\varepsilon_{p.pca}(\varepsilon_{cc}, x_{pca}) := \varepsilon_{p0inf} - \varepsilon_{cs} + \varepsilon_{cp.pca}(\varepsilon_{cc}, x_{pca})$$

Horizontal equilibrium

$$F_{pca}(\varepsilon_{cc}, x_{pca}) := \int_0^h \sigma_c(\varepsilon_{c.pca}(z, \varepsilon_{cc}, x_{pca})) \cdot b(z)\, dz + \sigma_s(\varepsilon_{s.pca}(\varepsilon_{cc}, x_{pca})) \cdot A_s \ldots + \sigma_p(\varepsilon_{p.pca}(\varepsilon_{cc}, x_{pca})) \cdot A_p$$

Moment equilibrium

$$M_{f.pca}(\varepsilon_{cc}, x_{pca}) := \int_0^h \sigma_c(\varepsilon_{c.pca}(z, \varepsilon_{cc}, x_{pca})) \cdot b(z) \cdot z\, dz \ldots + \sigma_s(\varepsilon_{s.pca}(\varepsilon_{cc}, x_{pca})) \cdot A_s \cdot d_s \ldots + \sigma_p(\varepsilon_{p.pca}(\varepsilon_{cc}, x_{pca})) \cdot A_p \cdot d_p$$

Location of neutral axis and strain in the top concrete fibre

Given

$$F_{pca}(\varepsilon_g, x_g) = 0 \qquad M_{f.pca}(\varepsilon_g, x_g) = M_{pca}$$

$$\begin{pmatrix} \varepsilon_{cc.pca} \\ x_{pca} \end{pmatrix} := \text{Find}(\varepsilon_g, x_g) \qquad x_{pca} = -562.602 \cdot mm$$

$$\varepsilon_{cc.pca} = -1.082 \times 10^{-4}$$

Curvature

$$\kappa_{pca} := \frac{\varepsilon_{cp.pca}(\varepsilon_{cc.pca}, x_{pca}) - \varepsilon_{cc.pca}}{d_p} \qquad \kappa_{pca} = -1.924 \times 10^{-4}\, \frac{1}{m}$$

Stress in top concrete fibre $\sigma_c(\varepsilon_{cc.pca}) = -3.51 \cdot MPa$

Stress in steel reinforcement $\sigma_s(\varepsilon_{s.pca}(\varepsilon_{cc.pca}, x_{pca})) = -102.609 \cdot MPa$

Strain in prestressing steel $\varepsilon_{p.pca}(\varepsilon_{cc.pca}, x_{pca}) = 6.063 \times 10^{-3}$

Fictitious concrete strain at the level of the CFRP

$\varepsilon_{cf.pca} := \varepsilon_{c.pca}(d_f, \varepsilon_{cc.pca}, x_{pca})$ $\varepsilon_{cf.pca} = -1.736 \times 10^{-4}$

B.4.4 Concrete crack initiation (cr)

Guess value $x_g := \frac{h}{2}$

Concrete strain in bottom fibre

$\varepsilon_{ct.cr.pc} := \frac{f_{ctk0.05}}{E_{cm}}$ $\varepsilon_{ct.cr.pc} = 7.838 \times 10^{-5}$

Concrete strain in top fibre

$\varepsilon_{cc.cr.pc}(x_{cr}) := \varepsilon_{ct.cr.pc} \cdot \left(1 - \frac{h}{h - x_{cr}}\right)$

Concrete strain distribution

$\varepsilon_{c.cr.pc}(z, x_{cr}) := \varepsilon_{cc.cr.pc}(x_{cr}) + \frac{\varepsilon_{ct.cr.pc} - \varepsilon_{cc.cr.pc}(x_{cr})}{h} \cdot z$

Strain in steel reinforcement

$\varepsilon_{s.cr.pc}(x_{cr}) := \varepsilon_{c.cr.pc}(d_s, x_{cr}) - \varepsilon_{cs}$

Concrete strain in level of prestressing steel

$\varepsilon_{cp.cr.pc}(x_{cr}) := \varepsilon_{c.cr.pc}(d_p, x_{cr})$

Strain of prestressing steel

$\varepsilon_{p.cr.pc}(x_{cr}) := \varepsilon_{p0inf} - \varepsilon_{cs} + \varepsilon_{cp.cr.pc}(x_{cr})$

Horizontal equilibrium

$F_{cr.pc}(x_{cr}) := \int_0^h \sigma_c(\varepsilon_{c.cr.pc}(z, x_{cr})) \cdot b(z)\, dz + \sigma_s(\varepsilon_{s.cr.pc}(x_{cr})) \cdot A_s \ldots$
$+ \sigma_p(\varepsilon_{p.cr.pc}(x_{cr})) \cdot A_p$

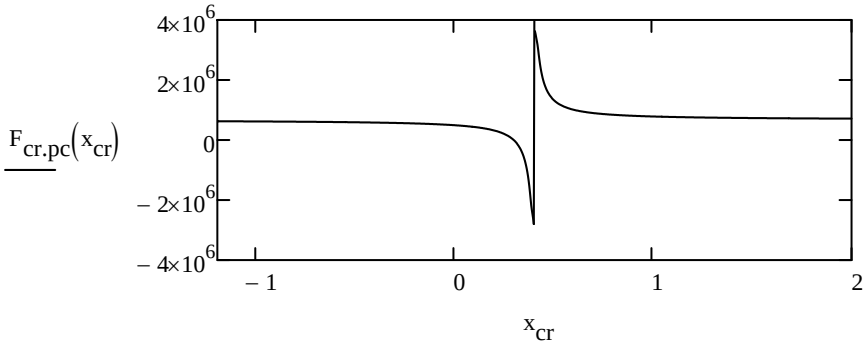

Location of neutral axis

$$x_{cr.pc} := \text{root}\left(F_{cr.pc}\left(x_g\right), x_g\right) \qquad x_{cr.pc} = 294.842 \cdot \text{mm}$$

Curvature

$$\kappa_{cr.pc} := \frac{\varepsilon_{cp.cr.pc}\left(x_{cr.pc}\right) - \varepsilon_{cc.cr.pc}\left(x_{cr.pc}\right)}{d_p} \qquad \kappa_{cr.pc} = 7.453 \times 10^{-4}\,\frac{1}{\text{m}}$$

Moment

$$M_{cr.pc} := \int_0^h \sigma_c\left(\varepsilon_{c.cr.pc}\left(z, x_{cr.pc}\right)\right) \cdot b(z) \cdot z \, dz + \left(\sigma_s\left(\varepsilon_{s.cr.pc}\left(x_{cr.pc}\right)\right) \cdot A_s\right) \cdot d_s \ldots + \sigma_p\left(\varepsilon_{p.cr.pc}\left(x_{cr.pc}\right)\right) \cdot A_p \cdot d_p$$

$$M_{cr.pc} = 122.069 \cdot \text{kN} \cdot \text{m}$$

Stress in top concrete fibre $\sigma_c\left(\varepsilon_{cc.cr.pc}\left(x_{cr.pc}\right)\right) = -6.923 \cdot \text{MPa}$

Stress in steel reinforcement $\sigma_s\left(\varepsilon_{s.cr.pc}\left(x_{cr.pc}\right)\right) = -120.225 \cdot \text{MPa}$

Stress in prestressing steel $\sigma_p\left(\varepsilon_{p.cr.pc}\left(x_{cr.pc}\right)\right) = 1251.395 \cdot \text{MPa}$

Cracking load $q_{cr.pc} := \frac{8 \cdot M_{cr.pc}}{l_0^{\,2}}$ $\qquad q_{cr.pc} = 4.709 \cdot \frac{\text{kN}}{\text{m}}$

B.4.5 Prestressing steel yield initiation (y)

Remaining steel strain until yielding

$$\varepsilon_{cp.y.pc} := \varepsilon_{py} - \varepsilon_{p0inf} \qquad \varepsilon_{cp.y.pc} = 6.163 \times 10^{-4}$$

Concrete strain in top fibre

$$\varepsilon_{cc.y.pc}\left(x_y\right) := \varepsilon_{cp.y.pc} \cdot \left(1 - \frac{d_p}{d_p - x_y}\right)$$

Concrete strain distribution

$$\varepsilon_{c.y.pc}(z, x_y) := \varepsilon_{cc.y.pc}(x_y) + \frac{\varepsilon_{cp.y.pc} - \varepsilon_{cc.y.pc}(x_y)}{d_p} \cdot z$$

Strain in steel reinforcement

$$\varepsilon_{s.y.pc}(x_y) := \varepsilon_{c.y.pc}(d_s, x_y) - \varepsilon_{cs}$$

Horizontal equilibrium for the additional strain

$$F_{y.pc}(x_y) := \int_0^{x_y} \sigma_c(\varepsilon_{c.y.pc}(z, x_y)) \cdot b(z)\, dz + \sigma_s(\varepsilon_{s.y.pc}(x_y)) \cdot A_s + \sigma_p(\varepsilon_{py}) \cdot A_p$$

Location of neutral axis

$$x_{y.pc} := \text{root}(F_{y.pc}(t_f), t_f) \qquad x_{y.pc} = 118.219 \cdot \text{mm}$$

Curvature

$$\kappa_{y.pc} := \frac{\varepsilon_{cp.y.pc} - \varepsilon_{cc.y.pc}(x_{y.pc})}{d_p} \qquad \kappa_{y.pc} = 2.966 \times 10^{-3} \frac{1}{\text{m}}$$

Moment

$$M_{y.pc} := \int_0^{x_{y.pc}} \sigma_c(\varepsilon_{c.y.pc}(z, x_{y.pc})) \cdot b(z) \cdot z\, dz + \sigma_s(\varepsilon_{s.y.pc}(x_{y.pc})) \cdot A_s \cdot d_s \ldots + \sigma_p(\varepsilon_{py}) \cdot A_p \cdot d_p$$

$$M_{y.pc} = 147.464 \cdot \text{kN} \cdot \text{m}$$

Stress in top concrete fibre $\sigma_c(\varepsilon_{cc.y.pc}(x_{y.pc})) = -10.663 \cdot \text{MPa}$

Stress in steel reinforcement $\sigma_s(\varepsilon_{s.y.pc}(x_{y.pc})) = -135.295 \cdot \text{MPa}$

Yielding load $q_{y.pc} := \frac{8 M_{y.pc}}{l_0^2}$ $\qquad q_{y.pc} = 5.689 \cdot \frac{\text{kN}}{\text{m}}$

B.4.6 Concrete failure (cc)

Concrete strain in top fibre

$$\varepsilon_{cc.u.cc.pc} := -\varepsilon_{cu}$$

Concrete strain distribution

$$\varepsilon_{c.u.cc.pc}(z, x_u) := \varepsilon_{cc.u.cc.pc} + \frac{-\varepsilon_{cc.u.cc.pc}}{x_u} \cdot z$$

Strain in steel reinforcement

$$\varepsilon_{s.u.cc.pc}(x_u) := \varepsilon_{c.u.cc.pc}(d_s, x_u) - \varepsilon_{cs}$$

Concrete strain in level of prestressing steel

$$\varepsilon_{cp.u.cc.pc}(x_u) := \varepsilon_{c.u.cc.pc}(d_p, x_u)$$

Strain in prestressing steel

$$\varepsilon_{p.u.cc.pc}(x_u) := \varepsilon_{p0inf} - \varepsilon_{cs} + \varepsilon_{cp.u.cc.pc}(x_u)$$

Horizontal equilibrium

$$F_{u.cc.pc}(x_u) := \int_0^{x_u} \sigma_c(\varepsilon_{c.u.cc.pc}(z, x_u))\cdot b(z)\, dz + \sigma_s(\varepsilon_{s.u.cc.pc}(x_u))\cdot A_s \ldots + \sigma_p(\varepsilon_{p.u.cc.pc}(x_u))\cdot A_p$$

Location of neutral axis

$$x_{u.cc.pc} := \text{root}(F_{u.cc.pc}(t_f), t_f) \qquad x_{u.cc.pc} = 19.381\cdot mm$$

Curvature

$$\kappa_{u.cc.pc} := \frac{\varepsilon_{cp.u.cc.pc}(x_{u.cc.pc}) + \varepsilon_{cu}}{d_p} \qquad \kappa_{u.cc.pc} = 0.181\,\frac{1}{m}$$

Moment

$$M_{u.cc.pc} := \int_0^{x_{u.cc.pc}} \sigma_c(\varepsilon_{c.u.cc.pc}(z, x_{u.cc.pc}))\cdot b(z)\cdot z\, dz \ldots + \sigma_s(\varepsilon_{s.u.cc.pc}(x_{u.cc.pc}))\cdot A_s\cdot d_s \ldots + \sigma_p(\varepsilon_{p.u.cc.pc}(x_{u.cc.pc}))\cdot A_p\cdot d_p \qquad M_{u.cc.pc} = 196.349\cdot kN\cdot m$$

Stress in steel reinforcement $\sigma_s(\varepsilon_{s.u.cc.pc}(x_{u.cc.pc})) = 122.943\cdot MPa$

Strain in the prestressing steel $\sigma_p(\varepsilon_{p.u.cc.pc}(x_{u.cc.pc})) = 1836.502\cdot MPa$

Check $\sigma_p(\varepsilon_{p.u.cc.pc}(x_{u.cc.pc})) \le f_{pud} = 0$ 1 = OK, 0 = Not OK

B.4.7 Rupture of prestressing steel (rp)

Concrete strain at the level of the prestressing steel

$$\varepsilon_{cp.u.rp.pc} := \varepsilon_{pud} - \varepsilon_{p0inf} - \varepsilon_{cs} \qquad \varepsilon_{cp.u.rp.pc} = 0.017$$

Concrete strain in top fibre

$$\varepsilon_{cc.u.rp.pc}(x_u) := \varepsilon_{cp.u.rp.pc}\cdot\left(1 - \frac{d_p}{d_p - x_u}\right)$$

Concrete strain distribution

$$\varepsilon_{c.u.rp.pc}(z, x_u) := \varepsilon_{cc.u.rp.pc}(x_u) + \frac{\varepsilon_{cp.u.rp.pc} - \varepsilon_{cc.u.rp.pc}(x_u)}{d_p}\cdot z$$

Strain in steel reinforcement

$$\varepsilon_{s.u.rp.pc}(x_u) := \varepsilon_{c.u.rp.pc}(d_s, x_u) - \varepsilon_{cs}$$

Horizontal equilibrium

$$F_{u.rp.pc}(x_u) := \int_0^{x_u} \sigma_c(\varepsilon_{c.u.rp.pc}(z, x_u))\cdot b(z)\, dz + \sigma_s(\varepsilon_{s.u.rp.pc}(x_u))\cdot A_s + \sigma_p(\varepsilon_{pud})\cdot A_p$$

Location of neutral axis

$$x_{u.rp.pc} := \text{root}(F_{u.rp.pc}(t_f), t_f) \qquad x_{u.rp.pc} = 24.405\cdot\text{mm}$$

Curvature

$$\kappa_{u.rp.pc} := \frac{\varepsilon_{cp.u.rp.pc} - \varepsilon_{cc.u.rp.pc}(x_{u.rp.pc})}{d_p} \qquad \kappa_{u.rp.pc} = 0.05725\,\frac{1}{m}$$

Moment

$$M_{u.rp.pc} := \int_0^{x_{u.rp.pc}} \sigma_c(\varepsilon_{c.u.rp.pc}(z, x_{u.rp.pc}))\cdot b(z)\cdot z\, dz \ ... + \sigma_s(\varepsilon_{s.u.rp.pc}(x_{u.rp.pc}))\cdot A_s\cdot d_s + \sigma_p(\varepsilon_{pud})\cdot A_p\cdot d_p \qquad M_{u.rp.pc} = 167.395\cdot\text{kN}\cdot\text{m}$$

Stress in top concrete fibre $\sigma_c(\varepsilon_{cc.u.rp.pc}(x_{u.rp.pc})) = -30.305\cdot\text{MPa}$

Stress in steel reinforcement $\sigma_s(\varepsilon_{s.u.rp.pc}(x_{u.rp.pc})) = -73.191\cdot\text{MPa}$

B.4.8 Determine governing failure mode

Assume concrete crushing and rupture of prestressing steel occur simultaneously

$$\varepsilon_{cp.crit.pc} := \varepsilon_{pud} - \varepsilon_{p0inf} - \varepsilon_{cs}$$

$$\varepsilon_{cc.crit.pc} := -\varepsilon_{cu}$$

Strain distribution

$$\varepsilon_{c.crit.pc}(z) := \varepsilon_{cc.crit.pc} + \frac{\varepsilon_{cp.crit.pc} - \varepsilon_{cc.crit.pc}}{d_p}\cdot z$$

Location of the neutral axis

$$x_{crit.pc} := root\left(\varepsilon_{c.crit.pc}\left(x_g\right), x_g\right) \qquad x_{crit.pc} = 54.945 \cdot mm$$

Strain in steel reinforcement

$$\varepsilon_{s.crit.pc} := \varepsilon_{c.crit.pc}\left(d_s\right) - \varepsilon_{cs}$$

From horizontal equilibrium, we obtain

$$A_{p.crit.pc} := -\frac{\sigma_s\left(\varepsilon_{s.crit.pc}\right) \cdot A_s + \int_0^{x_{crit.pc}} \sigma_c\left(\varepsilon_{c.crit.pc}(z)\right) \cdot b(z)\, dz}{\sigma_p\left(\varepsilon_{pud}\right)}$$

$$A_{p.crit.pc} = 1020.106 \cdot mm^2$$

Choose correct failure mode based on the critical prestressing steel area

$$M_{u.pc} := \begin{cases} M_{u.rp.pc} & \text{if } A_p \le A_{p.crit.pc} \\ M_{u.cc.pc} & \text{otherwise} \end{cases} \qquad M_{u.pc} = 167.395 \cdot kN \cdot m$$

$$\kappa_{u.pc} := \begin{cases} \kappa_{u.rp.pc} & \text{if } A_p \le A_{p.crit.pc} \\ \kappa_{u.cc.pc} & \text{otherwise} \end{cases} \qquad \kappa_{u.pc} = 0.05725 \frac{1}{m}$$

$$x_{u.pc} := \begin{cases} x_{u.rp.pc} & \text{if } A_p \le A_{p.crit.pc} \\ x_{u.cc.pc} & \text{otherwise} \end{cases} \qquad x_{u.pc} = 24.405 \cdot mm$$

$$\varepsilon_{cc.u.pc} := \begin{cases} \varepsilon_{cc.u.rp.pc}\left(x_{u.rp.pc}\right) & \text{if } A_p \le A_{p.crit.pc} \\ \varepsilon_{cc.u.cc.pc} & \text{otherwise} \end{cases} \qquad \varepsilon_{cc.u.pc} = -1.397 \times 10^{-3}$$

$$\varepsilon_{s.u.pc} := \begin{cases} \varepsilon_{s.u.rp.pc}\left(x_{u.rp.pc}\right) & \text{if } A_p \le A_{p.crit.pc} \\ \varepsilon_{s.u.cc.pc}\left(x_{u.cc.pc}\right) & \text{otherwise} \end{cases} \qquad \varepsilon_{s.u.pc} = -3.66 \times 10^{-4}$$

$$\varepsilon_{p.u.pc} := \begin{cases} \varepsilon_{pud} & \text{if } A_p \le A_{p.crit.pc} \\ \varepsilon_{p.u.cc.pc}\left(x_{u.cc.pc}\right) & \text{otherwise} \end{cases} \qquad \varepsilon_{p.u.pc} = 0.024$$

Gather moment and curvature results, including yielding step

$$M_{pc.y} := \begin{pmatrix} 0N \cdot m \\ M_{cr.pc} \\ M_{y.pc} \\ M_{u.pc} \end{pmatrix} = \begin{pmatrix} 0 \\ 122.069 \\ 147.464 \\ 167.395 \end{pmatrix} \cdot kN \cdot m \qquad \kappa_{pc.y} := \begin{pmatrix} \kappa_{ci.pc} \\ \kappa_{cr.pc} \\ \kappa_{y.pc} \\ \kappa_{u.pc} \end{pmatrix} = \begin{pmatrix} -2.096 \times 10^{-3} \\ 7.453 \times 10^{-4} \\ 2.966 \times 10^{-3} \\ 0.057 \end{pmatrix} \frac{1}{m}$$

Gather moment and curvature results, excluding yielding step

$$M_{pc.1} := \begin{pmatrix} 0\,N\cdot m \\ M_{cr.pc} \\ M_{u.pc} \end{pmatrix} \qquad \kappa_{pc.1} := \begin{pmatrix} \kappa_{ci.pc} \\ \kappa_{cr.pc} \\ \kappa_{u.pc} \end{pmatrix}$$

Determine what results to present, if yielding occurs upon cracking (i.e. yielding moment is less than the cracking moment), the moment-curvature relationship should exclude the yielding point from the graph.

$$M_{pc} := \begin{cases} M_{pc.1} & \text{if } M_{y.pc} < M_{cr.pc} \\ M_{pc.y} & \text{otherwise} \end{cases}$$

$$\kappa_{pc} := \begin{cases} \kappa_{pc.1} & \text{if } M_{y.pc} < M_{cr.pc} \\ \kappa_{pc.y} & \text{otherwise} \end{cases}$$

Failure load $q_{u.pc} := \dfrac{8\cdot M_{u.pc}}{l_0^{\,2}}$ $q_{u.pc} = 6.458\cdot\dfrac{kN}{m}$

Moment capacity is limited by ○ Concrete crushing ◉ Prestressing steel rupture

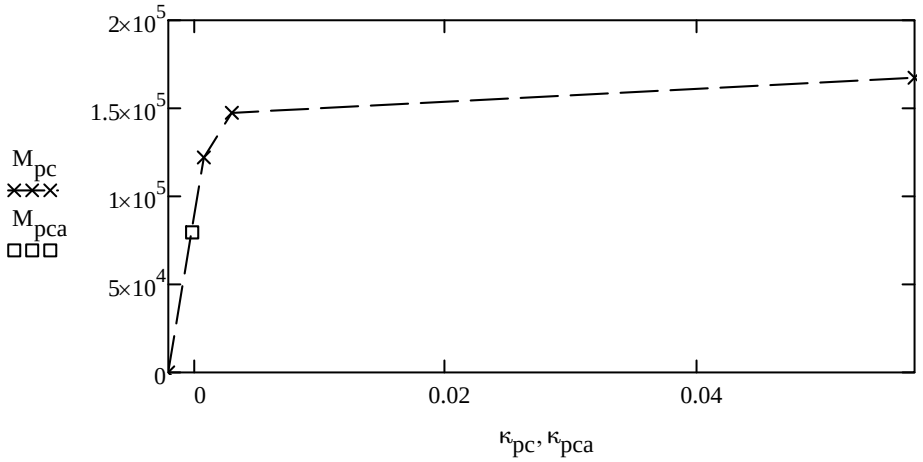

B.5 Analytical approach of CFRP strengthened prestressed concrete beam, SPC

Level of prestressing $\mu_f := 30\%$

Prestrain of CFRP $\varepsilon_{f0} := \mu_f\cdot\varepsilon_{fud}$

Total CFRP prestressing force $P_{f0} := E_{fd}\cdot\varepsilon_{f0}\cdot A_f$ $P_{f0} = 208.32\cdot kN$

per laminate $\dfrac{P_{f0}}{n_f} = 104.16\cdot kN$

B.5.1 Cross-sectional constants

Transformed concrete section

Distance from the centroidal axis

$$x_{gc.spc} := \frac{A_{c.f}\cdot\frac{t_f}{2} + A_{c.w1}\cdot\left(t_f + \frac{h_w}{2}\right) + A_{c.w2}\cdot\left(\frac{h_w}{3} + t_f\right) \ldots + \left(\alpha_{p.ef} - 1\right)\cdot A_p\cdot d_p + \left(\alpha_{s.ef} - 1\right)\cdot A_s\cdot d_s + A_f\cdot\alpha_f\cdot d_f}{A_{I.ef} + A_f} \qquad x_{gc.spc} = 126.957\cdot mm$$

Moment of inertia

Flange

$$I_{I.spc.f} := \frac{b_{eff}\cdot t_f^{\,3}}{12} + b_{eff}\cdot\left(t_f\right)\cdot\left(x_{gc.spc} - \frac{t_f}{2}\right)^2 \qquad I_{I.spc.f} = 5.546\times 10^{-4}\,m^4$$

Rectangular web part

$$I_{I.spc.w1} := \frac{b_{w.b}\cdot h_w^{\,3}}{12} + A_{c.w1}\cdot\left(t_f + \frac{h_w}{2} - x_{gc.spc}\right)^2 \qquad I_{I.spc.w1} = 7.145\times 10^{-4}\,m^4$$

Triangular web parts

$$I_{I.spc.w2} := 2\,\frac{h_w^{\,3}\cdot\frac{b_{w.t} - b_{w.b}}{2}}{36} + A_{c.w2}\cdot\left(t_f + \frac{1}{3}\cdot h_w - x_{gc.spc}\right)^2$$

$$I_{I.spc.w2} = 8.955\times 10^{-5}\,m^4$$

Prestressing steel

$$I_{I.spc.p.ef} := \left(\alpha_{p.ef} - 1\right)\cdot A_p\cdot\left(d_p - x_{gc.spc}\right)^2 \qquad I_{I.spc.p.ef} = 2.171\times 10^{-4}\,m^4$$

Reinforcement steel

$$I_{I.spc.s.ef} := \left(\alpha_{s.ef} - 1\right)\cdot A_s\cdot\left(x_{gc.spc} - d_s\right)^2 \qquad I_{I.spc.s.ef} = 1.434\times 10^{-5}\,m^4$$

CFRP reinforcement

$$I_{I.f} := A_f\cdot\left(x_{gc.spc} - d_f\right)^2 \qquad I_{I.f} = 1.271\times 10^{-5}\,m^4$$

Moment of inertia of uncracked section

$$I_{I.spc} := I_{I.spc.f} + I_{I.spc.w1} + I_{I.spc.w2} + I_{I.spc.p.ef} + I_{I.spc.s.ef} + I_{I.f}$$

$$I_{I.spc} = 1.603\times 10^{-3}\,m^4$$

Elastic section modulus

$$W_c := \frac{I_{I.spc}}{x_{gc.spc}} \qquad W_c = 0.013 \cdot m^3$$

B.5.2 After CFRP application (aca)

Guess values $x_g := -\frac{h}{2}$

$$\varepsilon_g := \frac{-\varepsilon_{cu}}{4}$$

Concrete strain in top fibre

$$\varepsilon_{cc.aca}(x_{aca}, \varepsilon_{cf.aca}) := \varepsilon_{cf.aca} \cdot \left(1 - \frac{d_f}{d_f - x_{aca}}\right)$$

Concrete strain distribution

$$\varepsilon_{c.aca}(z, x_{aca}, \varepsilon_{cf.aca}) := \varepsilon_{cc.aca}(x_{aca}, \varepsilon_{cf.aca}) + \frac{\varepsilon_{cf.aca} - \varepsilon_{cc.aca}(x_{aca}, \varepsilon_{cf.aca})}{d_f} \cdot z$$

Strain in steel reinforcement

$$\varepsilon_{s.aca}(x_{aca}, \varepsilon_{cf.aca}) := \varepsilon_{c.aca}(d_s, x_{aca}, \varepsilon_{cf.aca}) - \varepsilon_{cs}$$

Concrete strain in level of prestressing steel

$$\varepsilon_{cp.aca}(x_{aca}, \varepsilon_{cf.aca}) := \varepsilon_{c.aca}(d_p, x_{aca}, \varepsilon_{cf.aca})$$

Total prestressing steel strain

$$\varepsilon_{p.aca}(x_{aca}, \varepsilon_{cf.aca}) := \varepsilon_{p0inf} - \varepsilon_{cs} + \varepsilon_{cp.aca}(x_{aca}, \varepsilon_{cf.aca})$$

Total CFRP strain

$$\varepsilon_{f.aca}(\varepsilon_{cf.aca}) := \varepsilon_{f0} + \varepsilon_{cf.aca} - \varepsilon_{cf.pca}$$

Horizontal equilibrium

$$F_{aca}(x_{aca}, \varepsilon_{cf.aca}) := \int_0^h \sigma_c(\varepsilon_{c.aca}(z, x_{aca}, \varepsilon_{cf.aca})) \cdot b(z)\, dz + \sigma_s(\varepsilon_{s.aca}(x_{aca}, \varepsilon_{cf.aca})) \cdot A_s \cdots + \sigma_p(\varepsilon_{p.aca}(x_{aca}, \varepsilon_{cf.aca})) \cdot A_p + \varepsilon_{f.aca}(\varepsilon_{cf.aca}) \cdot E_f \cdot A_f$$

Moment equilibrium

$$M_{aca}(x_{aca}, \varepsilon_{cf.aca}) := \int_0^h \sigma_c(\varepsilon_{c.aca}(z, x_{aca}, \varepsilon_{cf.aca})) \cdot b(z) \cdot z\, dz \cdots + \sigma_s(\varepsilon_{s.aca}(x_{aca}, \varepsilon_{cf.aca})) \cdot A_s \cdot d_s \cdots + \sigma_p(\varepsilon_{p.aca}(x_{aca}, \varepsilon_{cf.aca})) \cdot A_p \cdot d_p + \varepsilon_{f.aca}(\varepsilon_{cf.aca}) \cdot E_f \cdot A_f \cdot d_f$$

Given

Conditions $F_{aca}(x_g, \varepsilon_g) = 0 \qquad M_{aca}(x_g, \varepsilon_g) = M_{pca}$

Find neutral axis and strain distribution

$$\begin{pmatrix} x_{aca} \\ \varepsilon_{cf.aca} \end{pmatrix} := \text{Find}(x_g, \varepsilon_g) \qquad x_{aca} = -37.591 \cdot \text{mm}$$

$$M_{aca}(x_{aca}, \varepsilon_{cf.aca}) = 79.574 \cdot \text{kN} \cdot \text{m}$$

Curvature

$$\kappa_{aca} := \frac{\varepsilon_{cf.aca} - \varepsilon_{cc.aca}(x_{aca}, \varepsilon_{cf.aca})}{d_f} \qquad \kappa_{aca} = -1.347 \times 10^{-3} \frac{1}{\text{m}}$$

Stress in top concrete fibre $\sigma_c(\varepsilon_{cc.aca}(x_{aca}, \varepsilon_{cf.aca})) = -1.667 \cdot \text{MPa}$

Stress in steel reinforcement $\sigma_s(\varepsilon_{s.aca}(x_{aca}, \varepsilon_{cf.aca})) = -96.868 \cdot \text{MPa}$

Stress in prestressing steel $\sigma_p(\varepsilon_{p.aca}(x_{aca}, \varepsilon_{cf.aca})) = 1148.765 \cdot \text{MPa}$

Stress in CFRP laminate $\varepsilon_{f.aca}(\varepsilon_{cf.aca}) \cdot E_f = 761.425 \cdot \text{MPa}$

B.5.3 Concrete crack initiation (cr)

Guess value $x_g := \frac{3}{4} \cdot h$

Concrete strain in bottom fibre

$$\varepsilon_{ct.cr.spc} := \frac{f_{ctk0.05}}{E_{cm}} \qquad \varepsilon_{ct.cr.spc} = 7.838 \times 10^{-5}$$

Concrete strain in top fibre

$$\varepsilon_{cc.cr.spc}(x_{cr}) := \varepsilon_{ct.cr.spc} \cdot \left(1 - \frac{h}{h - x_{cr}}\right)$$

Concrete strain distribution

$$\varepsilon_{c.cr.spc}(z, x_{cr}) := \varepsilon_{cc.cr.spc}(x_{cr}) + \frac{\varepsilon_{ct.cr.spc} - \varepsilon_{cc.cr.spc}(x_{cr})}{h} \cdot z$$

Strain in steel reinforcement

$$\varepsilon_{s.cr.spc}(x_{cr}) := \varepsilon_{c.cr.spc}(d_s, x_{cr}) - \varepsilon_{cs}$$

Concrete strain in level of prestressing steel

$$\varepsilon_{cp.cr.spc}(x_{cr}) := \varepsilon_{c.cr.spc}(d_p, x_{cr})$$

Strain in prestressing steel

$$\varepsilon_{p.cr.spc}(x_{cr}) := \varepsilon_{p0inf} - \varepsilon_{cs} + \varepsilon_{cp.cr.spc}(x_{cr})$$

Concrete strain in the level of CFRP reinforcement

$$\varepsilon_{cf.cr.spc}(x_{cr}) := \varepsilon_{c.cr.spc}(d_f, x_{cr})$$

Total strain the CFRP reinforcement

$$\varepsilon_{f.cr.spc}(x_{cr}) := \varepsilon_{f0} + \varepsilon_{cf.cr.spc}(x_{cr}) - \varepsilon_{cf.pca}$$

Horizontal equilibrium

$$F_{cr.spc}(x_{cr}) := \int_0^{x_{cr}} \sigma_c\left(\varepsilon_{c.cr.spc}(z, x_{cr})\right)\cdot b(z)\, dz + \sigma_s\left(\varepsilon_{s.cr.spc}(x_{cr})\right)\cdot A_s \ldots + \sigma_p\left(\varepsilon_{p.cr.spc}(x_{cr})\right)\cdot A_p + \varepsilon_{f.cr.spc}(x_{cr})\cdot E_f \cdot A_f$$

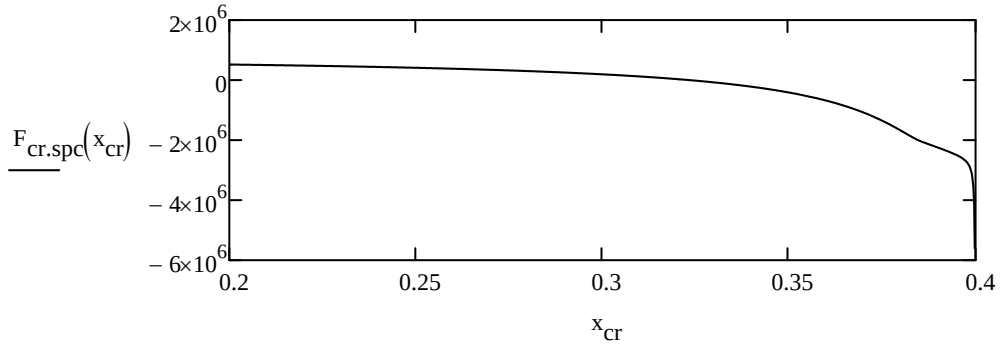

Location of neutral axis

$$x_{cr.spc} := \text{root}\left(F_{cr.spc}(x_g), x_g\right) \qquad x_{cr.spc} = 323.28\cdot mm$$

If Mathcad is unable to determine the location of the neutral axis even for an updated guess value, "Enable Evaluation" of the graph above and use the Trace function to determine its position. Right click and choose "Enable Evaluation" and manually enter the value here. Right click on the variable and choose "Disable Evaluation" if a value is found automatically.

$$x_{cr.spc} := 298.68mm$$

$$F_{cr.spc}(x_{cr.spc}) = 0\,N$$

Curvature

$$\kappa_{cr.spc} := \frac{\varepsilon_{cp.cr.spc}(x_{cr.spc}) - \varepsilon_{cc.cr.spc}(x_{cr.spc})}{d_p} \qquad \kappa_{cr.spc} = 1.022 \times 10^{-3}\,\frac{1}{m}$$

Moment

$$M_{cr.spc} := \int_0^{x_{cr.spc}} \sigma_c\left(\varepsilon_{c.cr.spc}(z, x_{cr.spc})\right)\cdot b(z)\cdot z\, dz \ldots + \sigma_s\left(\varepsilon_{s.cr.spc}(x_{cr.spc})\right)\cdot A_s \cdot d_s \ldots + \sigma_p\left(\varepsilon_{p.cr.spc}(x_{cr.spc})\right)\cdot A_p \cdot d_p + \varepsilon_{f.cr.spc}(x_{cr.spc})\cdot E_f \cdot A_f \cdot d_f$$

$$\frac{M_{cr.spc}}{M_{cr.pc}} - 1 = 50.422\cdot\% \qquad M_{cr.spc} = 183.619\cdot kN\cdot m$$

Stress in the top concrete fibre $\sigma_c\left(\varepsilon_{cc.cr.spc}\left(x_{cr.spc}\right)\right) = -10.1\cdot MPa$

Stress in steel reinforcement $\sigma_s\left(\varepsilon_{s.cr.spc}\left(x_{cr.spc}\right)\right) = -140.946\cdot MPa$

Stress in prestressing steel $\sigma_p\left(\varepsilon_{p.cr.spc}\left(x_{cr.spc}\right)\right) = 1247.306\cdot MPa$

Stress in CFRP reinforcement $\varepsilon_{f.cr.spc}\left(x_{cr.spc}\right)\cdot E_f = 850.823\cdot MPa$

Cracking load $q_{cr.spc} := \frac{8\cdot M_{cr.spc}}{l_0^{\,2}}$ $q_{cr.spc} = 7.084\cdot\frac{kN}{m}$

Stress limitations according to fib 14 section 4.6.2

For top concrete fibre

$0.45\cdot f_{ck} = 22.5\cdot MPa$ $\sigma_c\left(\varepsilon_{cc.cr.spc}\left(x_{cr.spc}\right)\right) \geq -0.45\cdot f_{ck} = 1$

For steel reinforcement

$0.8\cdot f_{yk} = 400\cdot MPa$ $\left|\sigma_s\left(\varepsilon_{s.cr.spc}\left(x_{cr.spc}\right)\right)\right| \leq 0.8\cdot f_{yk} = 1$

For prestressing steel

$0.8\cdot f_{p0.1k} = 1334\cdot MPa$ $\sigma_p\left(\varepsilon_{p.cr.spc}\left(x_{cr.spc}\right)\right) \leq 0.8\cdot f_{p0.1k} = 1$

For CFRP laminate

$0.8\cdot f_{fuk} = 2480\cdot MPa$ $\varepsilon_{f.cr.spc}\left(x_{cr.spc}\right)\cdot E_f \leq 0.8\cdot f_{fuk} = 1$

B.5.4 Prestressing steel yield initiation (y)

Guess value $x_g := \frac{h}{4}$

Concrete strain at the level of prestressing steel

$\varepsilon_{cp.y.spc} := \varepsilon_{py} - \varepsilon_{p0inf}$ $\varepsilon_{cp.y.spc} = 6.163 \times 10^{-4}$

Concrete strain in top fibre

$$\varepsilon_{cc.y.spc}\left(x_y\right) := \varepsilon_{cp.y.spc}\cdot\left(1 - \frac{d_p}{d_p - x_y}\right)$$

Concrete strain distribution

$$\varepsilon_{c.y.spc}\left(z, x_y\right) := \varepsilon_{cc.y.spc}\left(x_y\right) + \frac{\varepsilon_{cp.y.spc} - \varepsilon_{cc.y.spc}\left(x_y\right)}{d_p}\cdot z$$

Strain in the steel reinforcement

$$\varepsilon_{s.y.spc}\left(x_y\right) := \varepsilon_{c.y.spc}\left(d_s, x_y\right) - \varepsilon_{cs}$$

Concrete strain in the level of the CFRP

$$\varepsilon_{cf.y.spc}(x_y) := \varepsilon_{c.y.spc}(d_f, x_y)$$

Total strain in CFRP reinforcement

$$\varepsilon_{f.y.spc}(x_y) := \varepsilon_{f0} + \varepsilon_{cf.y.spc}(x_y) - \varepsilon_{cf.pca}$$

Horizontal equilibrium

$$F_{y.spc}(x_y) := \int_0^{x_y} \sigma_c\left(\varepsilon_{c.y.spc}(z, x_y)\right)\cdot b(z)\, dz + \sigma_s\left(\varepsilon_{s.y.spc}(x_y)\right)\cdot A_s + \sigma_p(\varepsilon_{py})\cdot A_p \cdots + \varepsilon_{f.y.spc}(x_y)\cdot E_f \cdot A_f$$

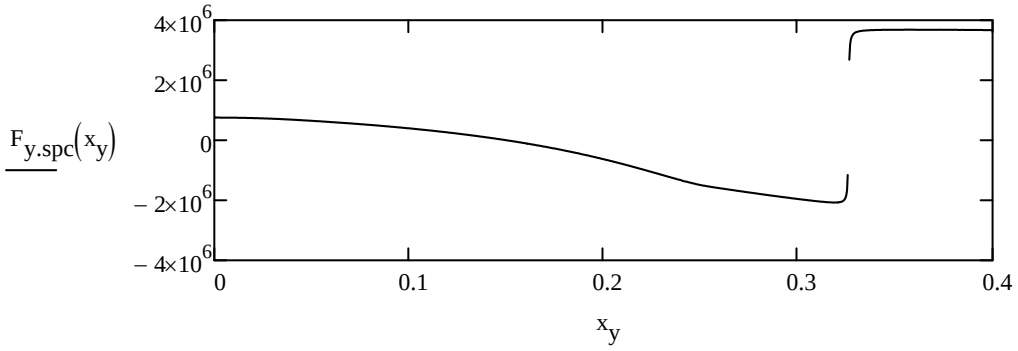

Location of neutral axis

$$x_{y.spc} := \text{root}\left(F_{y.spc}(x_g), x_g\right) \qquad x_{y.spc} = 149.672\cdot\text{mm}$$

If Mathcad is unable to determine the location of the neutral axis even for an updated guess value, "Enable Evaluation" of the graph above and use the Trace function to determine its position. Right click and choose "Enable Evaluation" and manually enter the value here. Right click on the variable and choose "Disable Evaluation" if a value is found automatically.

$$x_{y.spc} := 163.27\text{mm}$$

$$F_{y.spc}(x_{y.spc}) = -0\ \text{N}$$

Curvature

$$\kappa_{y.spc} := \frac{\varepsilon_{cp.y.spc} - \varepsilon_{cc.y.spc}(x_{y.spc})}{d_p} \qquad \kappa_{y.spc} = 3.495 \times 10^{-3}\ \frac{1}{\text{m}}$$

Moment

$$M_{y.spc} := \int_0^{x_{y.spc}} \sigma_c\left(\varepsilon_{c.y.spc}(z, x_{y.spc})\right)\cdot b(z)\cdot z\, dz + \sigma_s\left(\varepsilon_{s.y.spc}(x_{y.spc})\right)\cdot A_s\cdot d_s \cdots + \sigma_p(\varepsilon_{py})\cdot A_p\cdot d_p + \varepsilon_{f.y.spc}(x_{y.spc})\cdot E_f\cdot A_f\cdot d_f$$

$$M_{y.spc} = 229.931\cdot\text{kN}\cdot\text{m}$$

Stress in top concrete fibre $\qquad \varepsilon_{cc.y.spc}(x_{y.spc}) = -5.231 \times 10^{-4}$

Stress in steel reinforcement $\sigma_s\left(\varepsilon_{s.y.spc}\left(x_{y.spc}\right)\right) = -167.143 \cdot MPa$

Stress in CFRP laminate $\varepsilon_{f.y.spc}\left(x_{y.spc}\right) \cdot E_f = 961 \cdot MPa$

Yielding load $q_{y.spc} := \frac{8 \cdot M_{y.spc}}{l_0^{\,2}}$ $q_{y.spc} = 8.871 \cdot \frac{kN}{m}$

B.5.5 Concrete crushing (cc)

Guess value $x_g := t_f$

Concrete strain in top fibre

$\varepsilon_{cc.u.cc.spc} := -\varepsilon_{cu}$

Concrete strain distribution

$\varepsilon_{c.u.cc.spc}\left(z, x_u\right) := \varepsilon_{cc.u.cc.spc} + \frac{-\varepsilon_{cc.u.cc.spc}}{x_u} \cdot z$

Strain in steel reinforcement

$\varepsilon_{s.u.cc.spc}\left(x_u\right) := \varepsilon_{c.u.cc.spc}\left(d_s, x_u\right) - \varepsilon_{cs}$

Concrete strain in level of prestressing steel

$\varepsilon_{cp.u.cc.spc}\left(x_u\right) := \varepsilon_{c.u.cc.spc}\left(d_p, x_u\right)$

Total prestressing steel strain

$\varepsilon_{p.u.cc.spc}\left(x_u\right) := \varepsilon_{p0inf} - \varepsilon_{cs} + \varepsilon_{cp.u.cc.spc}\left(x_u\right)$

Concrete strain in level of the CFRP

$\varepsilon_{cf.u.cc.spc}\left(x_u\right) := \varepsilon_{c.u.cc.spc}\left(d_f, x_u\right)$

Total CFRP strain

$\varepsilon_{f.u.cc.spc}\left(x_u\right) := \varepsilon_{f0} + \varepsilon_{cf.u.cc.spc}\left(x_u\right) - \varepsilon_{cf.pca}$

Horizontal equilibrium

$$F_{u.cc.spc}\left(x_u\right) := \int_0^{x_u} \sigma_c\left(\varepsilon_{c.u.cc.spc}\left(z, x_u\right)\right) \cdot b(z)\, dz + \sigma_s\left(\varepsilon_{s.u.cc.spc}\left(x_u\right)\right) \cdot A_s \cdots + \sigma_p\left(\varepsilon_{p.u.cc.spc}\left(x_u\right)\right) \cdot A_p + \varepsilon_{f.u.cc.spc}\left(x_u\right) \cdot E_{fd} \cdot A_f$$

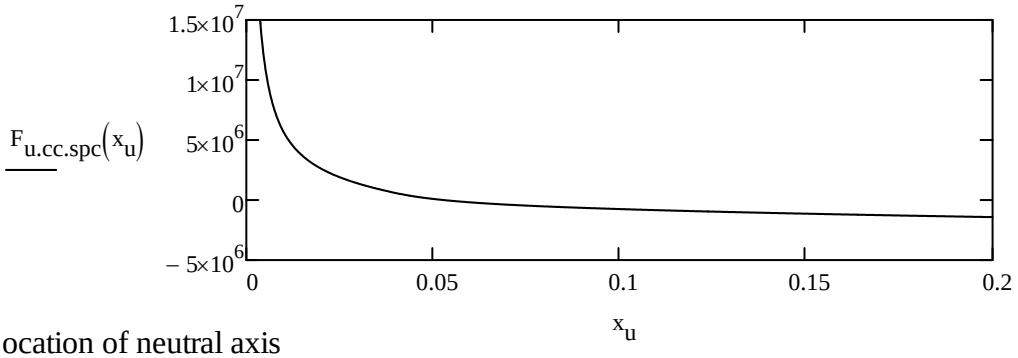

Location of neutral axis

$x_{u.cc.spc} := \text{root}\left(F_{u.cc.spc}\left(x_g\right), x_g\right)$ $\quad x_{u.cc.spc} = 52.434 \cdot \text{mm}$

If Mathcad is unable to determine the location of the neutral axis even for an updated guess value, "Enable Evaluation" of the graph above and use the Trace function to determine its position. Right click and choose "Enable Evaluation" and manually enter the value here. Right click on the variable and choose "Disable Evaluation" if a value is found automatically.

$x_{u.cc.spc} := 0.057\text{m}$

$F_{u.cc.spc}\left(x_{u.cc.spc}\right) = 0\ \text{N}$

Curvature

$$\kappa_{u.cc.spc} := \frac{\varepsilon_{cp.u.cc.spc}\left(x_{u.cc.spc}\right) + \varepsilon_{cu}}{d_p} \qquad \kappa_{u.cc.spc} = 0.067\ \frac{1}{\text{m}}$$

Moment

$$\begin{aligned} M_{u.cc.spc} := & \int_0^{x_{u.cc.spc}} \sigma_c\left(\varepsilon_{c.u.cc.spc}\left(z, x_{u.cc.spc}\right)\right) \cdot b(z) \cdot z \, dz \ \ldots \\ & + \sigma_s\left(\varepsilon_{s.u.cc.spc}\left(x_{u.cc.spc}\right)\right) \cdot A_s \cdot d_s \ \ldots \\ & + \sigma_p\left(\varepsilon_{p.u.cc.spc}\left(x_{u.cc.spc}\right)\right) \cdot A_p \cdot d_p \ \ldots \\ & + \varepsilon_{f.u.cc.spc}\left(x_{u.cc.spc}\right) \cdot E_{fd} \cdot A_f \cdot d_f \end{aligned} \qquad M_{u.cc.spc} = 497.058 \cdot \text{kN} \cdot \text{m}$$

Stress in steel reinforcement $\quad \sigma_s\left(\varepsilon_{s.u.cc.spc}\left(x_{u.cc.spc}\right)\right) = -434.783 \cdot \text{MPa}$

Stress in prestressing steel $\quad \sigma_p\left(\varepsilon_{p.u.cc.spc}\left(x_{u.cc.spc}\right)\right) = 1572.619 \cdot \text{MPa}$

Stress in CFRP laminate $\quad \varepsilon_{f.u.cc.spc}\left(x_{u.cc.spc}\right) \cdot E_{fd} = 3737.369 \cdot \text{MPa}$

Check $\quad \varepsilon_{f.u.cc.spc}\left(x_{u.cc.spc}\right) < \varepsilon_{fud} = 0$ $\quad$ 1 = OK, 0 = Not OK

B.5.6 Rupture of CFRP laminate (rc)

Guess value $\quad x_g := t_f$

Additional strain until CFRP reinforcement rupture

$$\varepsilon_{cf.u.rc.spc} := \varepsilon_{fud} - \varepsilon_{f0} + \varepsilon_{cf.pca} \qquad \varepsilon_{cf.u.rc.spc} = 0.011$$

Concrete strain in top fibre

$$\varepsilon_{cc.u.rc.spc}(x_u) := \varepsilon_{cf.u.rc.spc} \cdot \left(1 - \frac{d_f}{d_f - x_u}\right)$$

Concrete strain distribution

$$\varepsilon_{c.u.rc.spc}(z, x_u) := \varepsilon_{cc.u.rc.spc}(x_u) + \frac{\varepsilon_{cf.u.rc.spc} - \varepsilon_{cc.u.rc.spc}(x_u)}{d_f} \cdot z$$

Strain in steel reinforcement

$$\varepsilon_{s.u.rc.spc}(x_u) := \varepsilon_{c.u.rc.spc}(d_s, x_u) - \varepsilon_{cs}$$

Concrete strain in level of prestressing steel

$$\varepsilon_{cp.u.rc.spc}(x_u) := \varepsilon_{c.u.rc.spc}(d_p, x_u)$$

Total prestressing steel strain

$$\varepsilon_{p.u.rc.spc}(x_u) := \varepsilon_{p0inf} - \varepsilon_{cs} + \varepsilon_{cp.u.rc.spc}(x_u)$$

Horizontal equilibrium

$$F_{u.rc.spc}(x_u) := \int_0^{x_u} \sigma_c\left(\varepsilon_{c.u.rc.spc}(z, x_u)\right) \cdot b(z)\, dz + \sigma_s\left(\varepsilon_{s.u.rc.spc}(x_u)\right) \cdot A_s \ldots + \sigma_p\left(\varepsilon_{p.u.rc.spc}(x_u)\right) \cdot A_p + \varepsilon_{fud} \cdot E_{fd} \cdot A_f$$

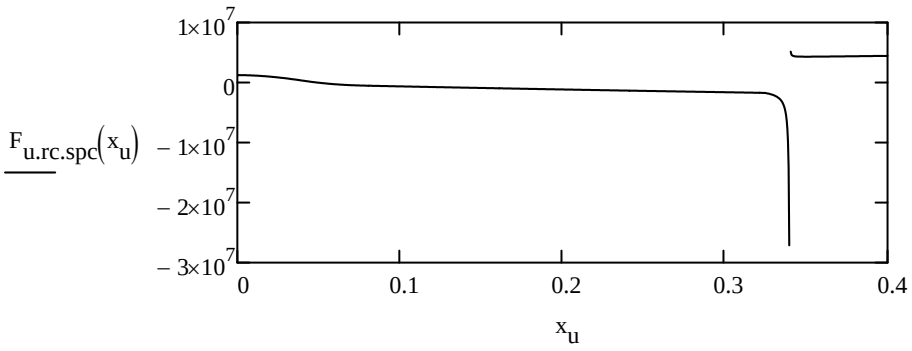

Location of neutral axis

$$x_{u.rc.spc} := \text{root}\left(F_{u.rc.spc}(x_g), x_g\right) \qquad x_{u.rc.spc} = 48.309 \cdot \text{mm}$$

If Mathcad is unable to determine the location of the neutral axis even for an updated guess value, "Enable Evaluation" of the graph above and use the Trace function to determine its position. Right click and choose "Enable Evaluation" and manually enter the value here. Right click on the variable and choose "Disable

$$x_{u.rc.spc} := 47.63\text{mm}$$

Evaluation" if a value is found automatically.

$$F_{u.rc.spc}\left(x_{u.rc.spc}\right) = 0\,N$$

Curvature

$$\kappa_{u.rc.spc} := \frac{\varepsilon_{cf.u.rc.spc} - \varepsilon_{cc.u.rc.spc}\left(x_{u.rc.spc}\right)}{d_f} \qquad \kappa_{u.rc.spc} = 0.038\,\frac{1}{m}$$

Moment

$$M_{u.rc.spc} := \int_0^{x_{u.rc.spc}} \sigma_c\left(\varepsilon_{c.u.rc.spc}\left(z, x_{u.rc.spc}\right)\right)\cdot b(z)\cdot z\,dz + f_{fud}\cdot A_f\cdot d_f \ \ldots$$
$$+ \sigma_s\left(\varepsilon_{s.u.rc.spc}\left(x_{u.rc.spc}\right)\right)\cdot A_s\cdot d_s \ \ldots$$
$$+ \sigma_p\left(\varepsilon_{p.u.rc.spc}\left(x_{u.rc.spc}\right)\right)\cdot A_p\cdot d_p$$

$$\frac{M_{u.rc.spc}}{M_{u.rp.pc}} - 1 = 128.045\cdot\% \qquad M_{u.rc.spc} = 381.736\cdot kN\cdot m$$

Strain in top concrete fibre $\varepsilon_{cc.u.rc.spc}\left(x_{u.rc.spc}\right) = -1.832 \times 10^{-3}$

Stress in top concrete fibre $\sigma_c\left(\varepsilon_{cc.u.rc.spc}\left(x_{u.rc.spc}\right)\right) = -33.097\cdot MPa$

Stress in steel reinforcement $\sigma_s\left(\varepsilon_{s.u.rc.spc}\left(x_{u.rc.spc}\right)\right) = -256.75\cdot MPa$

Stress in prestressing steel $\sigma_p\left(\varepsilon_{p.u.rc.spc}\left(x_{u.rc.spc}\right)\right) = 1517.638\cdot MPa$

B.5.7 Determine fictitious initial camber (ci)

$$\kappa_{ci.spc} := \kappa_{aca} - \frac{\kappa_{cr.spc} - \kappa_{aca}}{M_{cr.spc} - M_{aca}\left(x_{aca}, \varepsilon_{cf.aca}\right)}\cdot M_{aca}\left(x_{aca}, \varepsilon_{cf.aca}\right)$$

$$\kappa_{ci.spc} = -3.159 \times 10^{-3}\,\frac{1}{m}$$

B.5.8 Determine governing failure mode

Assume concrete crushing and rupture of prestressing steel occur simultaneously

$$\varepsilon_{cf.crit.spc} := \varepsilon_{fud} - \varepsilon_{f0} + \varepsilon_{cf.pca}$$

$$\varepsilon_{cc.crit.spc} := -\varepsilon_{cu}$$

Strain distribution

$$\varepsilon_{c.crit.spc}(z) := \varepsilon_{cc.crit.spc} + \frac{\varepsilon_{cf.crit.spc} - \varepsilon_{cc.crit.spc}}{d_p}\cdot z$$

Location of the neutral axis

$$x_{crit.spc} := root\left(\varepsilon_{c.crit.spc}\left(x_g\right), x_g\right) \qquad x_{crit.spc} = 78.369 \cdot mm$$

Strain in steel reinforcement

$$\varepsilon_{s.crit.spc} := \varepsilon_{c.crit.pc}\left(d_s\right) - \varepsilon_{cs}$$

Total strain in the prestressing steel

$$\varepsilon_{p.crit.spc} := \varepsilon_{p0inf} - \varepsilon_{cs} + \varepsilon_{c.crit.spc}\left(d_p\right)$$

From horizontal equilibrium, we obtain

$$A_{f.crit} := -\frac{\int_0^{x_{crit.spc}} \sigma_c\left(\varepsilon_{c.crit.spc}(z)\right) \cdot b(z)\, dz + \sigma_s\left(\varepsilon_{s.crit.spc}\right) \cdot A_s + \sigma_p\left(\varepsilon_{p.crit.spc}\right) \cdot A_p}{f_{fud}}$$

$$A_{f.crit} = 501.162 \cdot mm^2$$

Choose correct failure mode based on the critical CFRP reinforcement area

$$M_{u.spc} := \begin{cases} M_{u.rc.spc} & \text{if } A_f \le A_{f.crit} \\ M_{u.cc.spc} & \text{otherwise} \end{cases} \qquad M_{u.spc} = 381.736 \cdot kN \cdot m$$

$$\kappa_{u.spc} := \begin{cases} \kappa_{u.rc.spc} & \text{if } A_f \le A_{f.crit} \\ \kappa_{u.cc.spc} & \text{otherwise} \end{cases} \qquad \kappa_{u.spc} = 0.038\,\frac{1}{m}$$

$$x_{u.spc} := \begin{cases} x_{u.rc.spc} & \text{if } A_f \le A_{f.crit} \\ x_{u.cc.spc} & \text{otherwise} \end{cases} \qquad x_{u.spc} = 0.048\,m$$

$$\varepsilon_{cc.u.spc} := \begin{cases} \varepsilon_{cc.u.rc.spc}\left(x_{u.rc.spc}\right) & \text{if } A_f \le A_{f.crit} \\ \varepsilon_{cc.u.cc.spc} & \text{otherwise} \end{cases} \qquad \varepsilon_{cc.u.spc} = -1.832 \times 10^{-3}$$

$$\varepsilon_{s.u.spc} := \begin{cases} \varepsilon_{s.u.rc.spc}\left(x_{u.rc.spc}\right) & \text{if } A_f \le A_{f.crit} \\ \varepsilon_{s.u.cc.spc}\left(x_{u.cc.spc}\right) & \text{otherwise} \end{cases} \qquad \varepsilon_{s.u.spc} = -1.284 \times 10^{-3}$$

$$\varepsilon_{p.u.spc} := \begin{cases} \varepsilon_{p.u.rc.spc}\left(x_{u.rc.spc}\right) & \text{if } A_f \le A_{f.crit} \\ \varepsilon_{p.u.cc.spc}\left(x_{u.cc.spc}\right) & \text{otherwise} \end{cases} \qquad \varepsilon_{p.u.spc} = 0.017$$

$$\varepsilon_{f.u.spc} := \begin{cases} \varepsilon_{fud} & \text{if } A_f \le A_{f.crit} \\ \varepsilon_{f.u.cc.spc}\left(x_{u.cc.spc}\right) & \text{otherwise} \end{cases} \qquad \varepsilon_{f.u.spc} = 0.016$$

Determine additional loading until failure

$$\Delta M_{u.spc} := M_{u.spc} - M_{pca} \qquad \Delta q_{u.spc} := \frac{8 \cdot \Delta M_{u.spc}}{l_0^{\,2}} \qquad \Delta q_{u.spc} = 11.657 \cdot \frac{kN}{m}$$

Failure load

$$q_{u.spc} := \frac{8 \cdot M_{u.spc}}{l_0^{\,2}} \qquad q_{u.spc} = 14.727 \cdot \frac{kN}{m}$$

Gather moment and curvature results, including yielding step

$$M_{spc.y} := \begin{pmatrix} 0N \cdot m \\ M_{aca}\left(x_{aca}, \varepsilon_{cf.aca}\right) \\ M_{cr.spc} \\ M_{y.spc} \\ M_{u.spc} \end{pmatrix} \qquad \kappa_{spc.y} := \begin{pmatrix} \kappa_{ci.spc} \\ \kappa_{aca} \\ \kappa_{cr.spc} \\ \kappa_{y.spc} \\ \kappa_{u.spc} \end{pmatrix}$$

Gather moment and curvature results, excluding yielding step

$$M_{spc.1} := \begin{pmatrix} 0N \cdot m \\ M_{aca}\left(x_{aca}, \varepsilon_{cf.aca}\right) \\ M_{cr.spc} \\ M_{u.spc} \end{pmatrix} \qquad \kappa_{spc.1} := \begin{pmatrix} \kappa_{ci.spc} \\ \kappa_{aca} \\ \kappa_{cr.spc} \\ \kappa_{u.spc} \end{pmatrix}$$

Determine what results to present, if yielding occurs upon cracking (i.e. yielding momer less than the cracking moment), the moment-curvature relationship should exclude the yielding point from the graph.

$$M_{spc} := \begin{cases} M_{spc.1} & \text{if } M_{y.spc} < M_{cr.spc} \\ M_{spc.y} & \text{otherwise} \end{cases}$$

$$\kappa_{spc} := \begin{cases} \kappa_{spc.1} & \text{if } M_{y.spc} < M_{cr.spc} \\ \kappa_{spc.y} & \text{otherwise} \end{cases}$$

Moment capacity is limited by

- ○ Concrete crushing
- ◉ CFRP reinforcement rupture

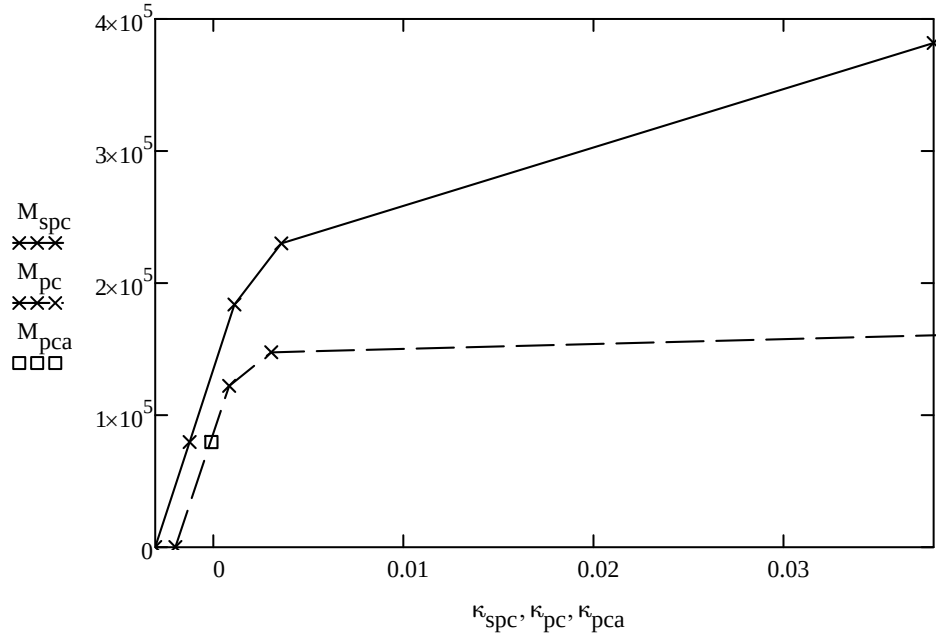

B.5.9 Contributions to the maximum shear stress

External load from Täljsten (2016) and CFRP prestressing force from Al-Emrani (2006)

External load

Additional load after CFRP application up to failure $\Delta q_{u.spc} = 11.657 \cdot \frac{kN}{m}$

Lever arm $z_0 := d_f - x_{u.spc}$ $z_0 = 0.292\,m$

Factor

$$\lambda := \sqrt{\frac{G_a \cdot b_{frp}}{t_a} \cdot \left(\frac{1}{E_{fd} \cdot A_f} + \frac{1}{E_{cd} \cdot A_c} + \frac{z_0}{E_{cd} \cdot W_c} \right)} \qquad \lambda = 38.89 \frac{1}{m}$$

Maximum shear stress

$$\tau_{max.q} := \frac{\Delta q_{u.spc}}{2} \cdot \frac{G_a}{t_a \cdot E_{cd} \cdot W_c} \cdot \frac{\left(a^2 + a \cdot l_0\right) \cdot \lambda + \frac{l_0}{2}}{\lambda^2} \qquad \tau_{max.q} = 7.938 \cdot MPa$$

CFRP prestressing

Factor

$$\omega := \sqrt{\frac{G_a \cdot b_{frp}}{t_a} \cdot \left(\frac{1}{E_f \cdot A_f} + \frac{1}{E_{cm} \cdot A_c} + \frac{h^2}{4 \cdot I_{I.spc} \cdot E_{cm}} \right)} \qquad \omega = 37.052 \frac{1}{m}$$

Maximum shear stress

$$\tau_{max.p} := \frac{P_{f0}}{E_f \cdot A_f} \cdot \frac{G_a}{t_a} \cdot \frac{\tanh\left(\frac{\omega \cdot l_0}{2}\right)}{\omega} = 73.822 \cdot MPa \qquad \tau_{max.p} = 73.822 \cdot MPa$$

B.6 Deflection

Long term load $q_l = 4.7 \cdot \frac{kN}{m}$

Loading prior to CFRP application $q_{pca} = 3.07 \cdot \frac{kN}{m}$

Moment distributions

Moment distribution for a uniformly distributed loa $M_f(x, q) := \frac{q \cdot x \cdot (l_0 - x)}{2}$

Remaining curvature from long term load

Moment contribution $M_\varphi(x) := M_f(x, q_l)$

Curvature $\kappa_\varphi(x) := \frac{M_\varphi(x)}{E_{cm} \cdot I_{I.pc}} \cdot \varphi$

Prior to CFRP application load

Moment contribution $M_{q.pca}(x) := M_f(x, q_{pca})$

Curvature contribution $\kappa_{q.pca}(x) := \frac{M_{q.pca}(x)}{E_{cm} \cdot I_{I.pc}}$

Cracking load

Prior to CFRP application

Moment contribution $M_{q.pc}(x) := M_f(x, q_{cr.pc})$

Curvature contribution $\kappa_{q.pc}(x) := \frac{M_{q.pc}(x)}{E_{cm} \cdot I_{I.pc}}$

After CFRP application

Moment contribution $M_{q.spc}(x) := M_f(x, q_{cr.spc})$

Curvature contribution $\kappa_{q.spc}(x) := \frac{M_{q.spc}(x)}{E_{cm} \cdot I_{I.spc}}$

Prestressing force

Eccentricity $e_p := d_p - x_{gc.pc} \qquad e_p = 202.971 \cdot mm$

Moment contribution $M_p(x) := -(P_{0inf} - F_{cs.p}) \cdot e_p$

Curvature contribution $\kappa_p(x) := \frac{M_p(x)}{E_{c.ef} \cdot I_{I.pc}}$

Shrinkage force

Eccentricity $e_s := d_s - x_{gc.pc}$ $e_s = -98.029 \cdot mm$

Moment contribution $M_{cs.s}(x) := F_{cs.s} \cdot e_s$

Curvature contribution $\kappa_s(x) := \frac{M_{cs.s}(x)}{E_{c.ef} \cdot I_{I.pc}}$

CFRP prestressing force

Eccentricity $e_f := d_f - x_{gc.spc}$ $e_f = 213.043 \cdot mm$

Moment contribution $M_{f.f}(x) := \begin{cases} -P_{f0} \cdot e_f & \text{if } a \le x \le l_0 - a \\ 0N \cdot m & \text{otherwise} \end{cases}$

Curvature contribution $\kappa_f(x) := \frac{M_{f.f}(x)}{E_{cm} \cdot I_{I.spc}}$

Support angle contributions

Function to determine support angle contributio $\theta_A(\kappa) := \int_0^{\frac{l_0}{2}} \kappa(x)\, dx$

From long term load $\theta_{A.\varphi} := \theta_A(\kappa_\varphi) = 0.025$

From cracking load

Unstrengthened $\theta_{A.pc} := \theta_A(\kappa_{q.pc}) = 9.969 \times 10^{-3}$

Strengthened $\theta_{A.spc} := \theta_A(\kappa_{q.spc}) = 0.015$

From prior to CFRP application load $\theta_{A.pca} := \theta_A(\kappa_{q.pca}) = 6.499 \times 10^{-3}$

From prestressing force $\theta_{A.p} := \theta_A(\kappa_p) = -0.037$

From shrinkage force $\theta_{A.s} := \theta_A(\kappa_s) = -2.589 \times 10^{-4}$

From CFRP $\theta_{A.f} := \theta_A(\kappa_f) = -3.861 \times 10^{-3}$

Deflection contributions

Function to determine deflection contributio $\delta_{fn}(x_1, \kappa) := \theta_A(\kappa) \cdot x_1 - \int_0^{x_1} \kappa(x) \cdot (x_1 - x)\, dx$

From long term load $\delta_\varphi(x_1) := \delta_{fn}(x_1, \kappa_\varphi)$

From cracking load $\delta_{q.pc}(x_1) := \delta_{fn}(x_1, \kappa_{q.pc})$

$\delta_{q.spc}(x_1) := \delta_{fn}(x_1, \kappa_{q.spc})$

From prior to CFRP application load $\delta_{q.pca}(x_1) := \delta_{fn}(x_1, \kappa_{q.pca})$

From prestressing force $\delta_p(x_1) := \delta_{fn}(x_1, \kappa_p)$

From shrinkage force $\delta_s(x_1) := \delta_{fn}(x_1, \kappa_s)$

From CFRP prestressing $\delta_f(x_1) := \delta_{fn}(x_1, \kappa_f)$

Deflection in studied states

Deflection prior to CFRP application

$\delta_{pca}(x) := \delta_\varphi(x) + \delta_{q.pca}(x) + \delta_s(x) + \delta_p(x)$

Deflection after CFRP application

$\delta_{aca}(x) := \delta_\varphi(x) + \delta_{q.pca}(x) + \delta_s(x) + \delta_p(x) + \delta_f(x)$

Deflection at cracking load for unstrengthened member

$\delta_{cr.pc}(x) := \delta_\varphi(x) + \delta_{q.pc}(x) + \delta_s(x) + \delta_p(x)$

Deflection at cracking load for strengthened member

$\delta_{cr.spc}(x) := \delta_\varphi(x) + \delta_{q.spc}(x) + \delta_s(x) + \delta_p(x) + \delta_f(x)$

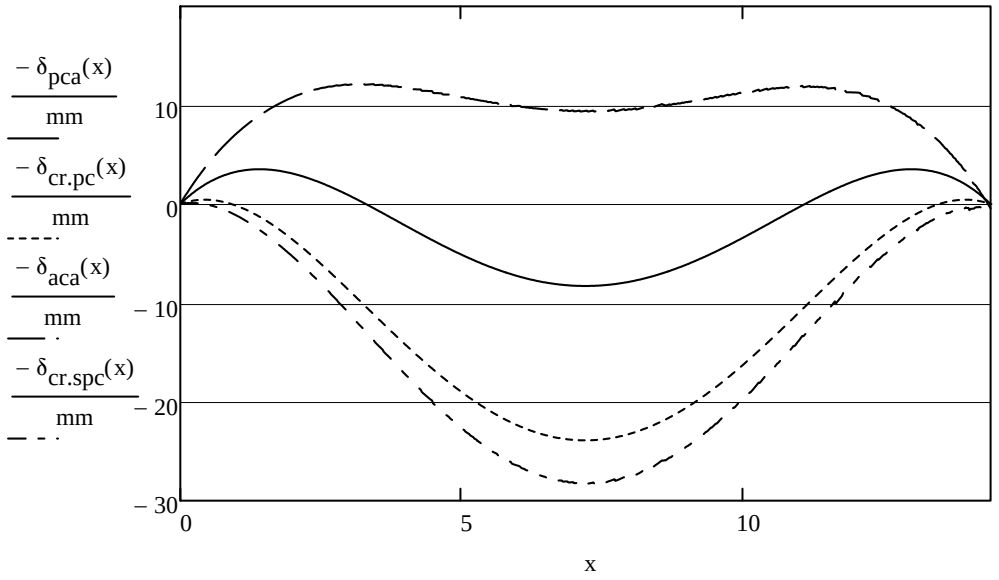

Deflection prior to CFRP application $\delta_{pca}\left(\frac{l_0}{2}\right) = 8.284 \cdot mm$

Deflection after CFRP application $\delta_{aca}\left(\frac{l_0}{2}\right) = -9.431 \cdot mm$

Deflection at cracking load for unstrengthened membe $\delta_{cr.pc}\left(\frac{l_0}{2}\right) = 23.901 \cdot mm$

Deflection at cracking load for strengthened member $\delta_{cr.spc}\left(\frac{l_0}{2}\right) = 28.205 \cdot mm$

For comparison $\frac{l_0}{400} = 36 \cdot mm$

B.7 Summary of results

B.7.1 Case settings

Dimensions of CFRP laminate $b_{frp} = 100 \cdot mm$

$t_{frp} = 1.4 \cdot mm$

Distance to CFRP laminate $d_f = 340 \cdot mm$

Number of laminates $n_f = 2$

Long term loading $q_l = 4.7 \cdot \frac{kN}{m}$

Loading prior to CFRP application $q_{pca} = 3.07 \cdot \frac{kN}{m}$

Prestressing level of CFRP $\mu_f = 30 \cdot \%$

B.7.2 Output

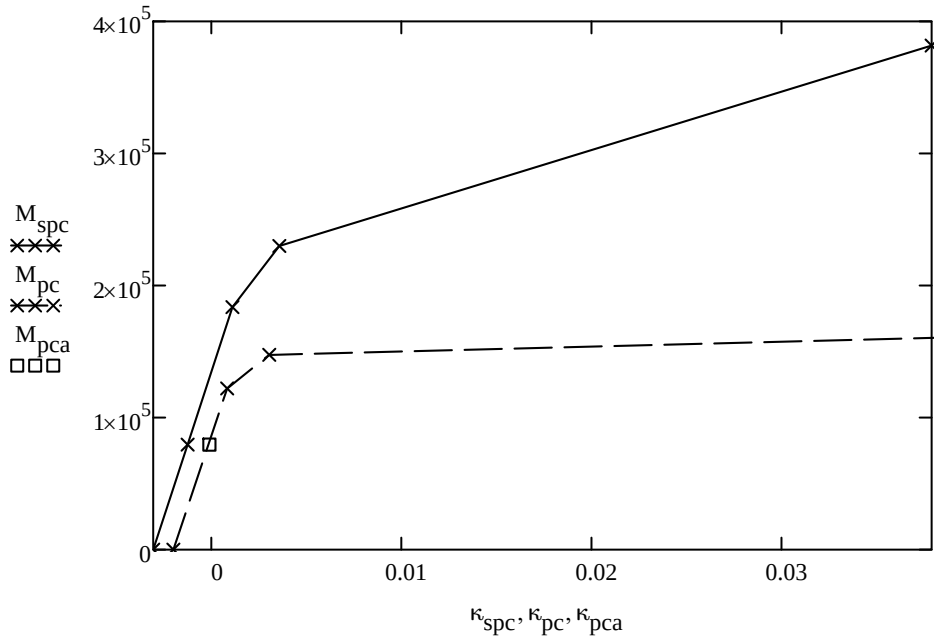

Quick checks

Neutral axises which are expected to be positive

Cracking $x_{cr.spc} \geq 0 = 1$

Yielding $x_{y.spc} \geq 0 = 1$

Failure $x_{u.spc} \geq 0 = 1$

Stress limitations according to fib 14 section 4.6.2

For top concrete fibre $\sigma_c\left(\varepsilon_{cc.cr.spc}\left(x_{cr.spc}\right)\right) \geq -0.45 \cdot f_{ck} = 1$

For steel reinforcement $\left|\sigma_s\left(\varepsilon_{s.cr.spc}\left(x_{cr.spc}\right)\right)\right| \leq 0.8 \cdot f_{yk} = 1$

For prestressing steel $\sigma_p\left(\varepsilon_{p.cr.spc}\left(x_{cr.spc}\right)\right) \leq 0.8 \cdot f_{p0.1k} = 1$

For CFRP laminate $\varepsilon_{f.cr.spc}\left(x_{cr.spc}\right) \cdot E_f \leq 0.8 \cdot f_{fuk} = 1$

SPC

Initial camber

Curvature $\kappa_{ci.spc} \cdot 10^3 = -3.159 \frac{1}{m}$

After CFRP application

CFRP prestressing force $P_{f0} = 208.32 \cdot kN$

Location of neutral axis $x_{aca} = -37.591 \cdot mm$

Curvature $\kappa_{aca} \cdot 10^3 = -1.35 \frac{1}{m}$

Stress in top concrete fibre $\sigma_c\left(\varepsilon_{cc.aca}\left(x_{aca}, \varepsilon_{cf.aca}\right)\right) = -1.667 \cdot MPa$

Stress in steel reinforcement $\sigma_s\left(\varepsilon_{s.aca}\left(x_{aca}, \varepsilon_{cf.aca}\right)\right) = -96.868 \cdot MPa$

Stress in prestressing steel $\sigma_p\left(\varepsilon_{p.aca}\left(x_{aca}, \varepsilon_{cf.aca}\right)\right) = 1148.76 \cdot MPa$

Stress in CFRP laminate $\varepsilon_{f.aca}\left(\varepsilon_{cf.aca}\right) \cdot E_f = 761.425 \cdot MPa$

Interfacial shear stress due to prestressing $\tau_{max.p} = 73.822 \cdot MPa$

Deflection $\delta_{aca}\left(\frac{l_0}{2}\right) = -9.431 \cdot mm$

Cracking

Location of neutral axis $x_{cr.spc} = 323.28 \cdot mm$

Curvartue $\kappa_{cr.spc} \cdot 10^3 = 1.022 \frac{1}{m}$

Cracking load $q_{cr.spc} = 7.084 \cdot \frac{kN}{m}$

Cracking moment $M_{cr.spc} = 183.619 \cdot kN \cdot m$

Stress in top concrete fibre $\sigma_c\left(\varepsilon_{cc.cr.spc}\left(x_{cr.spc}\right)\right) = -10.1 \cdot MPa$

Stress in steel reinforcement $\sigma_s\left(\varepsilon_{s.cr.spc}\left(x_{cr.spc}\right)\right) = -140.946 \cdot MPa$

Stress in prestressing steel $\sigma_p\left(\varepsilon_{p.cr.spc}\left(x_{cr.spc}\right)\right) = 1247.31 \cdot MPa$

Stress in CFRP laminate $\varepsilon_{f.cr.spc}\left(x_{cr.spc}\right) \cdot E_f = 850.823 \cdot MPa$

Deflection $\delta_{cr.spc}\left(\frac{l_0}{2}\right) = 28.205 \cdot mm$

Yielding

Location of neutral axis $x_{y.spc} = 149.672 \cdot mm$

Curvartue $\kappa_{y.spc} \cdot 10^3 = 3.495 \frac{1}{m}$

Yielding load $q_{y.spc} = 8.871 \cdot \frac{kN}{m}$

Yielding moment $M_{y.spc} = 229.931 \cdot kN \cdot m$

Stress in top concrete fibre $\sigma_c\left(\varepsilon_{cc.y.spc}\left(x_{y.spc}\right)\right) = -15.156 \cdot MPa$

Stress in steel reinforcement $\sigma_s\left(\varepsilon_{s.y.spc}\left(x_{y.spc}\right)\right) = -167.143 \cdot MPa$

Stress in CFRP laminate $\varepsilon_{f.y.spc}\left(x_{y.spc}\right) \cdot E_f = 961 \cdot MPa$

Failure

Moment capacity is limited by

- ○ Concrete crushing
- ◉ CFRP reinforcement rupture

Location of neutral axis $x_{u.spc} = 48.309 \cdot mm$

Curvartue $\kappa_{u.spc} \cdot 10^3 = 37.914 \frac{1}{m}$

Failure load $q_{u.spc} = 14.727 \cdot \frac{kN}{m}$

Failure moment $M_{u.spc} = 381.736 \cdot kN \cdot m$

Strain in top concrete fibre $\varepsilon_{cc.u.spc} \cdot 10^3 = -1.832$

Stress in top concrete fibre $\sigma_c\left(\varepsilon_{cc.u.spc}\right) = -33.097 \cdot MPa$

Stress in steel reinforcement $\sigma_s\left(\varepsilon_{s.u.spc}\right) = -256.75 \cdot MPa$

Stress in prestressing steel $\sigma_p\left(\varepsilon_{p.u.spc}\right) = 1517.638 \cdot MPa$

Stress in CFRP laminate $\varepsilon_{f.u.spc} \cdot E_{fd} = 2480 \cdot MPa$

PC

Initial camber

Location of neutral axis $x_{ci.pc} = 47.554 \cdot mm$

Curvature $\kappa_{ci.pc} \cdot 10^3 = -2.096 \frac{1}{m}$

Prior to CFRP application

Location of neutral axis $x_{pca} = -562.602 \cdot mm$

Curvartue $\kappa_{pca} \cdot 10^3 = -0.192 \frac{1}{m}$

Stress in top concrete fibre $\sigma_c(\varepsilon_{cc.pca}) = -3.51 \cdot MPa$

Stress in steel reinforcement $\sigma_s(\varepsilon_{s.pca}(\varepsilon_{cc.pca}, x_{pca})) = -102.609 \cdot MPa$

Stress in prestressing steel $\sigma_p(\varepsilon_{p.pca}(\varepsilon_{cc.pca}, x_{pca})) = 1212.56 \cdot MPa$

Deflection $\delta_{pca}\left(\frac{l_0}{2}\right) = 8.284 \cdot mm$

Cracking

Location of neutral axis $x_{cr.pc} = 294.842 \cdot mm$

Curvartue $\kappa_{cr.pc} \cdot 10^3 = 0.745 \frac{1}{m}$

Cracking load $q_{cr.pc} = 4.709 \cdot \frac{kN}{m}$

Cracking moment $M_{cr.pc} = 122.069 \cdot kN \cdot m$

Stress in top concrete fibre $\sigma_c(\varepsilon_{cc.cr.pc}(x_{cr.pc})) = -6.923 \cdot MPa$

Stress in steel reinforcement $\sigma_s(\varepsilon_{s.cr.pc}(x_{cr.pc})) = -120.225 \cdot MPa$

Stress in prestressing steel $\sigma_p(\varepsilon_{p.cr.pc}(x_{cr.pc})) = 1251.39 \cdot MPa$

Deflection $\delta_{cr.pc}\left(\frac{l_0}{2}\right) = 23.901 \cdot mm$

Yielding

Location of neutral axis $x_{y.pc} = 118.219 \cdot mm$

Curvartue $\kappa_{y.pc} \cdot 10^3 = 2.966 \frac{1}{m}$

Yielding load $q_{y.pc} = 5.689 \cdot \frac{kN}{m}$

Yielding moment $M_{y.pc} = 147.464 \cdot kN \cdot m$

Stress in top concrete fibre $\sigma_c\left(\varepsilon_{cc.y.pc}\left(x_{y.pc}\right)\right) = -10.663 \cdot MPa$

Stress in steel reinforcement $\sigma_s\left(\varepsilon_{s.y.pc}\left(x_{y.pc}\right)\right) = -135.295 \cdot MPa$

Failure

Moment capacity is limited by ○ Concrete crushing

● Prestressing steel rupture

Location of neutral axis $x_{u.pc} = 24.405 \cdot mm$

Curvartue $\kappa_{u.pc} \cdot 10^3 = 57.25 \frac{1}{m}$

Failure load $q_{u.pc} = 6.458 \cdot \frac{kN}{m}$

Failure moment $M_{u.pc} = 167.395 \cdot kN \cdot m$

Strain in top concrete fibre $\varepsilon_{cc.u.pc} \cdot 10^3 = -1.397$

Stress in top concrete fibre $\sigma_c\left(\varepsilon_{cc.u.pc}\right) = -30.305 \cdot MPa$

Stress in steel reinforcement $\sigma_s\left(\varepsilon_{s.u.pc}\right) = -73.191 \cdot MPa$

Stress in prestressing steel $\sigma_p\left(\varepsilon_{p.u.pc}\right) = 1571.236 \cdot MPa$

C Parameters for the studied double-T slab

Table C.1 Parameter values for concrete, steel reinforcement and prestressing steel.

Parameter	Value
Concrete, C50/60	
Partial factor, γ_c	1.5
Partial factor E-modulus, γ_{cE}	1.2
Creep coefficient, φ	2.5
Characteristic compressive strength, f_{ck}	50 MPa
Low characteristic tensile strength, $f_{ctk0,05}$	2.9 MPa
Mean tensile strength, f_{ctm}	4.1 MPa
Mean modulus of elasticity, E_{cm}	37 GPa
Ultimate compressive strain, ϵ_{cu}	0.0035
Shrinkage strain, ϵ_{cs}	0.0004
Steel reinforcement, B500B	
Partial factor, γ_s	1.15
Characteristic yield strength, f_{yk}	500 MPa
Modulus of elasticity, E_s	200 GPa
Yield strain, ϵ_{sy}	0.002174
Area, A_s	77 mm^2
Distance from top, d_s	25 mm
Prestressing steel, unknown	
Partial factor, γ_p	1.15
Relaxation factor, χ	8.5%
Characteristic yield strength, $f_{p0,1k}$	1640 MPa
Ultimate strength, f_{puk}	1829 MPa
Modulus of elasticity, E_p	200 GPa
Yield strain, ϵ_{py}	0.0075
Characteristic ultimate strain, ϵ_{puk}	0.027
Area, A_p	336 mm^2
Applied prestressing, σ_{p0i}	1450 MPa
Distance from top, d_s	326 mm

Table C.2 Parameter values for CFRP laminate and adhesive.

Parameter	Value
CFRP laminate, StoFRP Plate S	
Partial factor, γ_f	1.25
Partial factor E-modulus, γ_{fE}	1.1
Ultimate strength, f_{puk}	3100 MPa
Modulus of elasticity, E_f	170 GPa
Area, A_f	Depending on case
Distance from top, d_f	Depending on case
Adhesive, StoPox SK 41	
Modulus of elasticity, E_a	2 GPa
Poison's ratio, ν_a	0.3

D Raw data from case study

Limitations		
Concrete stress limit after strengthening	0	MPa
Concrete stress limit	-22,5	MPa
Reinforcement steel stress limit	400	MPa
Prestressing steel stress limit	1334	MPa
CFRP stress limit	2480	MPa
Maximum prestressing force per laminate	120	kN
Maximum allowable deflection	36	mm

Permanent loads	
Double-T slab	1,96 kN/m^2
Installations	0,3 kN/m^2
Insulation/membrane	0,06 kN/m^2
Protective layer	0,5 kN/m^3
Sedum	0,5 kN/m^2
Soil	16 kN/m^3

Variable loads	
Imposed load, q_k =	3,0 kN/m^2
Snow load, s_k =	1,5 kN/m^2
Shape coeff., μ =	0,8

Widths/depths/thicknesses	
Double-T slab width	1,198 m
Soil depth	0,1 m
Thickness protective layer	0,05 m

Permanent loads [kN/m^2]	
Double-T slab	1,96 kN/m^2
Installations	0,3 kN/m^2
Insulation/membrane	0,06 kN/m^2
Protective layer	0,025 kN/m^2
Sedum	0,5 kN/m^2
Soil	1,6 kN/m^2

Variable loads [kN/m^2]	
Imposed load, q_k =	3,0 kN/m^2
Snow load, $s_k \cdot \mu$ =	1,2 kN/m^2

Load combination and load combination factors

Combination	Permanent loads			Variable loads			
	General roof components	Sedum	Soil	Imposed		Snow	
					ψ_0		ψ_0
SLS 1	1		1			1	
SLS 2	1	1		1			
ULS 1: 6.10a	1,35		1,35			1,5	0,6
ULS 1: 6.10b	1,2		1,2			1,5	
ULS 2: 6.10a	1,35	1,35		1,5	0,7		
ULS 2: 6.10b	1,2	1,2		1,5			

Design loads

Combination	kN/m^2	kN/m	Governing eq.
SLS 1	5,15	6,16	
SLS 2	5,85	7,00	kN/m
ULS 1: 6.10a	6,41	7,67	7,83
ULS 1: 6.10b	6,53	7,83	
ULS 2: 6.10a	6,99	8,37	9,48
ULS 2: 6.10b	7,91	9,48	

Input

CFRP	
Dimensions [mm²]	80x1,4
Number of laminates	1
Placement	Bottom
Long term load [kN/m]	4,7
Load before strengthening [kN/m]	3,85

	Initial camber		Prior to strengthening						P_{tr} [kN]		After strengthening							Cracking								Yielding								Failure								ΔM [%]		Utilisation ratios for cracking (SLS) and failure (ULS)				Requirements fulfilled	Ductility index
Beam type	x [mm]	κ ·10⁻³ [1/m]	x [mm]	κ ·10⁻³ [1/m]	σ_{ut} [MPa]	σ_t [MPa]	σ_p [MPa]	δ [mm]	Total	per lamina/m	x [mm]	κ ·10⁻³ [1/m]	σ_{cc} [MPa]	σ_s [MPa]	σ_p [MPa]	σ_{cf} [MPa]	τ_{max} [MPa]	δ [mm]	x [mm]	κ ·10⁻³ [1/m]	q [kN/m]	M [kNm]	σ_{cc} [MPa]	σ_s [MPa]	σ_p [MPa]	σ_f [MPa]	δ [mm]	x [mm]	κ ·10⁻³ [1/m]	q [kN/m]	M [kNm]	σ_{cc} [MPa]	σ_s [MPa]	σ_p [MPa]	σ_f [MPa]	x [mm]	κ ·10⁻³ [1/m]	q [kN/m]	M [kNm]	ε_{cu} [%]	σ_{cc} [MPa]	σ_s [MPa]	σ_p [MPa]	σ_f [MPa]	Failure mode	Cracking	Failure	SLS 1	SLS 2	ULS 1	ULS 2		
PC	48	-2,096							-	-	-	-	-	-	-	-	-	-	295	0,745	4,71	122,1	-6,9	-120,2	1251,4	-	23,9	118	2,966	5,69	147,5	-10,7	-135,3	1450	-	24	57,25	6,46	167,4	-1,397	-30,3	-73,2	1571,2	-	RP	-	-	131%	149%	121%	147%	No	19,3
SPC 10%	-	-2,306							27,8	27,8	201,9	0,074	-4,78	-109,4	1221,8	262	17,6	12,5	298	0,768	4,97	128,9	-7,2	-121,9	1251,1	296	23,0	125	3,059	6,37	165,1	-11,5	-140,9	1450	426	36	39,44	10,34	267,9	-1,418	-30,5	-166,3	1524,1	2480	RC	5,6	60,0	124%	141%	76%	92%	No	12,9
SPC 20%	-	-2,436							55,6	55,6	-1204	-0,114	-4,40	-107,9	1212,0	524	35,3	9,3	303	0,805	5,37	139,3	-7,6	-124,7	1250,5	569	23,6	128	3,118	6,81	176,4	-12,0	-144,5	1450	700	38	35,20	10,28	266,5	-1,323	-29,5	-168,6	1515,0	2480	RC	14,1	59,2	115%	130%	76%	92%	No	11,3
SPC 30%	-	-2,602	625	0,258	-5,2	-110,9	1231,4	15,7	83,3	83,3	-409	-0,304	-4,02	-106,4	1202,0	786	52,9	6,1	307	0,842	5,77	149,6	-8,1	-127,5	1250,0	842	24,1	132	3,178	7,24	187,7	-12,5	-148,1	1450	973	40	30,95	10,23	265,1	-1,225	-28,3	-170,3	1505,8	2480	RC	22,5	58,4	107%	121%	77%	93%	No	9,7
SPC 40%	-	-2,788							111,1	111,1	-224	-0,499	-3,63	-104,9	1191,8	1048	70,5	3,0	311	0,880	6,17	159,9	-8,5	-130,3	1249,4	1114	24,7	136	3,238	7,68	199,0	-13,0	-151,7	1450	1247	42	26,69	10,17	263,6	-1,125	-27,0	-171,6	1496,6	2480	RC	31,0	57,4	100%	113%	77%	93%	No	8,2
SPC 50%	-	-2,986							138,9	138,9	-142	-0,697	-3,23	-103,4	1181,4	1309	88,2	0,4	315	0,918	6,57	170,2	-8,9	-133,2	1248,8	1387	25,9	139	3,298	8,11	210,2	-13,5	-155,3	1450	1520	46	22,44	10,11	262,0	-1,026	-25,4	-173,0	1487,5	2480	RC	39,4	56,5	94%	107%	77%	94%	No	6,8

Input

CFRP	
Dimensions [mm²]	100x1,4
Number of laminates	2
Placement	On the sides
Long term load [kN/m]	4,7
Load before strengthening [kN/m]	3,85

	Initial camber		Prior to strengthening						P_{tr} [kN]		After strengthening							Cracking								Yielding								Failure								ΔM [%]		Utilisation ratios for cracking (SLS) and failure (ULS)				Requirements fulfilled	Ductility index
Beam type	x [mm]	κ ·10⁻³ [1/m]	x [mm]	κ ·10⁻³ [1/m]	σ_{ut} [MPa]	σ_t [MPa]	σ_p [MPa]	δ [mm]	Total	per lamina/m	x [mm]	κ ·10⁻³ [1/m]	σ_{cc} [MPa]	σ_s [MPa]	σ_p [MPa]	σ_{cf} [MPa]	τ_{max} [MPa]	δ [mm]	x [mm]	κ ·10⁻³ [1/m]	q [kN/m]	M [kNm]	σ_{cc} [MPa]	σ_s [MPa]	σ_p [MPa]	σ_f [MPa]	δ [mm]	x [mm]	κ ·10⁻³ [1/m]	q [kN/m]	M [kNm]	σ_{cc} [MPa]	σ_s [MPa]	σ_p [MPa]	σ_f [MPa]	x [mm]	κ ·10⁻³ [1/m]	q [kN/m]	M [kNm]	ε_{cu} [%]	σ_{cc} [MPa]	σ_s [MPa]	σ_p [MPa]	σ_f [MPa]	Failure mode	Cracking	Failure	SLS 1	SLS 2	ULS 1	ULS 2		
PC	48	-2,096							-	-	-	-	-	-	-	-	-	-	295	0,745	4,71	122,1	-6,9	-120,2	1251,4	-	23,9	118	2,966	5,69	147,5	-10,7	-135,3	1450	-	24	57,25	6,46	167,4	-1,397	-30,3	-73,2	1571,2	-	RP	-	-	131%	149%	121%	147%	No	19,3
SPC 10%	-	-2,376							69,4	34,7	-1465	-0,097	-4,59	-109,0	1211,8	255	24,6	9,6	305	0,827	5,41	140,3	-7,9	-126,3	1250,2	290	24,0	132	3,183	7,01	181,8	-12,6	-148,3	1450	398	44	48,53	14,84	384,8	-2,130	-33,3	-263,3	1540,1	2480	RC	14,9	129,9	114%	129%	53%	64%	No	15,2
SPC 20%	-	-2,717							138,9	69,4	-266	-0,467	-4,01	-107,1	1191,5	510	49,2	3,4	315	0,920	6,22	161,3	-9,0	-133,4	1248,8	562	25,5	141	3,333	7,92	205,2	-13,8	-157,4	1450	671	46	43,37	14,79	383,3	-1,983	-33,3	-259,7	1529,2	2480	RC	32,2	129,0	99%	112%	53%	64%	No	13,0
SPC 30%	-	-3,112	625	0,258	-5,2	-110,9	1231,4	15,7	208,3	104,2	-123	-0,853	-3,40	-105,2	1170,2	764	73,8	-2,0	323	1,016	7,03	182,3	-10,0	-140,5	1247,4	834	27,7	149	3,485	8,81	228,5	-15,1	-166,6	1450	944	48	38,24	14,73	381,8	-1,840	-33,1	-256,9	1518,3	2480	RC	49,3	128,1	88%	100%	53%	64%	Yes	11,0
SPC 40%	-	-3,543							277,8	138,9	-67	-1,257	-2,77	-103,2	1147,8	1017	98,4	-7,8	330	1,112	7,84	203,2	-11,1	-147,7	1246,0	1106	29,5	157	3,640	9,71	251,6	-16,3	-175,9	1450	1217	51	33,11	14,67	380,2	-1,701	-32,6	-254,8	1507,4	2480	RC	66,5	127,1	79%	89%	53%	65%	No	9,1
SPC 50%	-	-4,008							347,2	173,6	-38	-1,684	-2,10	-101,2	1124,2	1268	123,0	-13,7	335	1,211	8,64	224,0	-12,2	-155,1	1244,5	1377	31,2	164	3,797	10,60	274,7	-17,5	-185,3	1450	1490	56	27,98	14,60	378,5	-1,565	-31,8	-253,0	1496,5	2480	RC	83,5	126,1	71%	81%	54%	65%	No	7,4

Input

CFRP	
Dimensions [mm²]	120x1,4
Number of laminates	2
Placement	On the sides
Long term load [kN/m]	4,7
Load before strengthening [kN/m]	3,85

	Initial camber		Prior to strengthening						P_{tr} [kN]		After strengthening							Cracking								Yielding								Failure								ΔM [%]		Utilisation ratios for cracking (SLS) and failure (ULS)				Requirements fulfilled	Ductility index
Beam type	x [mm]	κ ·10⁻³ [1/m]	x [mm]	κ ·10⁻³ [1/m]	σ_{ut} [MPa]	σ_t [MPa]	σ_p [MPa]	δ [mm]	Total	per lamina/m	x [mm]	κ ·10⁻³ [1/m]	σ_{cc} [MPa]	σ_s [MPa]	σ_p [MPa]	σ_{cf} [MPa]	τ_{max} [MPa]	δ [mm]	x [mm]	κ ·10⁻³ [1/m]	q [kN/m]	M [kNm]	σ_{cc} [MPa]	σ_s [MPa]	σ_p [MPa]	σ_f [MPa]	δ [mm]	x [mm]	κ ·10⁻³ [1/m]	q [kN/m]	M [kNm]	σ_{cc} [MPa]	σ_s [MPa]	σ_p [MPa]	σ_f [MPa]	x [mm]	κ ·10⁻³ [1/m]	q [kN/m]	M [kNm]	ε_{cu} [%]	σ_{cc} [MPa]	σ_s [MPa]	σ_p [MPa]	σ_f [MPa]	Failure mode	Cracking	Failure	SLS 1	SLS 2	ULS 1	ULS 2		
PC	48	-2,096							-	-	-	-	-	-	-	-	-	-	295	0,745	4,71	122,1	-6,9	-120,2	1251,4	-	23,9	118	2,966	5,69	147,5	-10,7	-135,3	1450	-	24	57,25	6,46	167,4	-1,397	-30,3	-73,2	1571,2	-	RP	-	-	131%	149%	121%	147%	No	19,3
SPC 10%	-	-2,406							83,3	41,7	-959	-0,147	-4,55	-109,0	1208,8	253	24,5	8,7	307	0,846	5,54	143,7	-8,1	-127,8	1249,9	289	24,3	135	3,223	7,21	186,8	-12,9	-150,8	1450	393	48	50,86	16,21	420,1	-2,418	-33,3	-309,2	1543,5	2480	RC	17,7	150,9	111%	126%	48%	59%	No	15,8
SPC 20%	-	-2,811							166,7	83,3	-212	-0,572	-3,92	-107,1	1185,2	506	49,0	2,2	318	0,959	6,48	168,0	-9,4	-136,2	1248,2	560	26,7	145	3,404	8,25	213,9	-14,4	-161,7	1450	666	49	45,49	16,15	418,7	-2,250	-33,3	-302,6	1532,2	2480	RC	37,6	150,1	95%	108%	48%	59%	No	13,4
SPC 30%	-	-3,279	625	0,258	-5,2	-110,9	1231,4	15,7	250,0	125,0	-98	-1,019	-3,26	-105,2	1160,3	757	73,5	-4,5	327	1,074	7,41	192,2	-10,7	-144,9	1246,5	832	28,8	154	3,588	9,29	240,8	-15,9	-172,8	1450	939	52	40,13	16,10	417,3	-2,087	-33,3	-296,8	1521,0	2480	RC	57,4	149,3	83%	94%	49%	59%	No	11,2
SPC 40%	-	-3,791							333,3	166,7	-53	-1,492	-2,56	-103,1	1133,8	1007	98,0	-11,1	334	1,191	8,34	216,2	-11,9	-153,7	1244,8	1103	30,9	163	3,776	10,32	267,5	-17,3	-184,1	1450	1211	55	34,79	16,04	415,8	-1,929	-33,3	-291,8	1509,7	2480	RC	77,1	148,4	74%	84%	49%	59%	No	9,2
SPC 50%	-	-4,348							416,6	208,3	-28	-1,997	-1,82	-101,1	1105,5	1255	122,5	-17,8	340	1,311	9,27	240,2	-13,2	-162,7	1243,0	1375	32,9	171	3,968	11,35	294,1	-18,8	-195,6	1450	1484	60	29,46	15,97	414,0	-1,774	-32,9	-287,4	1498,4	2480	RC	96,8	147,3	67%	76%	49%	59%	No	7,4

Input

CFRP	
Dimensions [mm^2]	80x1,4
Number of laminates	1
Placement	Bottom
Long term load [kN/m]	4,7
Load before strengthening [kN/m]	3,07

	Initial camber		Prior to strengthening						P_{f0} [kN]	
Beam type	x [mm]	$\kappa \cdot 10^{-3}$ [1/m]	x [mm]	$\kappa \cdot 10^{-3}$ [1/m]	σ_{cc} [MPa]	σ_s [MPa]	σ_p [MPa]	δ [mm]	Total	per laminate
PC	48	-2,096	-563	-0,192	-3,5	-102,6	1212,6	8,3	-	
SPC 10%	-	-2,213							27,8	27,8
SPC 20%	-	-2,397							55,6	55,6
SPC 30%	-	-2,594							83,3	83,3
SPC 40%	-	-2,799							111,1	111,1
SPC 50%	-	-3,014							138,9	138,9

	After strengthening								Cracking								
Beam type	x [mm]	$\kappa \cdot 10^{-3}$ [1/m]	σ_{cc} [MPa]	σ_s [MPa]	σ_p [MPa]	σ_f [MPa]	τ_{max} [MPa]	δ [mm]	x [mm]	$\kappa \cdot 10^{-3}$ [1/m]	q [kN/m]	M [kNm]	σ_{cc} [MPa]	σ_s [MPa]	σ_p [MPa]	σ_f [MPa]	δ [mm]
PC	-	-	-	-	-	-	-	-	295	0,745	4,71	122,1	-6,9	-120,2	1251,4	-	23,9
SPC 10%	-251	-0,383	-3,12	-101,1	1202,6	262	17,6	5,1	298	0,771	5,00	129,7	-7,2	-122,1	1251,0	318	23,3
SPC 20%	-145	-0,576	-2,73	-99,6	1192,4	524	35,3	1,9	303	0,808	5,40	140,1	-7,7	-124,9	1250,5	591	23,9
SPC 30%	-92	-0,774	-2,33	-98,1	1182,0	785	52,9	-1,3	307	0,845	5,80	150,4	-8,1	-127,7	1249,9	863	24,4
SPC 40%	-60	-0,976	-1,92	-96,6	1171,4	1046	70,5	-4,5	311	0,883	6,20	160,7	-8,5	-130,6	1249,4	1136	25,0
SPC 50%	-39	-1,183	-1,51	-95,1	1160,5	1307	88,2	-7,1	315	0,921	6,60	171,0	-9,0	-133,4	1248,8	1409	26,2

	Yielding								Failure									
Beam type	x [mm]	$\kappa \cdot 10^{-3}$ [1/m]	q [kN/m]	M [kNm]	σ_{cc} [MPa]	σ_s [MPa]	σ_p [MPa]	σ_f [MPa]	x [mm]	$\kappa \cdot 10^{-3}$ [1/m]	q [kN/m]	M [kNm]	ε_{cc} [%]	σ_{cc} [MPa]	σ_s [MPa]	σ_p [MPa]	σ_f [MPa]	Failure mode
PC	118	2,966	5,69	147,5	-10,7	-135,3	1450	-	24	57,25	6,46	167,4	-1,397	-30,3	-73,2	1571,2	-	RP
SPC 10%	125	3,063	6,40	166,0	-11,5	-141,2	1450	448	36	39,10	10,33	267,8	-1,410	-30,4	-166,5	1523,4	2480	RC
SPC 20%	129	3,123	6,84	177,3	-12,0	-144,8	1450	722	38	34,86	10,28	266,4	-1,315	-29,4	-168,7	1514,2	2480	RC
SPC 30%	132	3,183	7,28	188,6	-12,6	-148,4	1450	995	40	30,61	10,22	265,0	-1,217	-28,2	-170,4	1505,1	2480	RC
SPC 40%	136	3,243	7,71	199,8	-13,1	-152,0	1450	1269	42	26,35	10,16	263,4	-1,117	-26,8	-171,7	1495,9	2480	RC
SPC 50%	139	3,303	8,14	211,1	-13,6	-155,6	1450	1542	46	22,10	10,10	261,8	-1,018	-25,3	-173,1	1486,8	2480	RC

	ΔM [%]		Utilisation ratios for cracking (SLS) and failure (ULS)				Requirements fulfilled	Ductility index
Beam type	Cracking	Failure	SLS 1	SLS 2	ULS 1	ULS 2		
PC	-	-	131%	149%	121%	147%	No	19,3
SPC 10%	6,3	60,0	123%	140%	76%	92%	No	12,8
SPC 20%	14,8	59,2	114%	130%	76%	92%	No	11,2
SPC 30%	23,2	58,3	106%	121%	77%	93%	No	9,6
SPC 40%	31,7	57,4	99%	113%	77%	93%	No	8,1
SPC 50%	40,1	56,4	93%	106%	77%	94%	No	6,7

Input

CFRP	
Dimensions [mm^2]	100x1,4
Number of laminates	2
Placement	On the sides
Long term load [kN/m]	4,7
Load before strengthening [kN/m]	3,07

	Initial camber		Prior to strengthening						P_{f0} [kN]	
Beam type	x [mm]	$\kappa \cdot 10^{-3}$ [1/m]	x [mm]	$\kappa \cdot 10^{-3}$ [1/m]	σ_{cc} [MPa]	σ_s [MPa]	σ_p [MPa]	δ [mm]	Total	per laminate
PC	48	-2,096	-563	-0,192	-3,5	-102,6	1212,6	8,3	-	
SPC 10%	-	-2,348							69,4	34,7
SPC 20%	-	-2,737							138,9	69,4
SPC 30%	-	-3,159							208,3	104,2
SPC 40%	-	-3,613							277,8	138,9
SPC 50%	-	-4,101							347,2	173,6

	After strengthening								Cracking								
Beam type	x [mm]	$\kappa \cdot 10^{-3}$ [1/m]	σ_{cc} [MPa]	σ_s [MPa]	σ_p [MPa]	σ_f [MPa]	τ_{max} [MPa]	δ [mm]	x [mm]	$\kappa \cdot 10^{-3}$ [1/m]	q [kN/m]	M [kNm]	σ_{cc} [MPa]	σ_s [MPa]	σ_p [MPa]	σ_f [MPa]	δ [mm]
PC	-	-	-	-	-	-	-	-	295	0,745	4,71	122,1	-6,9	-120,2	1251,4	-	23,9
SPC 10%	-160	-0,560	-2,92	-100,7	1192,3	255	24,6	2,1	306	0,832	5,46	141,6	-7,9	-126,8	1250,1	307	24,5
SPC 20%	-75	-0,945	-2,31	-98,8	1171,1	509	49,2	-4,0	315	0,926	6,27	162,6	-9,0	-133,8	1248,7	579	26,0
SPC 30%	-38	-1,347	-1,67	-96,9	1148,8	761	73,8	-9,4	323	1,022	7,08	183,6	-10,1	-140,9	1247,3	851	28,2
SPC 40%	-17	-1,772	-1,00	-94,9	1125,2	1013	98,4	-15,3	330	1,118	7,89	204,5	-11,2	-148,2	1245,9	1123	30,0
SPC 50%	-4	-2,223	-0,29	-92,8	1100,1	1264	123,0	-21,2	336	1,217	8,69	225,3	-12,2	-155,6	1244,4	1394	31,7

	Yielding								Failure									
Beam type	x [mm]	$\kappa \cdot 10^{-3}$ [1/m]	q [kN/m]	M [kNm]	σ_{cc} [MPa]	σ_s [MPa]	σ_p [MPa]	σ_f [MPa]	x [mm]	$\kappa \cdot 10^{-3}$ [1/m]	q [kN/m]	M [kNm]	ε_{cc} [%]	σ_{cc} [MPa]	σ_s [MPa]	σ_p [MPa]	σ_f [MPa]	Failure mode
PC	118,2	2,966	5,69	147,5	-10,7	-135,3	1450	-	24	57,25	6,46	167,4	-1,397	-30,3	-73,2	1571,2	-	RP
SPC 10%	133	3,192	7,07	183,3	-12,6	-148,9	1450	415	44	48,20	14,84	384,7	-2,120	-33,3	-263,0	1539,4	2480	RC
SPC 20%	142	3,343	7,97	206,7	-13,9	-158,0	1450	688	46	43,05	14,79	383,3	-1,974	-33,3	-259,5	1528,5	2480	RC
SPC 30%	150	3,495	8,87	229,9	-15,2	-167,1	1450	961	48	37,91	14,73	381,7	-1,832	-33,1	-256,8	1517,6	2480	RC
SPC 40%	157	3,650	9,76	253,1	-16,4	-176,5	1450	1234	52	32,79	14,67	380,1	-1,693	-32,5	-254,6	1506,7	2480	RC
SPC 50%	164	3,807	10,65	276,1	-17,6	-185,9	1450	1507	56	27,66	14,60	378,4	-1,556	-31,7	-252,9	1495,8	2480	RC

	ΔM [%]		Utilisation ratios for cracking (SLS) and failure (ULS)				Requirements fulfilled	Ductility index
Beam type	Cracking	Failure	SLS 1	SLS 2	ULS 1	ULS 2		
PC	-	-	131%	149%	121%	147%	No	19,3
SPC 10%	16,0	129,8	113%	128%	53%	64%	No	15,1
SPC 20%	33,2	129,0	98%	112%	53%	64%	No	12,9
SPC 30%	50,4	128,0	87%	99%	53%	64%	Yes	10,8
SPC 40%	67,5	127,1	78%	89%	53%	65%	No	9,0
SPC 50%	84,6	126,0	71%	81%	54%	65%	No	7,3

Input

CFRP	
Dimensions [mm^2]	120x1,4
Number of laminates	2
Placement	On the sides
Long term load [kN/m]	4,7
Load before strengthening [kN/m]	3,07

	Initial camber		Prior to strengthening						P_{f0} [kN]	
Beam type	x [mm]	$\kappa \cdot 10^{-3}$ [1/m]	x [mm]	$\kappa \cdot 10^{-3}$ [1/m]	σ_{cc} [MPa]	σ_s [MPa]	σ_p [MPa]	δ [mm]	Total	per laminate
PC	48	-2,096	-563	-0,192	-3,5	-102,6	1212,6	8,3	-	
SPC 10%	-	-2,391							83,3	41,7
SPC 20%	-	-2,843							166,7	83,3
SPC 30%	-	-3,338							250,0	125,0
SPC 40%	-	-3,875							333,3	166,7
SPC 50%	-	-4,460							416,6	208,3

	After strengthening								Cracking								
Beam type	x [mm]	$\kappa \cdot 10^{-3}$ [1/m]	σ_{cc} [MPa]	σ_s [MPa]	σ_p [MPa]	σ_f [MPa]	τ_{max} [MPa]	δ [mm]	x [mm]	$\kappa \cdot 10^{-3}$ [1/m]	q [kN/m]	M [kNm]	σ_{cc} [MPa]	σ_s [MPa]	σ_p [MPa]	σ_f [MPa]	δ [mm]
PC	-	-	-	-	-	-	-	-	295	0,745	4,71	122,1	-6,9	-120,2	1251,4	-	23,9
SPC 10%	-144	-0,613	-2,88	-100,7	1189,2	253	24,5	1,3	308	0,853	5,60	145,1	-8,2	-128,3	1249,8	305	24,9
SPC 20%	-64	-1,054	-2,21	-98,8	1164,5	504	49,0	-5,2	319	0,966	6,54	169,4	-9,5	-136,8	1248,1	577	27,2
SPC 30%	-30	-1,522	-1,51	-96,8	1138,4	754	73,5	-11,9	327	1,081	7,47	193,6	-10,8	-145,4	1246,4	848	29,3
SPC 40%	-11	-2,020	-0,77	-94,7	1110,4	1003	98,0	-18,5	335	1,198	8,40	217,7	-12,0	-154,2	1244,7	1119	31,4
SPC 50%	0	-2,557	0,03	-92,6	1080,2	1250	122,5	-25,2	341	1,318	9,32	241,6	-13,3	-163,2	1242,9	1391	33,4

	Yielding								Failure									
Beam type	x [mm]	$\kappa \cdot 10^{-3}$ [1/m]	q [kN/m]	M [kNm]	σ_{cc} [MPa]	σ_s [MPa]	σ_p [MPa]	σ_f [MPa]	x [mm]	$\kappa \cdot 10^{-3}$ [1/m]	q [kN/m]	M [kNm]	ε_{cc} [%]	σ_{cc} [MPa]	σ_s [MPa]	σ_p [MPa]	σ_f [MPa]	Failure mode
PC	118,2	2,966	5,69	147,5	-10,7	-135,3	1450	-	24	57,25	6,46	167,4	-1,397	-30,3	-73,2	1571,2	-	RP
SPC 10%	135	3,234	7,27	188,4	-13,0	-151,4	1450	409	48	50,54	16,20	420,0	-2,408	-33,3	-308,8	1542,8	2480	RC
SPC 20%	146	3,415	8,31	215,5	-14,5	-162,3	1450	682	50	45,17	16,15	418,6	-2,240	-33,3	-302,2	1531,6	2480	RC
SPC 30%	155	3,599	9,35	242,4	-16,0	-173,4	1450	955	52	39,81	16,10	417,2	-2,078	-33,3	-296,4	1520,3	2480	RC
SPC 40%	163	3,787	10,38	269,1	-17,4	-184,7	1450	1228	56	34,47	16,04	415,7	-1,919	-33,3	-291,5	1509,0	2480	RC
SPC 50%	171	3,979	11,41	295,7	-18,8	-196,3	1450	1501	61	29,14	15,97	413,9	-1,765	-32,9	-287,2	1497,8	2480	RC

	ΔM [%]		Utilisation ratios for cracking (SLS) and failure (ULS)				Requirements fulfilled	Ductility index
Beam type	Cracking	Failure	SLS 1	SLS 2	ULS 1	ULS 2		
PC	-	-	131%	149%	121%	147%	No	19,3
SPC 10%	18,9	150,9	110%	125%	48%	59%	No	15,6
SPC 20%	38,8	150,1	94%	107%	48%	59%	No	13,2
SPC 30%	58,6	149,2	83%	94%	49%	59%	No	11,1
SPC 40%	78,3	148,3	73%	83%	49%	59%	No	9,1
SPC 50%	97,9	147,3	66%	75%	49%	59%	No	7,3

Input

CFRP	
Dimensions [mm²]	80x1,4
Number of laminates	1
Placement	Bottom
Long term load [kN/m]	4,7
Load before strengthening [kN/m]	2,35

	Initial camber		Prior to strengthening						P_{fr} [kN]		After strengthening							Cracking									Yielding							Failure									ΔM [%]		Utilisation ratios for cracking (SLS) and failure (ULS)				Requirements fulfilled	Ductility index
Beam type	x [mm]	κ ·10⁻³ [1/m]	x [mm]	κ ·10⁻³ [1/m]	σ_{α} [MPa]	σ_{t} [MPa]	σ_{fr} [MPa]	δ [mm]	Total	per laminate	x [mm]	κ ·10⁻³ [1/m]	σ_{cc} [MPa]	σ_{s} [MPa]	σ_{fr} [MPa]	σ_{fr} [MPa]	τ_{max} [MPa]	δ [mm]	x [mm]	κ ·10⁻³ [1/m]	q [kN/m]	M [kNm]	σ_{cc} [MPa]	σ_{s} [MPa]	σ_{fr} [MPa]	σ_{fr} [MPa]	δ [mm]	x [mm]	κ ·10⁻³ [1/m]	q [kN/m]	M [kNm]	σ_{α} [MPa]	σ_{s} [MPa]	σ_{fr} [MPa]	σ_{fr} [MPa]	δ [mm]	x [mm]	κ ·10⁻³ [1/m]	q [kN/m]	M [kNm]	ε_{su} [‰]	σ_{cc} [MPa]	σ_{s} [MPa]	σ_{fr} [MPa]	σ_{fr} [MPa]	Failure mode	Cracking	Failure	SLS 1	SLS 2	ULS 1	ULS 2		
PC	48	-2,096							-	-	-	-	-	-	-	-	-	-	295	0,745	4,71	122,1	-6,9	-120,2	1251,4	-	23,9	118	2,966	5,69	147,5	-10,7	-135,3	1450	-	24	57,25	6,46	167,4	-1,397	-30,3	-73,2	1571,2	-	RP	-	-	131%	149%	121%	147%	No	19,3
SPC 10%	-	-2,203							27,8	27,8	-58	-0,814	-1,56	-93,5	1184,2	262	17,6	-1,8	299	0,774	5,04	130,5	-7,3	-122,3	1251,0	338	23,5	125	3,068	6,44	166,9	-11,6	-141,4	1450	469	36	38,78	10,33	267,7	-1,403	-30,4	-166,7	1522,7	2480	RC	6,9	59,9	122%	139%	76%	92%	No	12,6
SPC 20%	-	-2,405							55,6	55,6	-34	-1,015	-1,15	-92,0	1173,6	523	35,3	-5,0	303	0,811	5,43	140,9	-7,7	-125,1	1250,4	611	24,1	129	3,127	6,87	178,2	-12,1	-145,0	1450	742	38	34,54	10,27	266,3	-1,308	-29,3	-168,9	1513,5	2480	RC	15,4	59,1	113%	129%	76%	92%	No	11,0
SPC 30%	-	-2,615	-9,7	-0,617	-2,0	-95,0	1194,5	1,4	83,3	83,3	-18	-1,220	-0,74	-90,5	1162,8	784	52,9	-8,1	308	0,848	5,83	151,2	-8,1	-127,9	1249,9	884	24,7	133	3,187	7,31	189,4	-12,6	-148,6	1450	1016	40	30,29	10,22	264,9	-1,210	-28,1	-170,5	1504,4	2480	RC	23,9	58,2	106%	120%	77%	93%	No	9,5
SPC 40%	-	-2,832							111,1	111,1	-7	-1,430	-0,31	-89,0	1151,6	1044	70,5	-11,3	312	0,886	6,23	161,5	-8,6	-130,8	1249,3	1157	25,3	136	3,247	7,74	200,7	-13,1	-152,2	1450	1289	43	26,03	10,16	263,3	-1,110	-26,7	-171,8	1495,2	2480	RC	32,3	57,3	99%	112%	77%	93%	No	8,0
SPC 50%	-	-3,057							138,9	138,9	2	-1,646	0,12	-87,5	1140,2	1305	88,2	-13,9	315	0,924	6,63	171,8	-9,0	-133,6	1248,8	1430	26,5	140	3,308	8,18	211,9	-13,6	-155,9	1450	1563	46	21,78	10,10	261,7	-1,011	-25,2	-173,3	1486,1	2480	RC	40,8	56,3	93%	106%	78%	94%	No	6,6

Input

CFRP	
Dimensions [mm²]	100x1,4
Number of laminates	2
Placement	On the sides
Long term load [kN/m]	4,7
Load before strengthening [kN/m]	2,35

	Initial camber		Prior to strengthening						P_{fr} [kN]		After strengthening							Cracking									Yielding							Failure									ΔM [%]		Utilisation ratios for cracking (SLS) and failure (ULS)				Requirements fulfilled	Ductility index
Beam type	x [mm]	κ ·10⁻³ [1/m]	x [mm]	κ ·10⁻³ [1/m]	σ_{α} [MPa]	σ_{t} [MPa]	σ_{fr} [MPa]	δ [mm]	Total	per laminate	x [mm]	κ ·10⁻³ [1/m]	σ_{cc} [MPa]	σ_{s} [MPa]	σ_{fr} [MPa]	σ_{fr} [MPa]	τ_{max} [MPa]	δ [mm]	x [mm]	κ ·10⁻³ [1/m]	q [kN/m]	M [kNm]	σ_{cc} [MPa]	σ_{s} [MPa]	σ_{fr} [MPa]	σ_{fr} [MPa]	δ [mm]	x [mm]	κ ·10⁻³ [1/m]	q [kN/m]	M [kNm]	σ_{α} [MPa]	σ_{s} [MPa]	σ_{fr} [MPa]	σ_{fr} [MPa]	δ [mm]	x [mm]	κ ·10⁻³ [1/m]	q [kN/m]	M [kNm]	ε_{su} [‰]	σ_{cc} [MPa]	σ_{s} [MPa]	σ_{fr} [MPa]	σ_{fr} [MPa]	Failure mode	Cracking	Failure	SLS 1	SLS 2	ULS 1	ULS 2		
PC	48	-2,096							-	-	-	-	-	-	-	-	-	-	295	0,745	4,71	122,1	-6,9	-120,2	1251,4	-	23,9	118	2,966	5,69	147,5	-10,7	-135,3	1450	-	24	57,25	6,46	167,4	-1,397	-30,3	-73,2	1571,2	-	RP	-	-	131%	149%	121%	147%	No	19,3
SPC 10%	-	-2,364							69,4	34,7	-41	-0,999	-1,34	-93,1	1173,5	254	24,6	-4,7	306	0,838	5,51	142,8	-8,0	-127,2	1250,0	323	24,9	133	3,201	7,12	184,7	-12,7	-149,4	1450	431	44	47,89	14,84	384,6	-2,111	-33,3	-262,8	1538,8	2480	RC	17,0	129,8	112%	127%	53%	64%	No	15,0
SPC 20%	-	-2,777							138,9	69,4	-15	-1,399	-0,70	-91,2	1151,3	507	49,2	-10,8	316	0,932	6,32	163,9	-9,1	-134,2	1248,6	595	26,5	142	3,352	8,03	208,1	-14,0	-158,5	1450	704	46	42,74	14,78	383,2	-1,965	-33,3	-259,3	1527,9	2480	RC	34,3	128,9	97%	111%	53%	64%	No	12,8
SPC 30%	-	-3,219							208,3	104,2	-0	-1,820	-0,02	-89,2	1128,0	759	73,8	-16,3	324	1,027	7,13	184,9	-10,2	-141,4	1247,2	867	28,7	150	3,504	8,92	231,3	-15,2	-167,7	1450	977	48	37,61	14,72	381,6	-1,823	-33,1	-256,6	1517,0	2480	RC	51,5	128,0	86%	98%	53%	64%	Yes	10,7
SPC 40%	-	-3,692							277,8	138,9	9	-2,266	0,68	-87,2	1103,1	1010	98,4	-22,1	330	1,124	7,94	205,8	-11,2	-148,6	1245,8	1139	30,4	158	3,659	9,82	254,5	-16,4	-177,0	1450	1251	52	32,48	14,66	380,0	-1,685	-32,5	-254,5	1506,1	2480	RC	68,6	127,0	78%	88%	53%	65%	No	8,9
SPC 50%	-	-4,203							347,2	173,6	16	-2,744	1,42	-85,1	1076,4	1259	123,0	-28,0	336	1,223	8,74	226,6	-12,3	-156,1	1244,3	1411	32,1	165	3,816	10,71	277,5	-17,6	-186,5	1450	1524	57	27,36	14,59	378,3	-1,548	-31,6	-252,8	1495,2	2480	RC	85,6	126,0	71%	80%	54%	65%	No	7,2

Input

CFRP	
Dimensions [mm²]	120x1,4
Number of laminates	2
Placement	On the sides
Long term load [kN/m]	4,7
Load before strengthening [kN/m]	2,35

	Initial camber		Prior to strengthening						P_{fr} [kN]		After strengthening							Cracking									Yielding							Failure									ΔM [%]		Utilisation ratios for cracking (SLS) and failure (ULS)				Requirements fulfilled	Ductility index
Beam type	x [mm]	κ ·10⁻³ [1/m]	x [mm]	κ ·10⁻³ [1/m]	σ_{α} [MPa]	σ_{t} [MPa]	σ_{fr} [MPa]	δ [mm]	Total	per laminate	x [mm]	κ ·10⁻³ [1/m]	σ_{cc} [MPa]	σ_{s} [MPa]	σ_{fr} [MPa]	σ_{fr} [MPa]	τ_{max} [MPa]	δ [mm]	x [mm]	κ ·10⁻³ [1/m]	q [kN/m]	M [kNm]	σ_{cc} [MPa]	σ_{s} [MPa]	σ_{fr} [MPa]	σ_{fr} [MPa]	δ [mm]	x [mm]	κ ·10⁻³ [1/m]	q [kN/m]	M [kNm]	σ_{α} [MPa]	σ_{s} [MPa]	σ_{fr} [MPa]	σ_{fr} [MPa]	δ [mm]	x [mm]	κ ·10⁻³ [1/m]	q [kN/m]	M [kNm]	ε_{su} [‰]	σ_{cc} [MPa]	σ_{s} [MPa]	σ_{fr} [MPa]	σ_{fr} [MPa]	Failure mode	Cracking	Failure	SLS 1	SLS 2	ULS 1	ULS 2		
PC	48	-2,096							-	-	-	-	-	-	-	-	-	-	295	0,745	4,71	122,1	-6,9	-120,2	1251,4	-	23,9	118	2,966	5,69	147,5	-10,7	-135,3	1450	-	24	57,25	6,46	167,4	-1,397	-30,3	-73,2	1571,2	-	RP	-	-	131%	149%	121%	147%	No	19,3
SPC 10%	-	-2,414							83,3	41,7	-37	-1,053	-1,30	-93,1	1170,2	252	24,5	-5,6	309	0,859	5,65	146,5	-8,3	-128,8	1249,7	321	25,4	136	3,244	7,33	190,0	-13,1	-152,0	1450	425	48	50,23	16,20	419,9	-2,398	-33,3	-308,4	1542,2	2480	RC	20,0	150,8	109%	124%	48%	59%	No	15,5
SPC 20%	-	-2,892							166,7	83,3	-12	-1,513	-0,60	-91,2	1144,5	502	49,0	-12,1	319	0,973	6,59	170,8	-9,6	-137,3	1248,0	592	27,7	146	3,425	8,37	217,0	-14,6	-163,0	1450	697	50	44,86	16,15	418,6	-2,231	-33,3	-301,9	1530,9	2480	RC	39,9	150,0	94%	106%	48%	59%	No	13,1
SPC 30%	-	-3,407	-9,7	-0,617	-2,0	-95,0	1194,5	1,4	250,0	125,0	2	-2,003	0,15	-89,1	1117,0	752	73,5	-18,8	328	1,088	7,52	195,0	-10,8	-145,9	1246,3	864	29,8	155	3,610	9,41	243,9	-16,1	-174,1	1450	970	52	39,51	16,09	417,1	-2,068	-33,3	-296,1	1519,6	2480	RC	59,7	149,2	82%	93%	49%	59%	No	10,9
SPC 40%	-	-3,968							333,3	166,7	11	-2,529	0,93	-87,0	1087,5	999	98,0	-25,4	335	1,205	8,45	219,0	-12,1	-154,7	1244,6	1135	31,9	164	3,798	10,44	270,6	-17,5	-185,4	1450	1243	56	34,17	16,03	415,6	-1,910	-33,3	-291,2	1508,4	2480	RC	79,4	148,3	73%	83%	49%	59%	No	9,0
SPC 50%	-	-4,583							416,6	208,3	17	-3,102	1,76	-84,8	1055,2	1244	122,5	-32,1	341	1,325	9,37	243,0	-13,4	-163,7	1242,8	1406	33,9	172	3,990	11,46	297,2	-18,9	-197,0	1450	1516	61	28,84	15,97	413,8	-1,756	-32,8	-287,0	1497,1	2480	RC	99,1	147,2	66%	75%	49%	59%	No	7,2